[redacted]

GIANNINI CONTROLS CORPORATION

FINAL REPORT

MARS PROBE/LANDER

DENSITY SENSING SYSTEM

Prepared for

NATIONAL AERONAUTICS AND SPACE ADMINISTRATION
LANGLEY RESEARCH CENTER
HAMPTON, VIRGINIA

CONTRACT NUMBER NAS1-5341

Prepared by

GIANNINI CONTROLS CORPORATION
CONTROL/NUCLEONICS DIVISION
Duarte, California

24 February 1966

GIANNINI CONTROLS CORPORATION

FINAL REPORT

MARS PROBE/LANDER DENSITY SENSING SYSTEM

Prepared For:

NATIONAL AERONAUTICS AND SPACE ADMINISTRATION
LANGLEY RESEARCH CENTER
HAMPTON, VIRGINIA

CONTRACT NUMBER NAS1-5341

Prepared by:

N. W. Gebbie

Dr. N. W. Gebbie
Research Physicist

Approved by:

D B Hakewessell

D. B. Hakewessell
Program Manager

GIANNINI CONTROLS CORPORATION

MARS PROBE/LANDER DENSITY SENSING SYSTEM

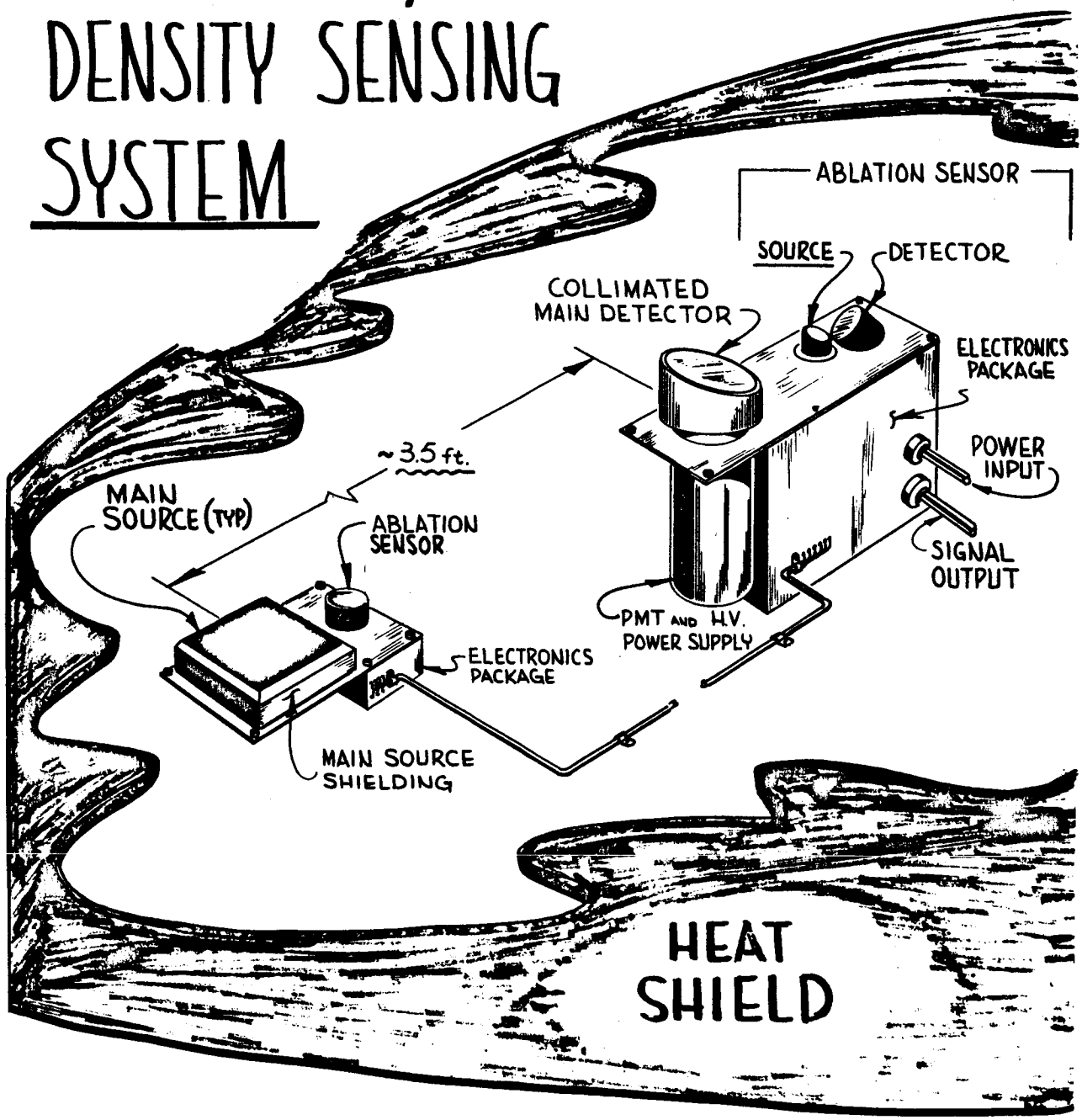

TABLE OF CONTENTS

TABLE OF CONTENTS (Cont'd)

TABLE OF CONTENTS (Cont'd)

TABLE OF CONTENTS (Cont'd)

LIST OF TABLES

LIST OF FIGURES

1.0 INTRODUCTION AND SUMMARY

Early in the 1970's, an unmanned vehicle will be used to probe the Martian atmosphere and land some apparatus on the planetary surface. A prime purpose of the mission is the measurement of the density of the Martian atmosphere at various altitudes for scientific knowledge and to aid in the design of future Mars Probe/Landers. The necessity of density measurements from a vehicle within the atmosphere itself is clear from the very considerable disagreement found among that data that are presently available[1], since these indicate surface pressures which differ by a factor of ten or more. Accordingly, Giannini Controls Corporation was awarded Contract Number NAS1-5341 from NASA-Langley Research Center in order to provide the conceptual design for a small reliable device capable of accurately measuring the atmospheric density while located in a vehicle descending through the Martian atmosphere. This conceptual design is presented by this Final Report of Contract NAS1-5341.

To carry out the density measurements, the γ ray backscatter technique is used. As shown schematically in Figure 1.0-1, a radiation source within the Mars Probe/Lander (MP/L) emits γ rays into the atmosphere surrounding the vehicle. These γ rays are scattered by the gas atoms compsiring the atmosphere, and some reach the detector located within the MP/L. As the gas density rises, so does the backscatter count rate. This density measuring technique has several distinct advantages. First, γ rays can pass through the heat shield. Thus, the device can be located within the

FIGURE 1.0-1

SCHEMATIC DENSITY SENSOR

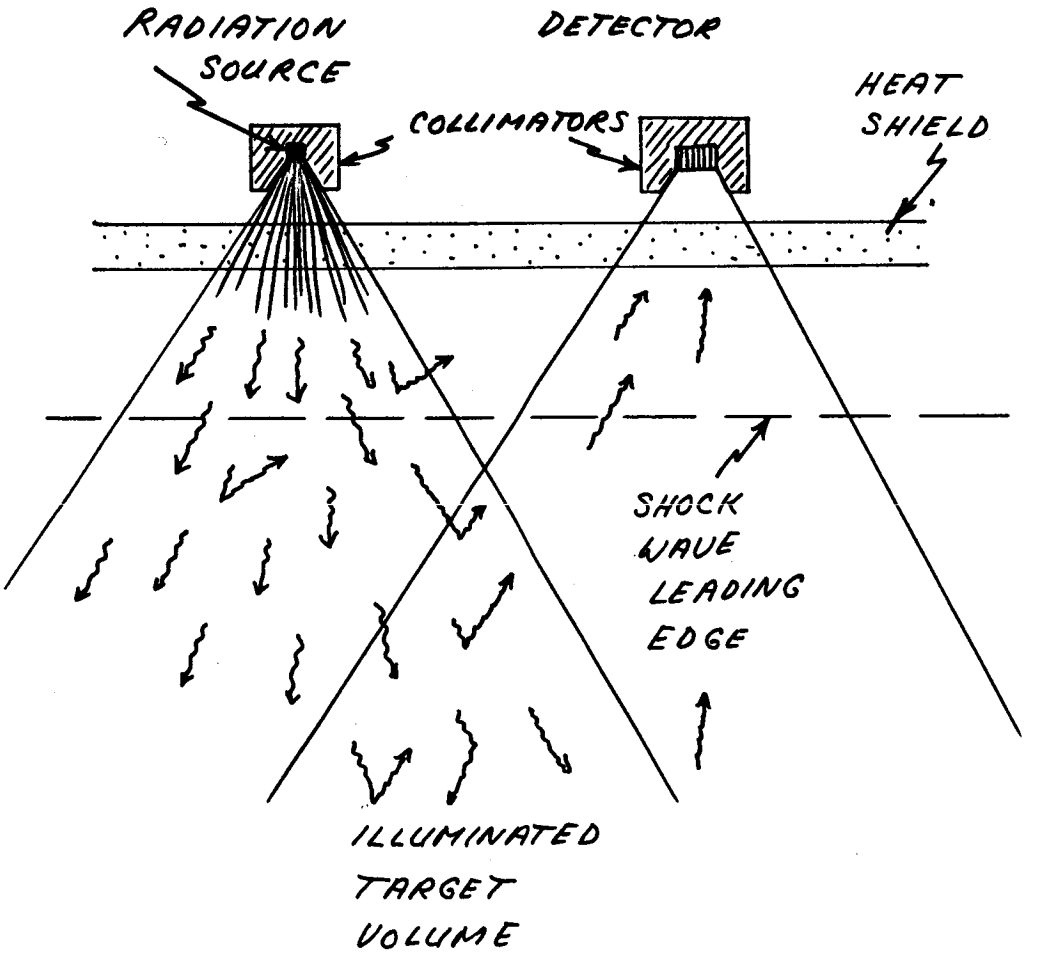

MP/L vehicle and yet carry out the measurements while the heat shield protects the vehicle during the high speed portion of the descent. No "window" or other possible weakening of the vehicle integrity is required. Secondly, the fields of view of both the source and the detector can be adjusted, as shown in Figure 1.0-1, so that only the density of the ambient atmosphere outside the plasma and shock wave is measured. Therefore, the density measurements can be carried out even when severe shock waves are formed during the entry into the atmosphere. Finally this γ ray backscattering technique is already a proven method of atmospheric density measurement, as shown during the experimental rocket flights conducted by NASA-LRC at Wallops Island.

While developing the conceptual design, the wide range of environmental conditions expected during the flight to Mars and the descent through the atmosphere has been carefully considered. Errors introduced by this environment are minimized by the careful physical arrangement of the source and detector and by using the density sensor to measure the ablation of the heat shield during the descent. As a result, this experiment also provides valuable bonus data such as heat shield characteristics and the background radiation. These extra results will aid in the planning and engineering required for follow-on missions.

The final conceptual design of the density sensor utilizes currently available hardware almost completely, such as integrated electronic circuits which are already in use for space applications. The few exceptions are clearly obtainable by simple modification

of current hardware. A summary of the important system parameters is shown in Table 1.0-I, and a sketch of the sensor appears prior to this first chapter. The following points are emphasized.

First, the system accuracy has been calculated for an operational range of $0^{o}C$ - $40^{o}C$, but the device is also capable of operating above and below this temperature range, though with reduced accuracy. In addition, storage at much lower temperatures will not impair the system. Also, the hard vacuum of space will have no effect.

Secondly, a large radioisotope source is a part of the density sensor, and radiation safety is an important consideration. When this source has been produced, it will be inserted by remote control into the shield and collimator to be used during the mission. When an additional flat plate of shielding has been temporarily placed over the collimator opening, there will be no radiation safety problem. In fact, the source and shield can be used as a desk paperweight by a scientist, and he will receive less radiation than the 100 millirem per week permitted for an indefinite period by the AEC. In particular, the dose rate at a distance of one meter is estimated at no more than 0.025 millirem per hour. Once the source has been installed within the MP/L vehicle, a temporary shield must be placed over that portion of the heat shield receiving radiation from the collimated source. No radiation control areas are then required.

Finally, there is the matter of the location of the density sensor within the MP/L vehicle. The best position is the most

TABLE 1.0-I

MAIN PARAMETERS OF THE CONCEPTUAL DESIGN

Mass:	3512 grams (7.75 pounds)
Volume:	~1600 cm^3 (~97 in^3)
Power:	5.81 watts drawn from the 28 volt dc supply aboard the MP/L
Accuracy:	±11.7% in a 1 second period at an altitude of 25 Km in the model 3 atmosphere (ρ = 2.3 x 10^{-6} gm/cm^3)
	±6.0% at 5 Km (ρ = 1.6 x 10^{-5} gm/cm^3)
Reliability:	105,000 hours of operation mean time between failures; system dormant during 8-month transit to Mars
Temperatures:	0^oC -40^oC operational range; may be stored at less than -20^oC provided is warmed up before Martian descent
Telemetry:	0-5 volts dc output (3) to be sampled each second
Radiation Source:	Gd-153 from reactor 100 Kev γ rays 236 days half-life 480 curies (1.8 grams of target - available at ORNL) Cost $35,000 total, delivered to NASA (with shield) Radiation Safety: AEC specifications complied with. No control area needed during vehicle assembly and launch.

forward position (e.g., the nose of a blunt cone vehicle), but such a position may not be available. Accordingly, the design has been carried out by conservatively assuming that the sensor will be located along one side of the vehicle and towards its front. If the front position does become available, the source strength can be reduced, and so can the system mass and volume.

The derivation and necessary documentation of the design parameters are presented in the following chapters of this final report. The first step is the development of the guidelines for the conceptual design.

2.0 DESIGN GUIDELINES

2.1 Introduction and Summary. The purpose of the density sensor is to measure the density of the Martian atmosphere as the vehicle bearing it descends to the Martian surface. However, before the device can be designed, it is necessary to formulate guidelines. This is done by considering the conditions under which the device must exist and then operate, as well as the desired accuracy, mass, power, volume, etc. The detailed considerations are in the following sections, and a summary of the guidelines is presented in Table 2.1-I.

2.2 Mission Profile. The mission starts with the assembly, testing, and calibration of the density sensor on earth. Sterilization is carried out, followed by further testing, insertion into the MP/L and possible final testing of the system. The entire MP/L, which is in a sterile container, is then loaded onto the Saturn 5 launch vehicle.

Once launched, the MP/L and its carrier bus pass through the Van Allen radiation belts around earth and spend eight months in transit to Mars. On reaching the vicinity of Mars, the MP/L and its carrier bus are placed in an orbit to await a propitious moment for the earth-based controllers to initiate the descent.

TABLE 2.1-I

DESIGN GUIDELINES

Accuracy: ±15% in one second at 25 km altitude in model 3 atmosphere (2.3×10^{-6} gm/cc)

Mass: 2270 gm (5 pounds)

Power: 5 watts drawn from 28V DC MP/L supply

Volume: 1640 cc (100 cubic inches)

Sterilization: 3 cycles of 36 hours at 145°C
1 cycle of 24 hours at 135°C
Surface decontamination with ethylene oxide

Hardware Availability: Off-shelf highly preferred
Minor developments allowed
No major development programs

Launch: See Figure 2.5-1 for environment

Trip to Mars: No system operation
Eight months duration
$\lesssim$ -20°C to +40°C
Hard vacuum possible
Space radiation - see Table 2.5-I

Mars Descent: On time < 30 minutes
20° entry angle at < 5 km/second
< 200g deceleration for 1 second
Heat shield ablation
Shock wave formation
0°C to 40°C operating temperature range
Power supply voltage variations
Maximum atmospheric density 4×10^{-5} gm/cc
Non-survival of impact

TABLE 2.1-I (Cont'd)

DESIGN GUIDELINES

Radiation Levels:	Personnel safety during assembly and pre-launch - AEC specifications
	Source integrity in fireball
	20 seconds at 3500°C
	several minutes at 1500°C
	Shield source from other MP/L apparatus
	Mars contamination to be avoided

The descent commences at an angle of about 20°C below the horizontal, and at a maximum velocity of 5 km/second. Retro-rockets are used. The density sensor commences operation and may, in fact, be activated up to 30 minutes before impact, depending on the preliminary measurements desired. When the MP/L vehicle enters the significant atmosphere (still at perhaps 5 km/sec.) a shock wave forms around it, and the heat shield partially ablates. The deceleration may reach 200 g for a second but less is expected. As the atmospheric drag reduces the vehicle velocity, the shock wave becomes less dense and is no longer folded back near the vehicle skin. While the vehicle is still traveling near the velocity of sound, a parachute sequence commences and the heat shield is released from the vehicle. The remainder of the descent (from about 5 km) is a slow parachute drop. The density sensor is not required to survive the impact.

During the descent, telemetering of data back to the orbiting bus continues except during the blackout due to the plasma formed during the heat shield ablation. Data is also stored in the survival instrument package for relay to the bus during the parachute phase. There may even be direct transmission of stored data to earth at a very low rate after impact.

2.3 System Accuracy. A number of earth-based observations[1] indicate a Martian atmospheric surface pressure of 17 ±9 to 85 ±4 millibars (mb), compared to the standard pressure of 1013 mb at earth sea level. In addition, there are the widely publicized Mariner 4 observations which have been used to calculate a surface

pressure of 5-8 mb. Obviously there are very serious discrepancies among the earth-based results.

However, when there is a γ ray backscatter density sensing system within a vehicle descending through the Martian atmosphere, the measurements are carried out within the atmosphere itself and much improved accuracy can be expected. The main limitations on the accuracy are the physical restrictions placed upon the apparatus. After preliminary studies and discussions with personnel at NASA-LRC, it was decided to set an accuracy goal of ±15% at 25 km above the Martian surface, assuming that the pressure and density there are approximately 0.54 mb and 2.3×10^{-6} gm/cc, respectively, as in the least dense engineering model atmosphere (number 3) specified by the Contract Work Statement[2]. The ±15% accuracy is a one-sigma accuracy; i.e., there is an approximately 2/3 probability that the actual density error will be less than 15%. It is to be obtained during a one-second period. At lower altitudes, where the density is greater, the accuracy improves.

By fitting a smooth curve through the consecutive density measurements, much better accuracy than the ±15% goal may be obtained. Nevertheless, a one-sigma accuracy of ±15% in one second at 25 km in the model 3 atmosphere serves as the accuracy guideline.

2.4 Mass, Power and Volume Goals. Some of the physical limitations upon the conceptual design obviously stem from the fact that sending a payload of instruments to Mars is a difficult and expensive procedure, and so the size of any particular experiment

should be minimized as much as possible. The Work Statement has set the following design goals:

Mass: 2270 grams (5 pounds)

Power: 5 watts drawn from the 28V DC battery supply in the descending probe

Volume: 1640 cubic centimeters (100 cubic inches)

2.5 Reliability. The most important requirement is that the system be reliable; i.e., the sensor must have a high probability of operating as planned while the Mars Probe/Lander is descending through the Martian atmosphere. Therefore, the conceptual design uses proven hardware so as to maximize the reliability.

In assessing the reliability of the conceptual design, there are, of course, the standard Mean Time Between Failures (MTBF) figures available for many of the different components. However, it is also necessary to consider the rather specialized conditions that will exist before and during the operation of the density sensor. First of all, the device itself must be sterilized; the following procedure has been specified in the Work Statement:

(a) Component sterilization of 3 cycles of 36 hours at 145°C in a dry atmosphere.

(b) Subassembly decontamination with ethylene oxide.

(c) Terminal sterilization of the MP/L for 24 hours at 135°C in a dry atmosphere.

Once the MP/L and its density sensor are onboard the Saturn 5, they must survive the launch environment. This is presently unknown, but for information purposes, the Apollo and Mariner 4 specifications are shown in Figure 2.5-1.

Then, there is the approximately eight-month transit to Mars, during which the density sensor is subjected to bombardment by various forms of radiation. The expected radiation environment is specified in Appendix A, and a summary is presented in Table 2.5-I. Since these are the radiation intensities expected on the outside of the carrier vehicle, the fluxes actually reaching the sensor through the shielding afforded by the bus and the MP/L are less severe. However, these worst case values are used for radiation damage calculations in order to be conservative. The complex flux reaching the detector during the Martian descent is described in Chapter 7.

In addition to the possibility of radiation damage, the eight-months "on-the-shelf" during transit must be considered. During most of this eight-month period, the entire MP/L and its contents may rest in a several psi argon atmosphere within a sterilization can until shortly before the Martian descent. Such an atmosphere aids significantly in avoiding the deterioration of equipment that can occur when more active gases are present.

LAUNCH ENVIRONMENT

FIGURE 2.5-1

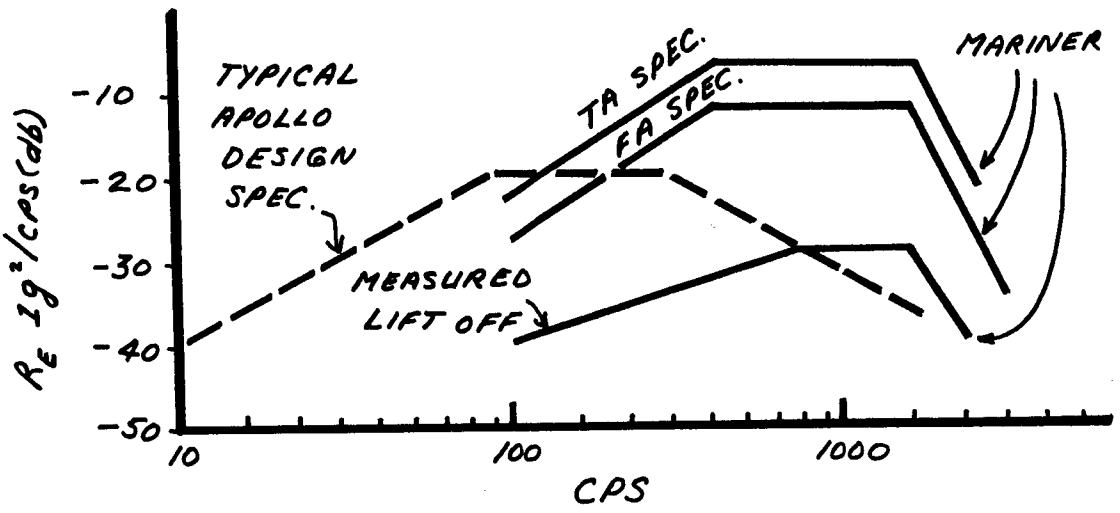

THERMAL SHOCK	75°C TO -46°C
VIBRATION	16.4g RMS NOISE - 3 MIN.
5g RMS NOISE	2g RMS SINE 15-40 CPS 9g RMS SINE 40-2000 CPS 600 SEC.
VIBRATION - LOW FREQ.	±1 SINE 1-4.4 CPS, 3 MIN 3g PEAK 4.4 CPS - 15 CPS
STATIC ACCELERATION	±14g 3 AXIS, 5 MIN
SHOCK	FIUE 200g, 0.7ms, 3 AXES

TABLE 2.5-I

RADIATION ENVIRONMENT OF THE DENSITY SENSING SYSTEM*

Earth Surface: Background present during testing is very strongly dependent on the physical surrounding and so is not specified. Radiation damage negligible.

Van Allen Belts:

Inner: $\leqslant 2 \times 10^4$ protons/cm^2/sec. with $40 < E_p < 110$ Mev

$\leqslant 2 \times 10^7$ electrons/cm^2/sec. with $5 < E_e$ Mev

Outer: $\leqslant 1 \times 10^8$ protons/cm^2/sec. with $0.1 < E_p < 5$ Mev

$\leqslant 4 \times 10^3$ protons/cm^2/sec. with $40 < E_p < 110$ Mev

$\leqslant 1 \times 10^6$ electrons/cm^2/sec. with $1.6 < E_e$ Mev

Solar Flares: Yearly fluxes are:

$1\text{-}6 \times 10^9$ protons/cm^2/year with $E_p > 30$ Mev

$1\text{-}10 \times 10^8$ protons/cm^2/year with $E_p > 100$ Mev

Cosmic Rays: $\sim$ 2-4 protons/cm^2/sec.

i.e., 7×10^7 to 1.3×10^8 protons/cm^2/year

Energy spectrum (E in Bev)

$$N(E)\Delta E = \frac{\Delta E}{(1+E)^n} \text{ particles/cm}^2\text{/sec.}$$

$n = 2.1$ for $2 < E < 15$ Bev

$= 2.5$ for $15 < E$

* See Appendix A for detailed description, particularly regarding flux variations in the Van Allen belts and the solar flare energy spectrum.

However, this neutral environment may be accidentally lost with the result that the apparatus spends a long period of time exposed to the hard vacuum of outer space. Therefore, mechanical devices with exposed moving parts are avoided, as are parts likely to undergo significant evaporation.

Next, the density sensor must survive the temperature extremes that occur during the voyage. The maximum expected is 40°C and the minimum may be less than -20°C. During the descent, the temperature is expected to be near the high end of this range, and the sensor must be capable of operating in the 0°C to 40°C range. During the descent, the voltage supplied to the density sensor from the 28 volt batteries may vary for some reason, so the conceptual design should be as insensitive as possible to such fluctuations.

2.6 MP/L Vehicle Structure. In designing the sensor, it is also necessary to consider the MP/L vehicle. At present, details are scarce, but a likely design is a blunt-nosed cone covered with a heat shield, all of which is decelerated during its descent by retro-rockets and atmospheric drag. The half-angle of the cone may be 50° to 60°, and the heat shield is assumed to be no more than a 2.5 cm thick ablator like Refrasil with a density of 0.5 gm/cc. This assumption is based on discussions with AVCO/RAD and NASA-LRC personnel. More recent discussions with NASA-LRC personnel indicate the possibility of a thin shield of beryllium. However, the first mentioned ablator appears to be a worst case, as far as the conceptual design is concerned, and is assumed.

The location of the density sensor aboard the MP/L has not yet been determined. One possibility is the most forward position, where the shock wave is thinnest (although densest). In this position, the source strength and cost would be least. However, such a position may be pre-empted by other apparatus, and so the conceptual design assumes a side position where the shock wave is about 30 cm thick, as compared to less than 7 cm at the nose. In either case, the density sensor is collimated so as to minimize the effect of the shock wave, which is of a higher density than the ambient atmosphere.

Due to the current lack of information regarding the MP/L vehicle, no important assumptions other than those above are made concerning the physical structure in which the density sensor will be embedded, except in Chapter 7 where the background radiation count rate is considered. The conceptual design has been made as independent as possible of the MP/L structure.

2.7 Hardware Availability. The conceptual design must use currently available and proven hardware as much as possible in order to demonstrate feasibility. Particularly to be avoided is hardware which depends upon a development program of uncertain outcome. This does not, however, eliminate simple and clearly feasible improvements in present-day apparatus, e.g., the ruggedization of a proportional counter.

It is also important that the chosen source of radiation be reasonably available. If a radioisotope is selected, it is realized that the desired size and type of source may not be on the shelf at Oak Ridge National Laboratory, but sufficient study should be carried out to indicate that it can be produced when needed.

2.8 Radiation Safety. Since the density sensor utilizes a source of γ radiation (be it a radioisotope or an X-ray tube), the design must reduce the radiation doses to acceptable levels. There are 4 cases to be considered.

First, there will be handling and installation of the source prior to launch. Avoidance of the need for controlled access areas is important, particularly during the hectic pre-launch countdown. Second, the source must not present a serious hazard in the event of a fireball accident, i.e., a launch vehicle explosion during the launch phase. In order to survive such an event, the source must withstand the initial period of very high temperature followed by a longer period at a lower temperature. These temperature periods are estimated to be:

20 seconds at 3500°C

several minutes at 1500°C

Actual test results are not available for the proposed launch vehicle.

The final 2 cases do not involve personnel, as they occur during the eight-month transit and descent. During the long transit, it is important the experiments within the MP/L and the bus are not adversely affected; i.e., there should not be structural radiation

damage and the background count rate contributed by the density sensor to other experiments during their operation should be at an acceptable level. Finally, it is desirable to avoid contamination of the Martian surface. Since the present plans call for a relatively soft parachute landing, any source which is designed to survive a fireball accident will also survive the impact on Mars, so Mars contamination avoidance presents no additional design constraints.

The design guidelines are summarized in Table 2.1-I at the start of this chapter. The next chapter contains the theoretical analysis of the γ ray scattering.

3.0 DERIVATION OF SYSTEM RESPONSE

3.1 Introduction and Summary. This chapter derives the system response as a function of various parameters, some of which have already been determined by the design guidelines of Chapter 2. Since very little information is available about the structure of the MP/L vehicle and the location therein of the density sensor, only a simplified derivation is carried out. However, experimental results from other density-sensing contracts have shown good agreement with the simply-derived system response, so Giannini Controls is confident that this analysis is the best available with our present information limitations and that it can be relied upon.

Using this theoretical system response, the geometrical arrangement of the source and detector is then selected, and an expression is developed to predict the rate at which γ rays will be scattered back from the Martian atmosphere to the detector. Finally, an examination of the system error leads to the conclusion that two ablation gages are required to measure the heat shield ablation over both the source and the detector. These conclusions along with other pertinent results, are summarized in section 3.4, and a brief outline is given in Table 3.1-I.

3.2 Scattering Theory and System Geometry Selection

3.2.1 Types of Interaction. Before studying the scattering theory, it is useful to examine the significant forms of interaction of γ rays with matter. The nine possible modes of interaction are discussed in Appendix B, but Compton scattering, photoelectric absorption, and pair production dominate so strongly for the γ ray

TABLE 3.1-I

SUMMARY OF THEORETICAL SYSTEM STUDY

Compton Scattering: Used to measure atmospheric density

System Geometry: Density sensor on MP/L vehicle side

Source-detector separation = 105 cm

Shock wave thickness = 30 cm

Heat shield thickness = 2.5 cm of 0.5 gm/cc

Source and detector have collimation half angles of $\sim 45°$ to avoid shock wave density measurement

Backscatter Count Rate: $I_s = 6.5 \times 10^{-5} I_o \rho_a \mu_{as} A_d \epsilon_d$ cps

where: I_o - source strength; ρ_a - atmospheric density; μ_{as} - scattering coefficient; A_d - detector area; ϵ_d - detector efficiency

Energy Discrimination: Required in detection system

Background Radiation: Prediction required

Ablation Gages: Required (2)

Calibration Error (total)	±5.3% at 25 km	±4.5% at 5 km
Ground Calibration	±3%	±3%
Ablation	±2%	--
Electronic Drift	±3%	±3%
Atmospheric Composition	±1%	±1%
Electronic Coincidence	±1%	±1%
Resolving Time	±2%	--

energies to be considered (10 Kev to 10 Mev), that the other processes can be neglected. These three important processes are:

(a) Compton Scattering - A γ ray scatters from a single electron which is in an orbit about a nucleus. This electron absorbs some of the γ ray energy and is freed from its orbit. The energy of the scattered γ ray depends on its original energy, the energy required to free the electron, and the angle of scattering.

(b) Photoelectric Absorption - The γ ray energy is completely transferred to an orbiting electron which then leaves its orbit.

(c) Pair Production - The γ ray interacts with the electric field about a nucleus or an electron and is converted into a positron and an electron. A minimum γ ray energy of 1.02 Mev is necessary.

Of these three interaction processes, pair production is avoided by using a radiation source of less than 1.02 Mev, and photoelectric absorption results in a high speed electron which travels away from the MP/L and has a negligible chance of producing a count in the detector of the density sensor. Therefore, only the Compton scattering need be considered.

3.2.2 Scattering Theory. The source and detector are located within the MP/L as shown schematically in Figure 3.2.2-1. Their separation is r. To avoid measuring the density of the shock wave, both are collimated so that their fields of view intersect only beyond the shock wave. Consider an elemental volume dV within this overlap region, and consider those γ rays which are emitted by the

FIGURE 3.2.2-1

SCHEMATIC SOURCE-DETECTOR CONFIGURATION

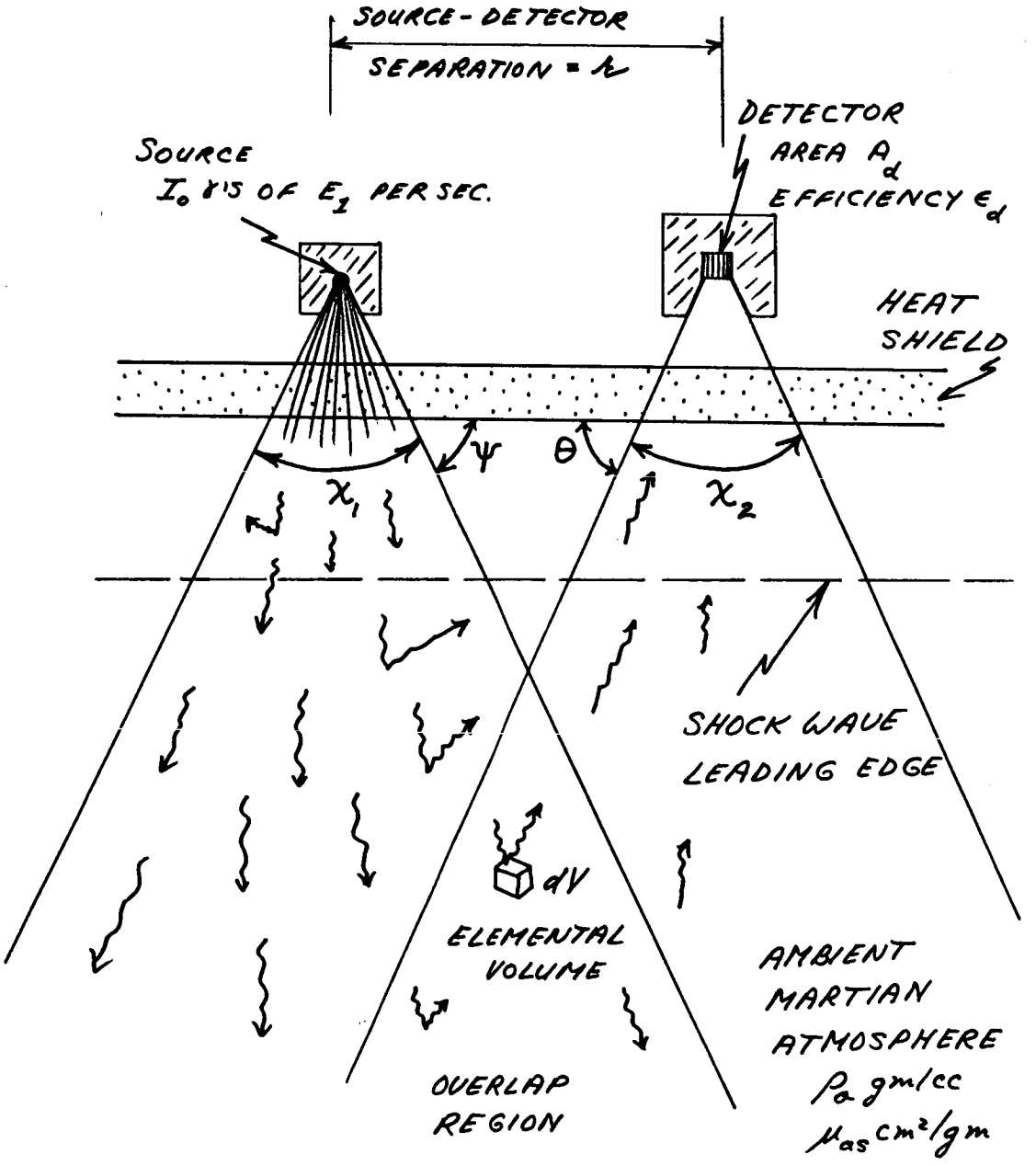

source, are scattered in dV, and then are detected, all with no other intervening interactions whatsoever. The γ ray flux N_1 at dV is given by:

$$N_1 = \frac{I_o P_1}{4\pi s_1^2} \quad \gamma\text{'s/cm}^2\text{/sec.} \qquad (3.2.2\text{-}1)$$

where: I_o is the source strength in photons/sec. emitted into 4π solid angle about the source

P_1 is the probability that a photon emitted towards dV will reach dV without an intervening interaction (such as being scattered in the heat shield, etc.)

s_1 is the distance of dV from the source, in cm

The rate dn_1 at which the primary γ rays are scattered in dV is:

$$dn_1 = N_1 \rho_a \mu_{as} dV \quad \gamma\text{'s/sec.} \qquad (3.2.2\text{-}2)$$

where: ρ_a is the density of the Martian atmosphere outside the shock wave, in gm/cm^3

μ_{as} is the photon scattering coefficient of the ambient Martian atmosphere, in cm^2/gm

Combining equations 3.2.2-1 and 2,

$$dn_1 = \frac{I_o P_1 \rho_a \mu_{as} dV}{4\pi s_1^2} \quad \gamma\text{'s/sec.} \qquad (3.2.2\text{-}3)$$

The next step is to determine the count rate from the detector due to dn_1. This is:

$$dn_2 = dn_1 \times \frac{w(\beta,E_1)\ P_2}{1} \times \frac{A_d\ \epsilon_d}{4\pi s_2^2} \quad \text{cps} \qquad (3.2.2\text{-}4)$$

where: dn_2 is the rate at which photons scattered in dV are recorded by the detector, in counts/sec.

$w(\beta,E_1)$ is a correction factor applied to the scattering coefficient μ_{as} to allow for the anisotropy of the scattering process

β is the angle through which the γ ray is scattered

E_1 is the energy of the γ rays emitted by the radiation source

P_2 is the probability that a photon scattered towards the detector from dV will reach it without an intervening interaction

A_d is the detector area, in cm^2

ϵ_d is the detector efficiency

S_2 is the distance from dV to the detector

Combining equations 3.2.2-3 and 4,

$$dn_2 = \frac{I_o\ P_1}{4\pi s_1^2} \times \frac{\rho_a\ \mu_{as} w(\beta,E_1)}{1} \times \frac{P_2\ A_d\ \epsilon_d}{4\pi s_2^2} \times dV \qquad (3.2.2\text{-}5)$$

counts/second

The total backscatter count rate I_s due to γ rays from the source which reach the detector by means of a single scatter in the overlap region of the source and detector collimated volumes, is obtained by integrating the elemental count rate dn_2 over the overlap region V, i.e.,

$$I_s = \int_V dn_2 \qquad (3.2.2\text{-}6)$$

When I_s is evaluated it is found to be a function of I_o, ρ_a, μ_{as}, A_d, ϵ_d, E_1, ψ, θ, χ_1, χ_2, and r.

3.2.3 Selection of System Geometry. Of the parameters found in the expression for I_s, the ones I_o, ρ_a, μ_{as}, A_d, ϵ_d, and E_1 are independent of the system geometry. Accordingly, they are fixed and the system geometry is made as efficient as possible by manipulating the geometry-defining parameters ψ, θ, χ_1, χ_2, and r. Assuming the reasonable MP/L vehicle structure outlined in section 2.6, the system geometry optimization is described in Appendix C. The results are shown in Figure 3.2.3-1 for the case of a density sensor located along the side of a blunt-nose MP/L cone vehicle where the shock wave is expected to be about 30 cm thick.

If the density sensor is located in the nose of the MP/L, where the shock wave is much thinner, the source-detector separation will be reduced by a factor of 3 and the source strength I_o also can be reduced by a factor of 3. However, it is expected that the density sensor may not be able to obtain the nose position and so it is assumed throughout the remainder of this final report that the sensor geometry is as shown in Figure 3.2.3-1. For this geometry, the count rate I_s is given by:

$$I_s = 6.5 \times 10^{-5} I_o \rho_a \mu_{as} A_d \epsilon_d \text{ counts/sec.} \qquad (3.2.3\text{-}1)$$

FIGURE 3.2.3-1

SOURCE-DETECTOR GEOMETRY *

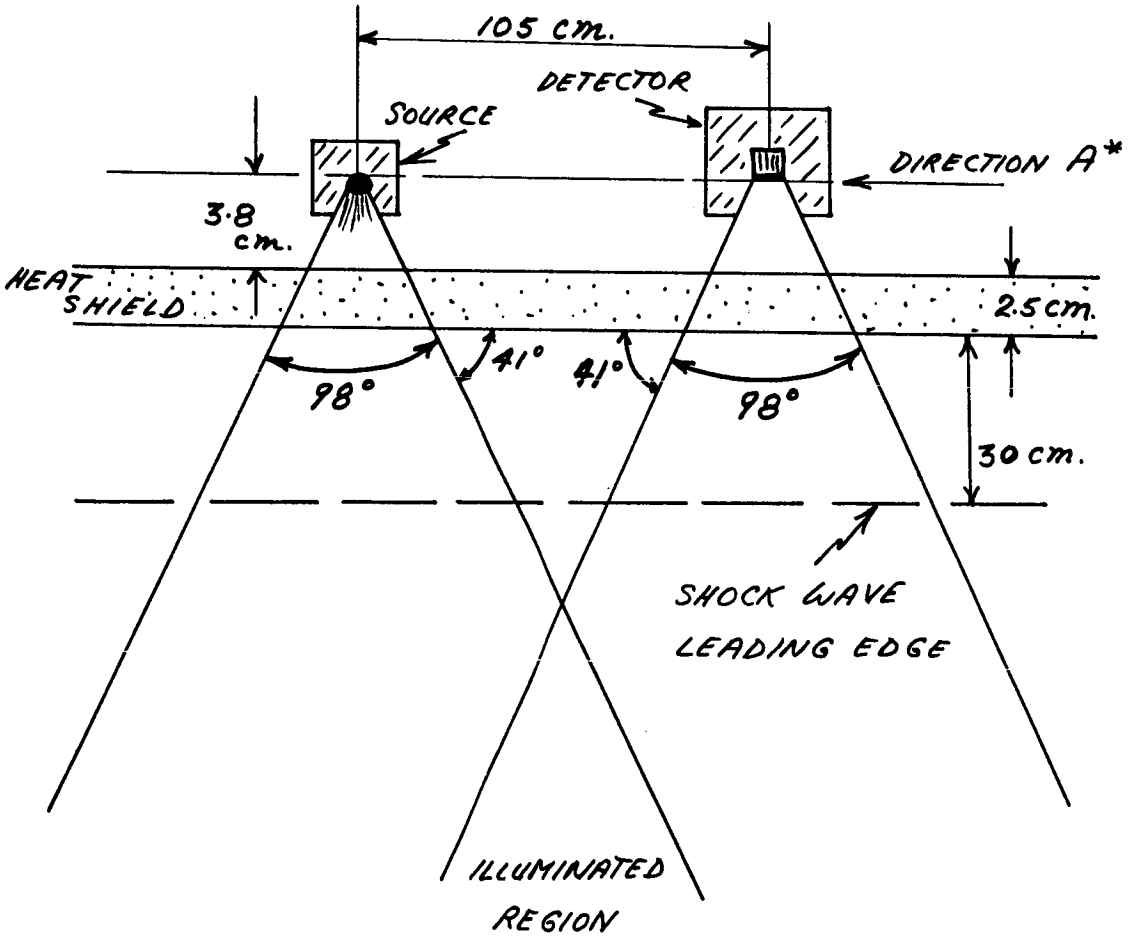

*WHEN SEEN ALONG DIRECTION A, SOURCE AND DETECTOR VIEWING ANGLES ARE 90°.

The parameter E_1, representing the energy of the γ rays emitted from the source, is implicit in μ_{as} and ϵ_d.

Equation 3.2.3-1 predicts only the count rate resulting from γ rays of energy E_1 which leave the source, reach the region of overlap for the collimated source and detector without further interaction, scatter once in the overlap volume, reach the detector without further interaction, and then are detected. Obviously, counts will be recorded that do not correspond to the above sequence of events. These counts may be divided into 2 groups--those which are indicative of the ambient density of the Martian atmosphere, and those that are not. The first group is useful and their inclusion will benefit the density sensing experiment. They can arise when a source γ ray undergoes a low angle scatter in the heat shield followed by a scatter in the overlap volume and subsequent detection. A brief survey of the possibility of such an event indicates that it (and others of similar types) are not sufficiently numerous to justify the effort needed to accurately predict their effect. Therefore, equation 3.2.3-1 is used for the conceptual design even though it gives a pessimistic estimate of the useful count rate I_s.

On the other hand, there are those counts which are definitely not indicative of the ambient atmospheric density. Such counts may arise when a γ ray scatters in the heat shield, proceeds along the heat shield to scatter in the shield right over the detector, and is then detected. Cosmic ray counts, etc. are also in this category. All such counts cause an error in the indicated

atmospheric density. Their importance and proposed ways of reducing or eliminating them are discussed in the following section on error analysis.

3.3 Error Analysis. In this section, an analytical expression is developed for the system error as a function of many system parameters. Unless otherwise specified, all errors are one-sigma statistical errors; i.e., there is an approximately 2/3 probability that the error occurring during the density measurement is less than the quoted one-sigma value.

3.3.1 Overall Error Expression. The data received from the sensor's detector consists of the total count rate I_d recorded during successive one-second intervals. This rate is the sum of the actual background rate I_b and the actual source atmospheric backscatter rate I_s, where I_s is defined in section 3.2.2. Therefore:

$$I_d = I_s + I_b \qquad (3.3.1\text{-}1)$$

The atmospheric density ρ_m that is calculated from these results will be the best estimate of I_s multiplied by a measured calibration constant k. Since the calculated value of I_s is the measured total rate I_d minus the calculated background rate I_{bc}, therefore:

$$\rho_m = k(I_d - I_{bc}) = k(I_s + I_b - I_{bc}) \qquad (3.3.1\text{-}2)$$

From this, the density error $\Delta\rho_m$ is:

$$\frac{\Delta\rho_m}{\rho_m} = \frac{\Delta k}{k} + \frac{\Delta I_s}{I_s} + \frac{\Delta I_b}{I_s} - \frac{\Delta I_{bc}}{I_s} \qquad (3.3.1\text{-}3)$$

where it is assumed that I_{bc} and I_b are so close in value that the quantity $(I_s + I_b - I_{bc})$ can be replaced by I_s above. The symbols of 3.3.1-3 are explained as follows:

ρ_m is the measured density calculated from equation 3.3.1-2

$\Delta\rho_m$ is the error in the measured density ρ_m

k is the measured calibration constant of the apparatus. It relates the atmospheric density to the rate at which the atmosphere backscatters γ rays from the source.

Δk is the error in k

I_s is the count rate due to γ rays which reach the detector by means of a lone interaction--a scatter in the volume formed by the overlapping of the collimated source and detector viewing volumes

ΔI_s is the error in I_s

ΔI_b is the statistical error in the background radiation count rate I_b

ΔI_{bc} is the uncertainty in the calculation of the background radiation count rate

The foregoing errors are now described in greater detail.

3.3.2 Source Error ΔI_s. The one-sigma statistical uncertainty ΔI_s in the count rate I_s is:

$$\frac{\Delta I_s}{I_s} = \pm \frac{I_s}{I_s} = \pm \frac{1}{\sqrt{I_s}} \qquad (3.3.2\text{-}1)$$

It can be reduced by increasing I_s.

3.3.3 Background Error ΔI_b. The one-sigma statistical uncertainty in the radiation background count rate I_b will be:

$$\frac{\Delta I_b}{I_s} = \frac{\sqrt{I_b}}{I_s} \qquad (3.3.3\text{-}1)$$

The background count rate arises from the following causes:

(a) Cosmic rays interact with the detector, the MP/L vehicle, the Martian atmosphere, and the Martian surface to produce radiations (γ, p, n, etc.) which reach the detector and are counted.

(b) Radioisotopes in the Martian surface layer.

(c) Solar flares contribute by all the methods given for cosmic rays in (a).

(d) There is direct transmission from the source to the detector.

(e) The γ rays reach the detector by scattering in the MP/L structure.

(f) Multiple scattering within the relatively dense shock wave layer permits extraneous γ rays to reach the detector.

(g) Combinations of (e) and (f) occur.

(h) A small additional radiation source used for circuit stabilization contributes.

The quantity ΔI_b represents the root of the sum of the squares of the one-sigma errors for each of the above contributors.

Since the background count rates from the above causes depend on the detector selected, the actual radiation background calculations are done in Chapter 7.

From the preceding descriptions of the causes of background radiation, it is clear that this unwanted count rate can be very significant. Therefore, the conceptual design is such that the electrical pulses resulting from virtually all of the background counts are rejected and so do not contribute to the total detector

count rate I_d. This is possible because most of the background counts produce electrical pulses whose magnitudes differ from those due to the backscattered γ rays. This difference is utilized by the electronics to reject them. In the remainder of this report, the "background count rate" will refer only to those background pulses which are not rejected by the electronics, unless otherwise specified.

3.3.4 Background Prediction Error ΔI_{bc}. Although there is considerable data available to predict the most likely values of the radiation background contributors listed in 3.3.3, there will be some difference between the most probable actual rate and the predicted background rate. This prediction I_{bc} will have a one-sigma statistical uncertainty ΔI_{bc} which is the root of the sum of the squares of the prediction uncertainties for the different sources of background radiation. The background radiation and its prediction uncertainties are calculated in Chapter 7.

3.3.5 Calibration Error Δk. The count rate I_s is related to the measured ambient atmospheric density by $\rho_m = k\ I_s$. Once the calibration constant k has been determined during the pre-launch tests, the atmospheric density ρ_m can be calculated. However, k is subject to error, as follows.

3.3.5.1 Pre-Launch Error Δk_1. When the calibration is being carried out, it will be done in a large evacuated sphere. Past experience indicates that there will be some uncertainty attached to the experimentally determined k. This uncertainty is estimated at ±3%, i.e.,

$$\frac{\Delta k_1}{k} = \pm 0.03$$

where Δk_1 is the error in k resulting from inaccuracies in the pre-launch calibration procedure.

3.3.5.2 Ablation Error Δk_2. The radiation source emits into the Martian atmosphere through a heat shield. If this shield remains in its original condition, allowance can be made for its effect upon both the emitted γ flux and the γ flux returning to the detector. However, the high speed of the vehicle during the entry into the Martian atmosphere will cause part of the shield to ablate, and so the effective source strength will increase. Thus, the calibration constant k will be altered since the count rate I_s rises as the shield ablates even if the atmospheric density remains constant.

If the radiation source is emitting 100 Kev photons, the proposed heat shield (consisting of 2.5 cm of 0.5 gm/cm^3 of Refrasil-like material) will reduce the count rate I_s by $\sim$ 40%. Since it is not possible to accurately predict the rate of ablation during the descent through the Martian atmosphere, it is necessary to add two ablation gages to the conceptual design in order to measure the ablation that occurs in the heat shield over both the source and the detector. These gages are detailed in Chapter 6. Since they are not perfectly accurate, there will remain an additional uncertainty in the heat shield ablation. This uncertainty is represented by:

$$\pm \frac{\Delta k_2}{k}$$

It is estimated at ±2% for the case of a 100 Kev γ ray source.

3.3.5.3 Electronic Error Δk_3. When a γ ray strikes the detector, the net result is an electrical pulse whose magnitude is proportional to the energy deposited in the detector. This pulse, and those due to other radiations, are routed through various electronic subsystems where they are amplified, measured, etc. Since a range of possible operating conditions is expected during the descent to the Martian surface, the electronics may change their mode of operation, or "drift", and produce a change in the density sensor's output even though the input remains constant. Thus, an error Δk_3 is introduced and must be allowed for.

Included in Δk_3 is the effect of the long period of inactivity during the eight-month transit to Mars, with its exposure to space radiations, etc. At the end of this dormant period, the apparatus is turned on and must perform certain simple self-calibrating procedures. Some small error may appear here also.

Since Giannini Controls has had considerable experience in designing high stability miniaturized electronic systems, the electronic drift is not expected to be a serious problem and should not exceed:

$$\frac{\Delta k_3}{k} = \pm 0.03$$

3.3.5.4 Atmospheric Composition Error Δk_4. The technique used to measure the atmospheric density is the Compton scattering of γ rays from the atomic electrons of the atmospheric atoms. As long as these gas atoms all have the same number of electrons per unit mass, the backscatter count rate is constant for a given density regardless of the gases present. This is the case for all three model atmospheres specified in the Contract Work Statement--the specified gases are CO_2 and N_2. Other possible gases, however, are hydrogen (i.e., water vapor) and argon.

In H_2O, the electrons per unit mass ratio is 0.555 (versus 0.500 for N_2 and CO_2). The ratio for argon is 0.45. Therefore, if the Martian atmosphere is pure H_2O or argon, the error in the measured density is:

H_2O	+11%
A	-10%

However, the observations of the Martian atmosphere indicate insignificant amounts of H_2O. Also, the highest suggested argon content is about 30%, which would lead to a -3% error.

Since there is every indication that the MP/L will soft-land an experiment to identify the different gases that are present, the density error due to the atmospheric composition should be less than ±1%. Accordingly,

$$\frac{\Delta k_4}{k} = \pm 0.01$$

is chosen.

3.3.5.5 Coincidence Error Δk_5. When γ rays are detected at random time intervals, some may occur so close together that only one count is registered, and so an error is introduced into the measured density ρ_m. As the count rate rises, this coincidence loss becomes increasingly important, but much of the resulting error can be eliminated by careful testing and calibration of the density sensor prior to leaving earth. In addition, later sections of this report indicate that the expected count rates due to the backscattering of γ rays are such that coincidence losses will be negligible.

However, it is possible that the Martian descent will be carried out in the presence of severe background radiation, e.g., a solar flare. Although the electronic subsystems are designed to reject almost all electronic pulses which are not due to back-scattered γ rays, the presence of many rejected extraneous pulses will keep the electronics busy for part of each one-second counting period and so may cause counts due to γ rays scattered from the atmosphere to be ignored. Since the start of the descent from the Mars orbit is to be chosen by the earth controllers, major solar flares can be avoided, and so the uncertainty Δk_5 in the allowance made for coincidence losses is very small. An error allotment of $\frac{\Delta k_4}{k} = \pm 0.01$ is made. A random error is given because a prediction of the coincidence losses will be made and so the remaining error is random in nature.

3.3.5.6 Resolving Time Error Δk_6. When the density sensor is parachuting slowly through the Martian atmosphere, the ambient atmospheric density during a one-second sampling period is virtually constant, and the backscatter count rate I_s is representative of this density.

Prior to that, the velocity may be quite high (up to 5 km/sec.) and the ambient density may change considerably during a one-second sampling period. Therefore, it will be difficult to know to which radar-indicated altitude the count rate I_s corresponds since the altitude and the ambient density changed considerably during the recording of the I_s counts.

Fortunately, there are two circumstances which reduce the uncertainty that may arise from the foregoing conditions. First, the MP/L enters the atmosphere at the shallow angle of about 20° below the horizontal, and so its vertical velocity is much less than the maximum entry velocity of 5 km/sec. and the ambient density changes at a slower rate than suggested earlier. Secondly, no discontinuities or relatively abrupt changes in atmospheric density are envisioned. Since the mass of the planet Mars is known, the percentage change of the atmospheric density per unit of altitude can be estimated and used to interpret the data.

Detailed estimates of the resolving time error Δk_6 due to the change in the atmospheric density during a one-second sample period are presented in Appendix D. At 25 km, the estimate is that:

$$\frac{\Delta k_6}{k} \leqslant \pm 0.02$$

The error is random because a prediction will be made of the resolving time error, thus leaving only a random residual error. Once the parachute portion of the descent is underway, this error becomes negligible.

3.3.5.7 Summary of Calibration Error Δk. The six contributors to the calibration error Δk have been described in the preceding subsections. They are all random and independent of each other. Therefore, the total calibration error Δk can be expressed as:

$$\frac{\Delta k}{k} = \frac{\sqrt{(\Delta k_1)^2+(\Delta k_2)^2+(\Delta k_3)^2+(\Delta k_4)^2+(\Delta k_5)^2+(\Delta k_6)^2}}{k} \qquad (3.3.5.7\text{-}1)$$

where all symbols have been explained earlier.

The value of $\frac{\Delta k}{k}$ is ± 0.053 at 25 km and ± 0.045 at 5 km. The reduction with decreasing altitude is due to the much lower velocity (thus negligible resolving time error) and the removal of the heat shield (thus no ablation gage error).

3.3.6 Error Summary. As shown in section 3.3.1, the error $\Delta\rho_m$ in the measured atmospheric density ρ_m is given by:

$$\frac{\Delta\rho_m}{\rho_m} = \frac{\Delta k}{k} + \frac{\Delta I_s}{I_s} + \frac{\Delta I_b}{I_s} - \frac{\Delta I_{bc}}{I_s} \qquad (3.3.6\text{-}1)$$

Since all of Δk, ΔI_s, ΔI_b and ΔI_{bc} are random and independent of each other, the system error becomes:

$$\frac{\Delta\rho_m}{\rho_m} = \pm\sqrt{(\frac{\Delta k}{k})^2+(\frac{\Delta I_s}{I_s})^2+(\frac{\Delta I_b}{I_s})^2+(\frac{\Delta I_{bc}}{I_s})^2} \qquad (3.3.6\text{-}2)$$

with all symbols as explained in section 3.3.1.

3.4 Summary of System Response. The preceding subsections of this chapter have examined various aspects of the proposed density sensing system. In most cases, the results are in terms of system parameters which are not specified until later in this report. The significant results are:

(a) System Geometry. Due to the expected sensor location within the MP/L and the likely shock wave configuration, the source and detector are separated by 105 cm to optimize the system response. This arrangement was shown schematically in Figure 3.2.3-1. Using this geometry, the density sensor can be located to one side of the MP/L vehicle nose.

(b) Backscatter Count Rate. The backscatter count rate I_s due to γ rays from the source is given by:

$$I_s = 6.5 \times 10^{-5} I_o \rho_a \mu_{as} A_d \epsilon_d \text{ counts/sec.}$$

where I_o is the source strength (γ's/sec.), ρ_a is the atmospheric density outside the shock wave (gm/cm^3), μ_{as} is the atmospheric scattering coefficient (cm^2/gm), and A_d and ϵ_d are the detector area (cm^2) and efficiency, respectively.

(c) Heat Shield Ablation. To compensate for this, two ablation gages are required to record the ablation of those portions of the heat shield over the source and the detector.

(d) Energy Discrimination. Energy discrimination must be applied to the radiations recorded by the detector in order to eliminate most of the background radiation count rate. The remaining background must then be estimated and subtracted from the total detector count rate.

(e) System Error. This is summarized in section 3.3.6 and prior subsections. It applies to only the 0 to 5 volts DC analog voltage supplied to the telemetry. No errors due to the subsequent telemetering are included.

(f) Telemetry Needs. Every second, the 0-5V DC detector output must be sampled. In addition, the similar outputs of the two ablation gages must also be sampled each second.

In the following chapters of this report, the various components of the conceptual design are presented. The design, which is guided by the guidelines of Chapter 2 and the system response study of this chapter, did not evolve in the order presented in the next chapters. Rather, all parts underwent continual design and redesign as new data became available and their effects on other components were studied. For easier comprehension, however, the design is presented in distinct sections, starting with the source, then the detector, the electronics, and finally the necessary auxiliary systems for gain control and ablation measurement. Once the design is complete, the final error analysis is carried out.

4.0 SOURCE SELECTION

4.1 Introduction and Summary. This chapter selects the radiation source for the conceptual design of the density sensor. First, specific guidelines for the final selection of the source are generated by more carefully examining the design guidelines given in Chapter 2. After applying these, it is decided to use the radioisotope Gadolinium 153 (Gd-153). Further details are then given concerning this source, particularly regarding its availability and physical characteristics. Finally, the mechanical design of the entire source assembly is presented. A summary of the pertinent details of the source and its assembly is presented in Table 4.1-I.

4.2 Source Selection Guidelines

4.2.1 Source Strength. The most important guideline is the source strength necessary to carry out the density measurements. From equation 3.2.3-1, the backscatter count rate I_s is given by:

$$I_s = 6.5 \times 10^{-5} I_o \mu_{as} \rho_a A_d \epsilon_d \qquad (4.2.1\text{-}1)$$

for the case where the source and detector are 105 cm apart and their collimation is as described in Figure 3.2.3-1. I_o is the source strength, μ_{as} is the scattering coefficient of the ambient atmosphere, ρ_a is the density, and A_d and ϵ_d are the detector area and efficiency respectively. By substituting the appropriate μ_{as} and ρ_a values for an altitude of 25 km in the model 3 atmosphere, and using a 5 cm diameter by 1.25 cm thick NaI(Tl) detector, the value of I_s becomes:

TABLE 4.1-I

SOURCE SELECTION SUMMARY

Source: Gd-153

Half-life of 236 days

100 Kev γ rays are 46% abundant after internal conversion

152 and 173 Kev γ rays are each ~ 0.5% abundant

480 curies--1.8 grams of gadolinium metal, now in stock at ORNL

Gadolinium melts at 1275°C

Production: Gd-152 + n in ORNL reactor

~ 210 days of irradiation

Cost:

Target material for irradiation	~$24,000
Reactor Irradiation	~ 7,000
Handling, other costs	~ 4,000
TOTAL	~$35,000 delivered to NASA

Mass: 1070 grams including shield

Radiation Level: 2.5 mrem/hour at 10 cm when delivered to NASA (including flat plate temporary shield over collimator). Put temporary shield of 1.5 cm of lead on outside of MP/L heat shield near location of density sensor source.

$$I_s = 3.17 \times 10^{-10} I_o \qquad (4.2.1\text{-}2)$$

which can be translated into 230 counts/second from a 20 γ curie source of 100 Kev γ rays, where a 1 γ curie source of 100 Kev radiation emits 3.7×10^{10} 100 Kev γ rays/second. The statistical accuracy of 230 cps is ±6.6% for a one-second sampling period. Therefore, a 20 γ curie source of 100 Kev γ rays is used as a guide-line for the descent through the Martian atmosphere. A period of 300 days is presumed to elapse between the delivery of the source by the AEC and the time at which the Mars descent commences.

4.2.2 Reliability and Availability. The selected source must be available in the required strength and must also have a very high probability of successful operation after the stress of the launch environment, the eight-month dormancy during the transit to Mars, and during the rough operating conditions of the descent through the Martian atmosphere. Regarding availability, it is realized that the selected source may not be literally "available" at once. However, there should be no serious doubt about its being ready well before the start of the mission, which may be as early as 1971, but more likely 1973.

Implicit in the term "availability" is the cost of the source. An approximate guideline here is $50,000. This does not necessarily rule out an expensive X-ray tube development program since the additional cost may be justified by the use of the improved tube for other government purposes.

4.2.3 Power Consumption. Since the power available in the MP/L vehicle is quite limited, the design goal for the entire density sensor is 5 watts drawn from the 28 volt battery supply. In addition, the operational period for the density sensor may be as long as 30 minutes, though 15 minutes is more likely.

4.2.4 Volume and Mass. Both the volume and mass available for the source assembly are severely restricted since the respective design goals for the entire density sensor are 1640 cc and 2270 grams respectively.

A γ-radioisotope source assembly consists of the radioisotope, its container, and the necessary shielding.

An X-ray source consists of the X-ray tube, shielding, and a power supply which steps up the 28V DC battery power to the many thousand volt potential required to operate the tube. Depending on the power requirements, this supply may include additional batteries. Finally, if the tube is not operated continuously, there will be electronic control devices to pulse it as required.

If a hybrid source is used, (a β emitting radioisotope plus target), it will hopefully emit no γ rays except those due to its β rays striking the target material. Although an on-off shutter device can vastly reduce the shielding necessary for personnel safety, considerable shielding mass may be required to shield the source from the detector during the density-sensing operation. This depends on the emitted γ ray spectrum. In addition, there is the control mechanism for the on-off shutter.

In any case, the shielding mass will be very important. A 1000 gram source mass guideline is assumed in view of the 2270 gram design goal for the entire density sensor.

4.2.5 γ Ray Energy. The factors which influence the selection of the γ ray energy are identified by following the sequence of events leading from the source to the detector.

First, there is the self-absorption of the source itself. As the emitted γ ray energy decreases, a lower proportion of the photons emitted from the nuclei actually escape. Some of this self-absorption can be reduced by spreading the source material out in a thin flat plate shape, but such a shape is unwieldy and difficult to shield and collimate. Therefore, higher energies are desirable. As a guideline, note that at least 50% of the 60 Kev γ rays from Am-241 undergo self-absorption.

Once the γ rays have emerged from the source material, they must be shielded and collimated so that they reach the detector only by a backscatter in the atmosphere. The effectiveness of shielding is extremely dependent on the energy. Since a source approximately equivalent to at least 20 γ curies of 100 Kev radiation is to be used in a geometry where source and detector are 105 cm apart, and since a source mass guideline of 1000 grams has been set, it is possible to place restrictions upon the γ ray energies allowed for the source. This is done in Appendix E. If a different size and efficiency of detector is used, the source size requirements will change, likely in the upward direction since the suggested detector is already 100% efficient and has an area of 20 cm^2 on its

main face. If a larger detector area is used this increases the photomultiplier tube size considerably and seriously jeopardizes the mass allowance.

As a result of the calculations carried out in Appendix E, the guidelines of Table 4.2.8-I have been generated for the γ ray energy. "Main Emission" refers to the γ ray energy used for the density measurement.

As the progress of the γ rays is followed after they leave the source, no further energy guidelines are generated.

4.2.6 Heat Production. By its very purpose, a radiation source is a producer of energy. This production may be continuous (γ and β radioisotopes) or only upon demand (X-ray tube). However, when heat is produced it must be dissipated before it can harm the density sensor, other apparatus, or the MP/L vehicle itself. Since the density sensor is located within the MP/L vehicle which itself is in a sterile can during the eight-month transit to Mars, any radioisotope onboard should be so limited that its heat production rate is only a couple of watts. Otherwise heat dissipation may become a major engineering problem. In this connection, note that 1000 γ curies (or β curies) of a 100 Kev source produce 0.6 watts.

In the case of the X-ray tube, each milliampere of current at 150,000 volts is roughly equivalent to a 1000 γ curie source of 100 Kev energy. Its heat output is 150 watts; depending on the length of operation, a many watt heat output may be acceptable.

4.2.7 Radiation Safety. The selected source must be such that the radiation doses to personnel meets AEC specifications. In addition, the source should remain intact in the event of a fireball accident on the launch pad. Therefore, any radioisotope that is selected should not have a low melting or boiling point--the higher the better in view of the fireball conditions of:

3500°C for 20 seconds

1500°C for several minutes

4.2.8 Summary of Guidelines. These are presented in Table 4.2.8-I.

4.3 Source Type Selection. In this subsection, the possible use of hybrid, X-ray tube and γ radioisotope sources is considered.

4.3.1 Hybrid. This source is called a hybrid source because it is a cross between a γ radioisotope and an X-ray tube. In it, the electrons from a β emitting radioisotope bombard a target to produce bremsstrahlung as is done in an X-ray tube. The β's are not monoenergetic, but have energies ranging continuously from zero to some maximum. A sample hybrid source γ energy spectrum is shown in Figure 4.3.1-1 and includes the characteristic K X-ray peak.

An advantage of a hybrid source is that the production of the high speed electrons is more reliable than in an X-ray tube. Also, by having a beryllium shutter between the radioisotope and the target, it is possible to turn the bremsstrahlung on and off as desired, unlike the γ radioisotope. From the available literature[4,5,6] it is concluded that the efficiency of these

TABLE 4.2.8-I

SOURCE SELECTION GUIDELINES

Reliability: Operate successfully for 15-30 minutes after eight months in space.

Availability: Definitely available well prior to a 1971 or 1973 launch date. Avoid uncertain development programs.

Cost: Less than $50,000.

Source Strength: Equivalent to about 20 γ curies (7.4×10^{11} γ's/sec.) of 100 Kev radiation. Allow for radioisotope decay during transit. Select a half-life of at least 50 days.

Power Consumption: For more than several watts, additional batteries (mass) required.

Mass: About 1000 grams, including shielding and any auxiliary power supplies and voltage converters.

Heat Production: Only several watts over long periods (months) Indeterminate over short periods (minutes)

γ Ray Energy: Main emission $\geqslant$ 50 Kev

Main emission $\leqslant$ 250 Kev

Additional γ's of: $>$300 Kev, $<$10%
$>$400 Kev, $<$ 3%
$>$700 Kev, $<$ 1%
$>$1000 Kev, $<$ 0.5%

Boiling Point: Well over 1500°C

FIGURE 4.3.1-1

RADIATION SPECTRA

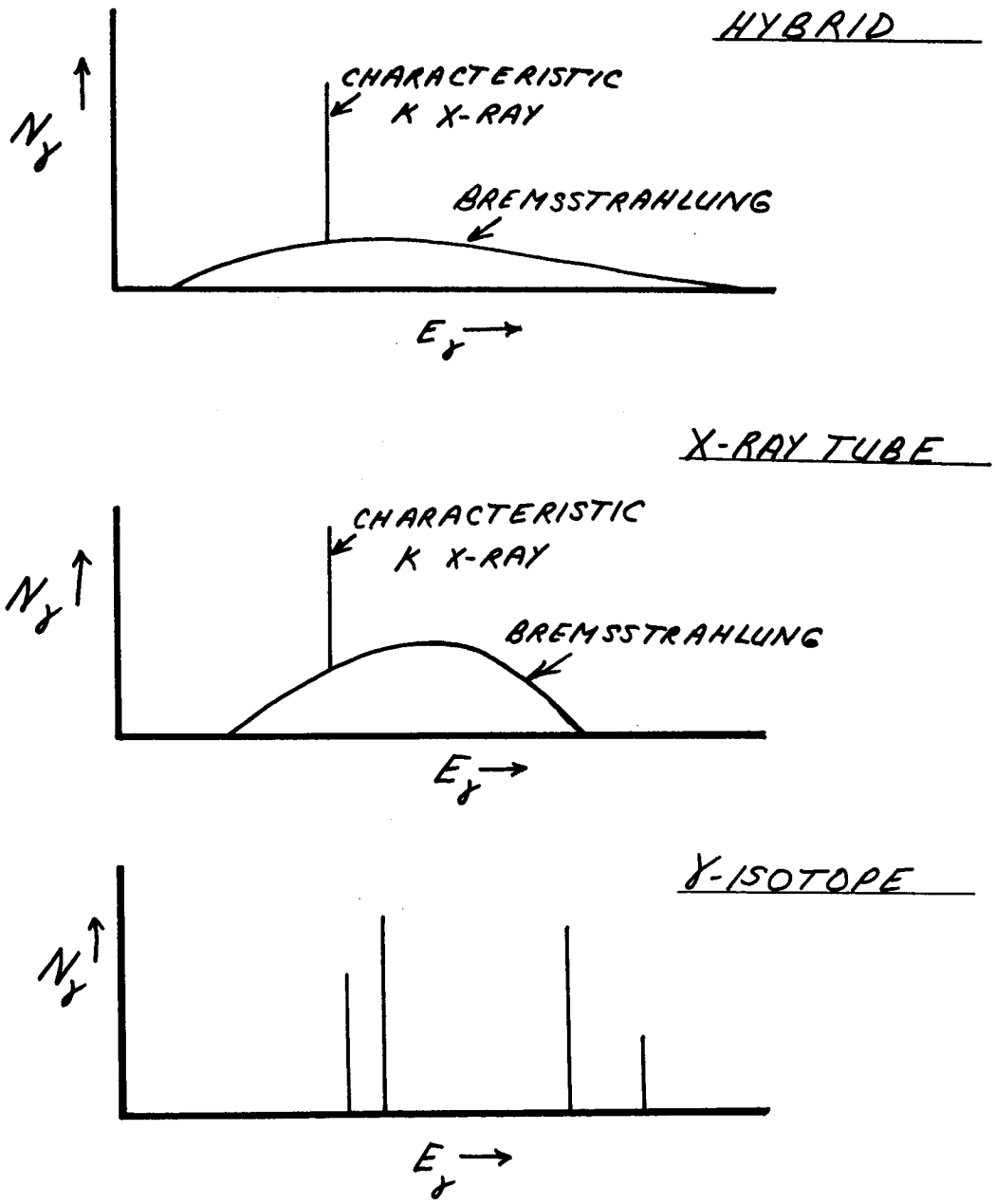

sources (number of γ rays, per β ray) rises with the β ray energy and the atomic number of the target material. Unfortunately, as the β energy rises, so does the energy of the γ rays and the necessary shielding mass. After studying the available spectra[4], it is apparent that the best hybrid source for our purposes would be composed of a β radioisotope, of 1.0 Mev maximum β energy, which is spread thin between 2 thin layers of a high Z material. Lead layers have been used by Starfelt et al[4], but depleted uranium or americium is suggested so as to increase the K X-ray energy to approximately 100 Kev, which is markedly less subject to absorption prior to reaching the Martian atmosphere. Both depleted uranium and americium are radioactive, but americium emits nothing more difficult to shield than 60 Kev γ rays, while the approximately 1 Mev γ rays from the U-238 decay chain are few in number ($\sim 10^4$/gram/sec.) due to the long half-life of the uranium.

Extrapolating from Starfelt's results[4], it is apparent that the type of source suggested above would be $\sim$ 4% efficient; i.e., a 500 β curie source spread and sandwiched appropriately would be equivalent to a 20 γ curie source of 100 Kev radiation. Its heat production, assuming an average β energy of 0.7 Mev, would be 2.1 watts, which is probably acceptable.

However, even if the appropriate β isotope is available (with at least a 100 day half-life and no γ ray emissions of consequence), the resultant source is inferior to a γ radioisotope.

First, the hybrid source has a spreadout energy spectrum due to the bremsstrahlung and so energy discrimination of the detected radiations to reduce the background count rate will result in only part of the spectrum being used, perhaps 50%, thus doubling the source strength. Also, the spread upward of the bremsstrahlung portion of the energy spectrum raises the shielding requirement above that necessary for a γ radioisotope whose emission(s) are concentrated at lower energies.

Next, there is the third disadvantage, namely physical size. Potentially, a 20 γ curie radioisotope source is much more compact than a 500 to 1000 β curie source. Also, the β source has to be spread out between the target layers and the result may be an extremely unwieldy source shape, not to mention a high shielding mass. Finally, the above described source does not have the on-off capability that was mentioned as a potential advantage over a γ isotope. This can still be achieved, but the source strength increases since the target layers will likely be located farther away from the β isotope.

It is therefore concluded that a hybrid source would be more awkward, larger, and harder to shield than a γ radioisotope source. Also, its heat production would be from 2 watts upward, compared to perhaps 0.2 watts for the γ isotope. Despite the possibility of an on-off capability, a γ radioisotope source is definitely preferable and so the hybrid source need not be considered unless there is no suitable γ isotope source.

4.3.2 X-Ray Tube. An X-ray tube source consists of an anode and cathode with a large potential difference between them--about 150 Kv to get a bremsstrahlung spectrum with a maximum intensity at ~100 Kev, see Figure 4.3.1-1. Heating the cathode causes it to emit electrons which are then accelerated to 150 Kv before striking the anode. At the anode, the electron beam produces bremsstrahlung. For a 150 Kv beam of electrons, each milliampere of current is equivalent to about 1000 γ curies of 100 Kev γ rays. Therefore, a 20 γ curie X-ray source requires 3.0 watts of power for the electron beam alone. Stepping up the 28V DC spacecraft power supply to 150 Kv DC will involve a power loss of about 50%, so the beam current alone will draw about 6 watts. Also, about 6 watts are needed to heat the filament, which is the source of electrons. This brings the total source power requirements to 12 watts, compared to zero for the other possible source types.

In addition to a power disadvantage, an X-ray tube source suffers a mass disadvantage. Past experience by Giannini Controls indicates that the mass of the tube and its high voltage power will be about 4000 grams, which exceeds the 2270 gram design goal for the entire density sensor.

If very good radioisotope sources are not available, a 4000 gm X-ray source requiring 12 watts may still be accepted in order that the very important density-sensing experiment can be carried out. However, there is serious doubt about the reliability of the X-ray tube after the eight-month transit to Mars.

It is common practice to re-age X-ray tubes after they have been on the shelf for sometime, and so the tube cannot be expected to operate at its designed voltage until a re-aging period of minutes to perhaps hours has passed. Conversations with manufacturers indicate that this disadvantage may be overcome by a development program, but this is not certain. Also, the program would cost in excess of the $50,000 price tag placed on the source for the mission. Therefore, although an X-ray tube source has a number of potential advantages (for example, a pulsed X-ray system could ignore the radiation background), it is only backup in case no acceptable radioisotope can be found. If the ensuing years prior to the Mars mission result in great improvements in high performance X-ray tubes, it then may be worthwhile to reconsider, particularly if there are radioisotope difficulties.

4.3.3 γ Radioisotope. This source contains energetically unstable nuclei which achieve stability by reducing their excess energy. Though this energy reduction process frequently commences with the emission of an α or β particle, or the nuclear capture of an orbiting electron, somewhere in the sequence of events the nucleus may emit one or more γ rays. These γ rays have certain discrete energies only, and a sample energy spectrum is shown schematically in Figure 4.3.1-1.

As stated in the preceding subsections, a γ radioisotope source has a number of advantages over the hybrid and X-ray tube sources provided it is available and can meet the source selection guidelines previously given in Table 4.2.8-I. Since no appropriate source is immediately available, the entire table of ~1300 nuclides has been examined in detail and a preliminary selection of possible sources has been made. These have been investigated in further detail (generally regarding availability) and the final selection of Gd-153 has been made.

4.4 Preliminary γ Radioisotope Selection. This preliminary selection is carried out using the γ ray energy guidelines of Table 4.2.8-I and a minimum half-life of about 50 days. The results are in Table 4.4-I. Some sources which do not entirely meet the guidelines are included because some other quanlity of them is particularly attractive, e.g., long half-life or low cost.

The information in Table 4.4-I has been obtained from references 7, 8, 9, 11 and 12. The production methods for each isotope are given as Accelerator (proton bombardment of a target), Fission (the isotope results from the fissioning of nuclei in a reactor) and Reactor (neutron capture by a target in a reactor). The γ ray abundancies are usually the percentage of the nuclear disintegrations that result in a γ ray escaping from its source atom; i.e., internal conversion is allowed for. Often, only the abundances of the γ rays relative to each other are known, and so the symbol R appears in the Abundance column to indicate this.

TABLE 4.4-I

PRELIMINARY γ-RADIOISOTOPE SOURCE SELECTION

ISOTOPE	HALF-LIFE	PRODUCTION	E_γ (Kev)	ABUNDANCE
Am-241	458y	Reactor	60	40
Au-195	183d	Accelerator	31	1R
			99	12R
			130	2R
Cd-109	470d	Accelerator Reactor	88	4
Ce-139	140d	Accelerator Reactor	166	100R
Ce-144	285d	Fission	33	
			41	
			53	
			59	
			80	
			95	
			134	98R
			145	
			700	1.5R
			1500	0.3R
			2180	0.8R
Co-57	267d	Accelerator	14	6
			122	88
			136	10
Dy-159	144d	Accelerator Reactor	58	25R
			200	
			290	
			360	

TABLE 4.4-I (Cont'd)

ISOTOPE	HALF-LIFE	PRODUCTION	E_γ (Kev)	ABUNDANCE
Eu-149	106d	Accelerator	256	
			285	
			330	
			582	
Eu-155	1.8y	Accelerator Fission	19	
			27	
			45	
			60	
			87	100R
			105	63R
Gd-151	120d	Accelerator	22	44R
			154	60R
			175	27R
			244	45R
			308	8R
Gd-153	236d	Accelerator Reactor	70	2
			83	<1
			97	21
			103	25
			152	<1
			173	<1
Hg-203	47d	Accelerator Reactor	279	100R
Lu-173	1.3y	Accelerator	79	
			101	
			172	
			273	
Pm-145	18y	Accelerator	67	10R
			73	23R

TABLE 4.4-I (Cont'd)

ISOTOPE	HALF-LIFE	PRODUCTION	E_γ (Kev)	ABUNDANCE
Rh-101	5y	Accelerator	127	
			195	
Sm-145	340d	Accelerator	49	
		Reactor	61	14
Sn-119m	250d	Accelerator	65	100R
		Fission Reactor		
Tc-97m	91d	Accelerator	96	100R
Te-123m	104d	Accelerator	89	100R
		Reactor	159	100R
Tm-170	127d	Accelerator	84	3
		Reactor		
Tm-171	680d	Accelerator	67	2

In all, a total of 21 radioisotopes out of the approximately 1300 known nuclides pass the preliminary selection. Some well-known ones that fail because of the very large shielding mass they require are Ba-133, Co-60, Cs-137, Ir-192, and Se-75. In addition, Re-183 is omitted because its γ ray spectrum of 22 γ rays between 83 and 407 Kev is too complex for practical use. The next subsection further reduces the number of possible isotopes.

4.5 Final γ Radioisotope Selection. The first step in narrowing the selection is to check on the production rate of those radioisotopes available only from the ORNL isotope accelerator. It is soon found that Co-57 has the highest production rate (about 3.5 curies per week), and since the γ ray energies emitted by Co-57 are ideal, it is clear that Co-57 is the best choice if an accelerator produced source is to be used. This eliminates Au-195, Eu-149, Gd-151, Lu-173, Pm-145, Rh-101, Tc-97m and Tm-171, all of which are available from the accelerator alone. When using the production rate as a criterion, the half-lives of the different isotopes are also considered since a low production rate is somewhat offset by the lower rate of source decay during the eight-month transit to Mars.

The 12 remaining radioisotopes available by fission or neutron bombardment in a reactor have been examined with the aid of ORNL personnel. The criteria used are:

(a) Necessary shielding mass due to both γ energy and physical size of source.

(b) Heat production rate during eight-month transit to Mars (particularly important for those isotopes where the γ rays of interest have a low abundance, e.g., Tm-171).

(c) γ Ray Energy - must penetrate the heat shield.

(d) Half-life - assume 300 days from end of source production till Mars descent.

(e) Reactor production rate, including use of enriched targets.

(f) Cost.

It is concluded that Gd-153 is the best reactor-produced source. A comparison with Co-57 indicates that Gd-153 is the best radioisotope to use, and so it has been selected. The following subsection describes Gd-153 in greater detail. The γ rays to be used from Gd-153 have energies of 97 and 103 Kev. In calculations they are treated as having an average energy of 100 Kev.

4.6 Properties of the Gd-153 Source

4.6.1 Production. Gd-153 is produced when Gd-152 captures a thermal (low energy) neutron in a nuclear reactor. The targets which ORNL currently uses to make Gd-153 are composed of:

Gd-152	13.26 ±0.05%
Gd-154	7.0% ±0.05%
Gd-155	23.68% ±0.05%
Gd-156	20.92% ±0.05%
Gd-157	11.63% ±0.05%
Gd-158	14.16% ±0.05%
Gd-160	9.34% ±0.05%
Calcium	0.02% ±0.05%

A spectroscopic analysis of the target material does not indicate any other isotopes present. When the target is subjected to neutron bombardment, the only radioisotope formed in a significant quantity is Gd-153. The cost of the target material is $13 per milligram.

Because Gd-155 and 157 have extremely high thermal neutron capture cross-sections, the first week of irradiation will produce almost no Gd-153. After that week, however, most of the Gd-155 and 157 will have been converted to other stable isotopes (Gd-156 and 158) and the rate of conversion of the Gd-152 to Gd-153 will be approximately 1% per day of the remaining Gd-152. To achieve the rapid removal of the Gd-155 and 157, it is necessary to use thin (0.2 gm/cm^2) gadolinium target foils. These will be neutron "sinks" at first and must be arranged so that they do not "shadow" each other and thus reduce the effect thermal neutron flux on each other. During the first week in the assumed $10^{15} n/cm^2/sec.$ flux, less than 1% of the thermal neutrons striking the targets will pass through without being captured.

If the neutron flux depression caused by all the foils is too much of a load for the reactor (particularly the ORNL reactor), it will be necessary to irradiate each foil separately for about a week in order to convert nearly all the Gd-155 and 157. After a maximum of two weeks separate irradiation, all the foils can be irradiated together in the same reactor.

4.6.2 Source Strength Delivered from ORNL. Earlier in this report, it was calculated that the source strength should be equivalent to 20 γ curies of 100 Kev radiation during the descent through the Martian atmosphere. These calculations were simple in nature because only an approximate guideline was needed--the source had not been chosen, and relatively little was known about the MP/L vehicle structure. With the source now chosen, detailed calculations are necessary to estimate the source strength actually required. As before a γ curie emits 3.7×10^{10} γ rays per second of a specified energy.

4.6.2.1 Fireball Protection. An estimate of the conditions if there is a fireball accident on the launch pad is:

3500°C for 20 seconds

1500°C for several minutes

The tantalum shielding around most of the source has a melting point of 2996°C and so will survive without difficulty, but gadolinium metal melts at 1250°C and its compounds generally melt at lower temperatures (e.g., $GdCl_3$ at 609°C). Therefore, it is necessary to protect the source from the heat that enters through the collimator opening. This protection should be sufficient to contain

a molten source and also sufficient to prevent vaporization during the initial 3500°C period. To do this, a sandwich of 0.25 mm titanium plus 6.5 mm of ablation material (0.5 gm/cc) plus 0.13 mm of tantalum has been chosen. The outer titanium sheet (.125 mm) is only for structural strength during assembly, etc., and will be destroyed in the initial heat since its melting point is 1725°C. However, the ablator will then take over the source protection and will outlast the initial 20 second hot period. During the longer 1500°C period that follows, the ablator may disappear, but the inner titanium layer will not melt and so the source will be protected.

However, this titanium plus ablator sandwich will reduce the γ ray flux, so the source size should be increased by a factor of 1.09 to compensate.

4.6.2.2 Detector Casing. As the γ rays pass through the mechanical container of the NaI(Tl) crystal, some are scattered and rendered useless for counting as part of the atmosphere back-scatter. An aluminum detector casing (on the face) of 0.75 mm is assumed and the source must be increased by a factor of 1.05 to compensate.

4.6.2.3 Collimation Effects. Previously, a point source was assumed when calculating the proportion of the γ rays escaping through the collimator opening, but this is no longer the case.

The combined collimation efficiency of the conceptual design of the source and detector is only 1/3 as great as that originally calculated for the point source and detector. Therefore, a factor of 3.0 has been introduced to compensate for these collimation effects.

4.6.2.4 Time Decay. During the assumed 300 days between the delivery of the source and its descent through the Martian atmosphere, it will decay with a half-life of 236 days. Thus, the original source strength must be increased by a factor of 2.42 as compensation.

4.6.2.5 Self-Absorption. γ rays which have emerged from one source atom may interact with another source atom prior to emerging from the source as a whole. It has been decided to fabricate the source from pieces of 0.2 gm/cm^2 gadolinium metal, and so the aforementioned self-absorption requires an increase in the source strength by a factor of 1.33.

4.6.2.6 Source Strength Summary. The source strength at delivery from Oak Ridge must be:

$$20 \times 1.09 \times 1.05 \times 3.0 \times 2.42 \times 1.33 = 220 \ \gamma \text{ curies}$$

Since the actual abundance of the approximately 100 Kev γ rays is 46%[12] after allowance for losses due to internal conversion, the source that is ordered will be:

$$220/0.46 = 480 \text{ curies}$$

The design and fabrication of the source are described next.

4.7 Design and Fabrication

4.7.1 Physical Size and Cost. If the target material, containing 13.26% Gd-152, could be placed in a very, very high neutron flux, it could not achieve a greater concentration, i.e., specific activity, than 483 curies/gram. In practice, the specific activity will be less since the source will decay somewhat while it is being irradiated.

Assuming that the source is being fabricated on either the newest ORNL reactor or in the Savannah River Reactors during their high flux mode of operation, a minimum thermal neutron flux of $10^{15}/cm^2/sec$. can be assumed. From this, a specific activity of approximately 310 curies per gram can be obtained by careful selection of the irradiation period and assuming the minimum listed thermal neutron capture cross-section of 120 barns for Gd-152. However, to allow for irradiation delays and interruptions due to the servicing of the reactor, a lower specific activity of 270 curies/gram is assumed.

Thus, the isotope mass required will be 480/270 = 1.8 grams, at a cost of $1.8 \times 13 \times 10^3 \doteq \$23,400$ for the target material.

Prior to irradiation, the gadolinium foil will be cut into 6 pieces of 6.3 mm (1/4 inch) by 25 mm (1 inch) by a thickness of $0.2\ gm/cm^2$--the exact physical thickness will depend on the gadolinium compound selected. Since the standard ORNL irradiation capsules are a little more than 6.4 mm I.D. by $\gtrsim$51 mm long, it will be possible to place 2 of these foils end to end in the same capsule. Including the preliminary irradiations to eliminate the

Gd-155 and 157, plus interruptions to service the reactor, the total irradiation time per capsule should not exceed 210 days (30 weeks) at a cost of $75/week, thus bringing the total irradiation cost to 30 x 75 x 3 = $6,750. In practice, a higher neutron flux may be available and it may be possible to irradiate all six foils in the same capsule once the Gd-155 and 157 has been removed. Either of these happenings would considerably reduce the total irradiation cost, but they are not assumed here.

Therefore, the total source cost will be (23,400) + (6750) + handling and machining (particularly of the shielding). This is estimated to total approximately $35,000 delivered to NASA.

4.7.2 Gamma Ray Spectrum. The latest data indicate the following spectrum[10]:

E_γ (Kev)	Transition Strength	Emitted Strength
54	$\ll 0.1$	
68	$\ll 0.04$	
70	8.1	2%
75	0.26	
83	0.70	
89	0.23	
97	100	21%
103	73	25%
152	< 0.6	
173	< 0.6	

The second column in the above table shows the relative possibility that the different transitions of the first column will occur in a Gd-153 nucleus. After losses to internal conversion have been included, the emitted strengths of column 3 are found; i.e., the 97 and 103 Kev γ's have a total abundance of 46%--46 of them escape from Gd-153 atoms for each 100 Gd-153 decays.

4.7.3 Source and Shield Construction. The source-shield configuration is shown in Figure 4.7.3-1. Its total mass is 1070 grams, including the fireball protection sandwich. It is assembled as follows. The thickness of the shielding and its shape are determined in Appendix F.

First, all parts are machined and precision fitted together before irradiation of the gadolinium foils. After the foil irradiation, the assembly process is carried out by remote control since the source strength is approximately 220 γ curies. The 6 pieces of 25 mm by 6.3 mm foil are placed side by side in the indentation prepared for them in the tantalum shield base. They form a rectangle of 25 mm by 38 mm. The fireball shield is then placed over the foils; its bent edges of 0.25 mm titanium make its positioning a relatively simple matter. Next, each of the four sides of the shield are fastened on by screws, and so hold the fireball shield in place (this shield should be made somewhat too thick so that it is compressed as the shield sides are screwed on). After a temporary shield consisting of $\lesssim$1 cm of tantalum (or 1.5 cm of lead) in the form of a flat plate is placed over the collimator opening, the source assembly can be removed from the remote assembly installation and sent to NASA in a standard container.

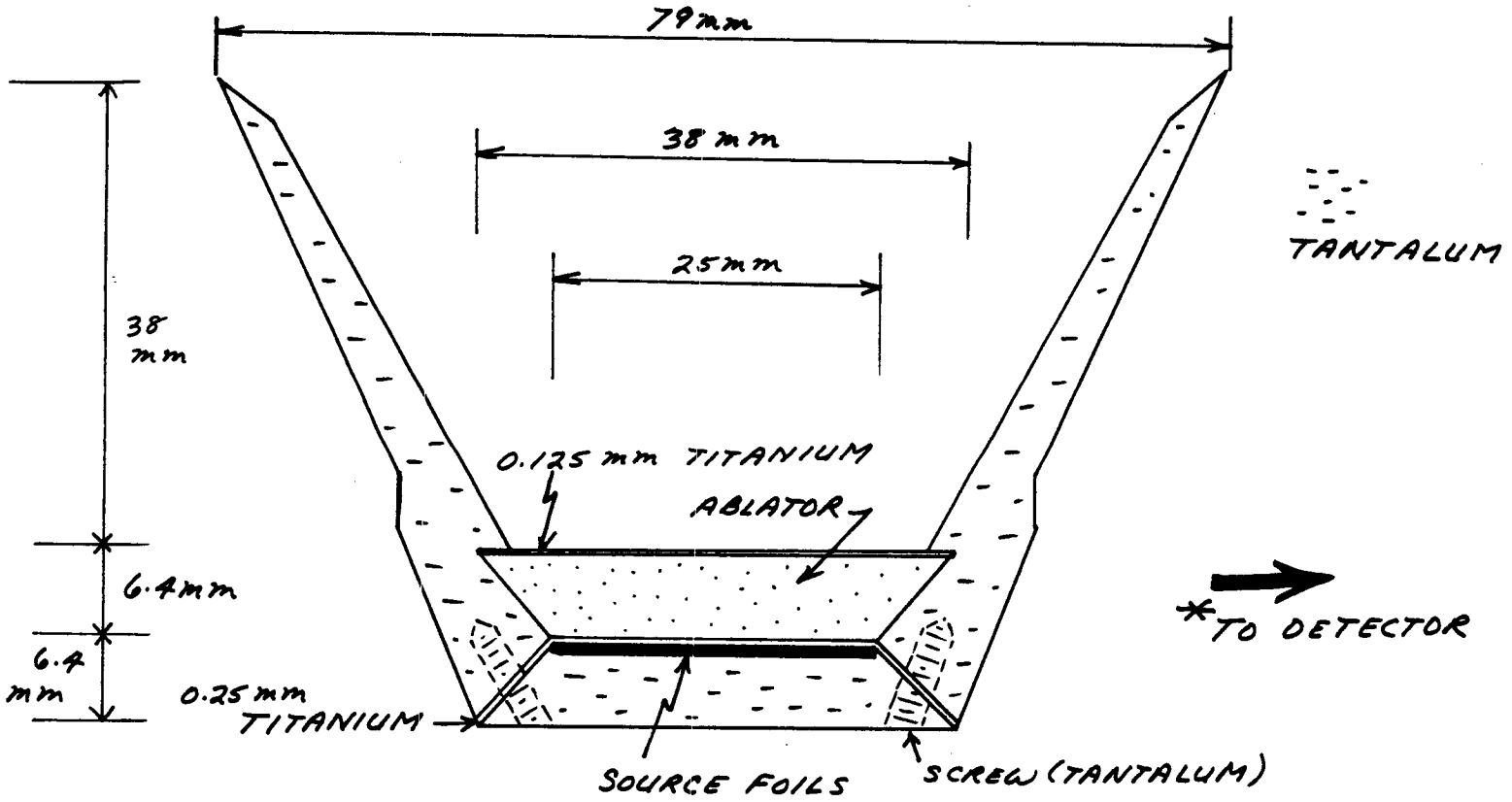

FIG. 4.7.3-1
CONT'D

SOURCE & SHIELD CONSTRUCTION*

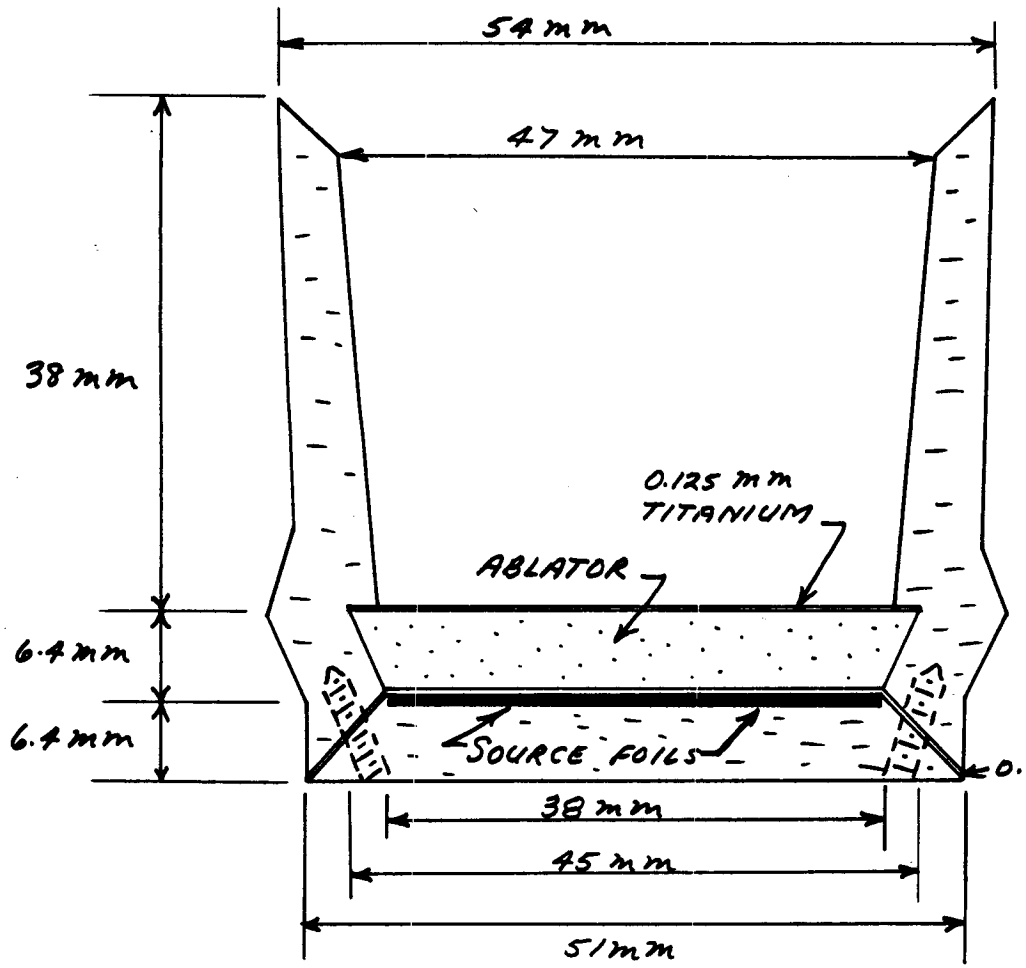

SOURCE & SHIELD CONSTRUCTION*

*VIEW FROM MAIN DETECTOR

TANTALUM

FIG. 4.7.3-1 CONT'D

4.7.4 Radiation Levels. At one meter from the original source (unshielded) the dose rate will be approximately 11 rem/hour; hence the need for remote assembly. However, once the source is in its shield (which has an effective thickness of at least 6.3 mm in all directions, including the flat plate temporarily placed over the collimator), the dose rate at a meter will be approximately .025 mrem/hour. At 10 cm, the dose will not exceed 2.5 mrem/hour.

The foregoing dose rates are maximum estimates since the actual shielding is thicker than 6.3 mm in most directions. Once the source has been placed inside the MP/L vehicle, a 1.5 cm lead shield should be hung over the outside of the vehicle at that point where the collimated γ rays strike the heat shield. Then there should be no need for a controlled radiation area around the vehicle.

5.0 MAIN DETECTION SYSTEM

5.1 Introduction and Summary. The purpose of this system is to detect those γ rays which have undergone a single scatter in the Martian atmosphere after having been emitted by the main radiation source. At the same time, the system must be designed to discriminate against radiations other than the backscattered γ rays.

This chapter outlines the guidelines for choosing the detector and applies them to the various possible detectors. A 5 cm diameter by 1.25 cm thick NaI(Tl) crystal is then chosen. The light pulses produced in this scintillator are converted into electrical pulses and amplified by a photomultiplier tube. Further signal conditioning is carried out to minimize the effects of background radiation, and the final output from the detection system is a 0 to 5 volt DC signal.

To compensate for the range of possible environments in which the detector may have to operate, a secondary system called an Automatic Gain Control (AGC) is used; it requires a very small radioactive source for calibration purposes. The important mechanical and electronic details of the complete detection system are presented in this chapter. The total power required is 3.0 watts drawn from the 28V DC MP/L power supply; the detector and its supporting electronics total 1657 gm.

Note that the ablation gage subsystems (whose need is made clear in Chapter 3) are treated separately in Chapter 6.

5.2 Detector Selection Criteria. The general system guidelines of Chapter 2 apply to the detection system, namely reliability, availability, mass, power and volume, of which reliability is the most important. Included under the category of reliability are the effects of sterilization and the launch environment, the hard vacuum and radiation of space, temperature and supply voltage variations, etc. In addition, certain other criteria apply specifically to the detector. These are efficiency, effective area of exposure, energy resolution, and saturation at high count rates; they are discussed in greater detail in the following subsections.

5.2.1 Efficiency and Area of Exposure. As indicated in the previous chapter, the system operates with acceptable accuracy when using a source equivalent to about 90 γ curies of 100 Kev radiation and a detector having the detection capability of 20 cm^2 of 100% efficiency. If either the area or the efficiency is decreased, the source strength must be correspondingly increased so that the product of source strength (γ curies), detector area (cm^2), and efficiency (100% = 1.0) is kept at 60 x 20 x 1 = 1200.

5.2.2 Energy Resolution. Since primary γ rays from the source, which undergo a single backscatter in the Martian atmosphere prior to being detected, have energies within a limited and well-defined range, it is possible to largely exclude the counts due to background radiations of other energies. The effectiveness of this exclusion is very strongly dependent upon the energy resolution capability of the detector. The narrower the range of the voltage pulse heights corresponding to the absorption of a given amount of

radiation energy, the better the energy resolution and hence the better the rejection of background radiation of energies other than those corresponding to backscatter γ rays.

In view of the possible intensity of the background radiation expected during the descent through the Martian atmosphere, this energy resolution capability is very important.

5.2.3 Count Rate Saturation. Every time an incident radiation is detected, a finite time is required before the detector returns to its original condition. If another radiation should reach the detector during this finite "recovery" time, the detector may apparently add the second radiation to the first and so its output is not an accurate indication of the incident radiation flux. This effect is reduced as the recovery time decreases.

As regards the backscatter count rate, this will not exceed 10,000 cps unless the Martian atmosphere is denser than even the densest of the 3 model atmospheres specified in the Contract Work Statement--very unlikely in view of the Mariner 4 data. However, there is the possibility of a small solar flare during the Martian descent despite the selection of the descent time by the earth controllers. In that case, radiation fluxes of a thousand counts/sec./cm^2 may penetrate the MP/L walls and reach the detector. Therefore, it is desirable to minimize the detector area to avoid saturation.

5.3 Selection of the Detector. The four types of detectors that are considered are solid state detectors, proportional counters, plastic scintillation counters, and NaI(Tl) scintillators. These are examined in the following paragraphs.

5.3.1 Solid State Detectors. The lithium drift detectors in present use are unable to withstand the sterilization temperature of 145°C and so need not be considered further. However, Technical Measurement Corporation of Palo Alto, California, is currently manufacturing a solid state detector tested to withstand all the specified mechanical and temperature environments. Its efficiency for the detection of approximately 80 Kev γ rays is $\lesssim 3\%$ at best, and no marked improvement is expected by the manufacturer. Therefore, some 600 cm^2 of detector area would be necessary to maintain the required count rate without increasing the source strength and cost. Although some compactness might be obtained by stacking the detectors, this low efficiency is a very strong deterrent to their use. In addition, the solar flare and cosmic ray particles striking the detectors during the eight-month transit may cause a serious deterioration in their performance. This is not certain due to insufficient data regarding the structure of the MP/L and the bus carrying it to Mars. However, preliminary calculations indicate that the dose rate would be on the verge of causing significant damage.

Therefore, solid state detectors are rejected because of their very low efficiency and their possible susceptibility to radiation damage.

5.3.2 Proportional Counters. These are more efficient than solid state detectors and an efficiency of 20% or better for 72-84 Kev γ rays could possibly be obtained by the use of high pressure xenon gas in the counter. However, the energy resolution is perhaps 40% at 80 Kev and so energy discrimination is difficult. Accordingly, proportional counters are rated low because of their poor efficiency and energy resolution.

5.3.3 Plastic Scintillator. A scintillator made of plastic alone has an efficiency of approximately 10% for a 1 cm thickness, but the addition of a 15% lead by weight raises the efficiency to 20% or better. Unfortunately, the energy resolution is as poor as for a proportional counter and there is some question as to the ability of the detector to withstand sterilization.

Therefore, plastic scintillators are rated low.

5.3.4 Sodium Iodide. This has the best energy resolution and efficiency of all the detectors. Furthermore, rocket flights have been carried out by NASA-LRC using a 10 cm diameter by 2.5 cm thick NaI(Tl) crystal as the detector for atmospheric density measurements using the γ ray backscatter technique. Although a more severe mechanical environment is possible for the MP/L, a 5 cm by 1.25 cm crystal is expected to be sufficiently strong. Regarding sterilization, NaI(Tl) may crack under severe thermal shock, but an hour spent raising the MP/L to sterilization temperatures is quite long enough to completely avoid this possibility. Finally, NaI(Tl) can handle 100,000 cps, and this is more than sufficient for a 20 cm^2 detector.

Therefore, NaI(Tl) is chosen for its efficiency and energy resolution, plus the fact that it is already in use in similar experiments within the earth's atmosphere. The next part of this chapter describes the selected detection system.

5.4 Outline of the Detection System. A schematic block diagram of the system is shown in Figure 5.4-1. Its operation can be described as follows.

First, radiation interacts with the NaI(Tl) crystal and produces a flash of light (scintillation) whose magnitude is proportional to the energy deposited in the crystal. The light photons comprising the scintillation spread throughout the crystal and some reach the end of the photomultiplier tube that is optically coupled to the scintillator. This end of the tube is the photocathode, and the light photons expel a number of electrons from it. These are then accelerated through several hundred volts to the next "stage" of the tube where their newly acquired kinetic energy is sufficient to expel an increased number of electrons. This process of electron multiplication continues through many stages and results in an electrical output pulse whose magnitude is nearly proportional to the radiation energy deposited in the detector. Due to statistical processes in the detection system, there is a narrow range of possible pulse magnitudes corresponding to a particular energy, and the width of this range (divided by its average magnitude) is the energy resolution of the system.

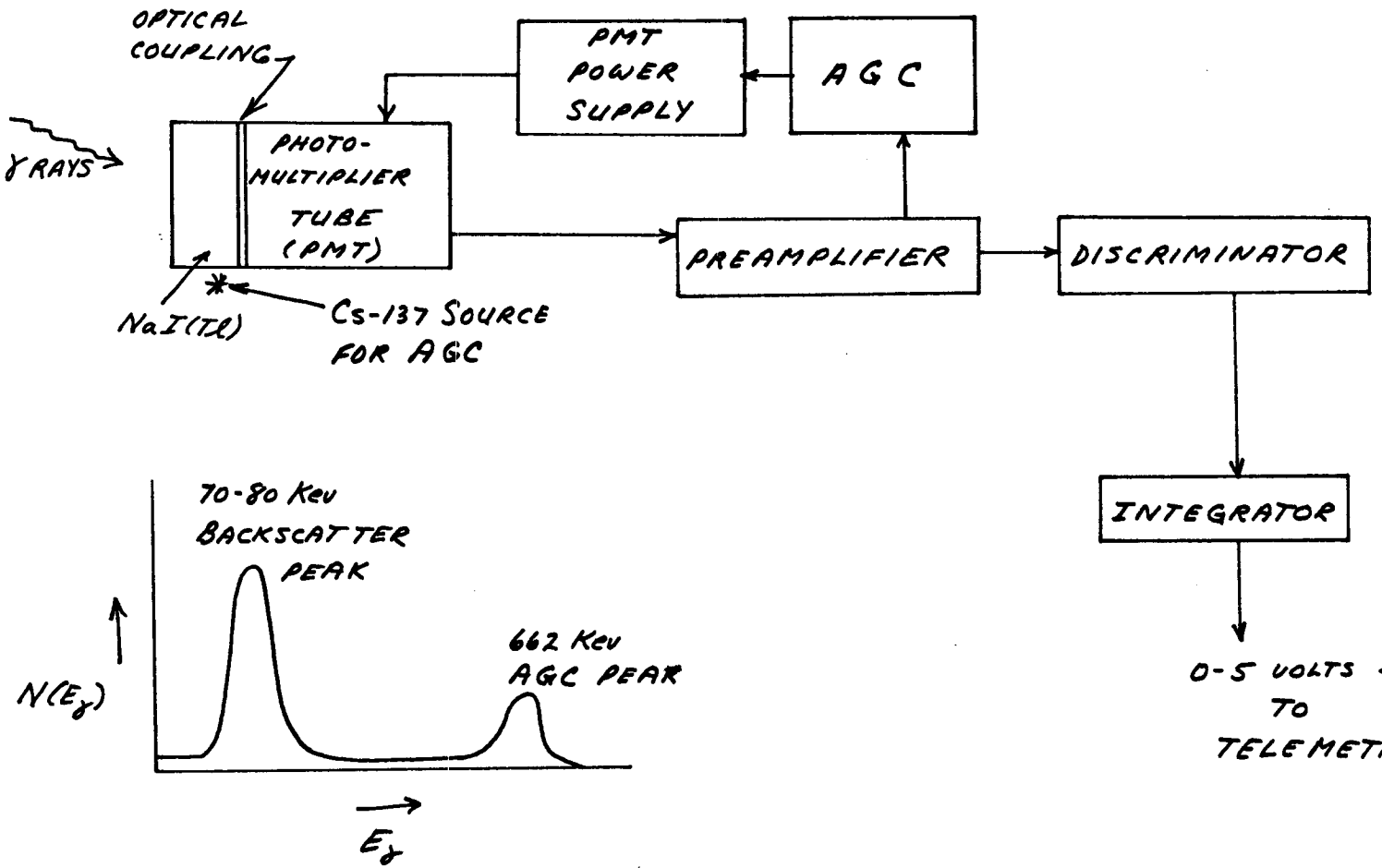

DETECTION SYSTEM SCHEMATIC FIG. 5.4-1

After leaving the photomultiplier tube, the electrical pulses are further amplified in a preamplifier and then sent to both the AGC circuitry and the remainder of the processing electronics. Consider these latter first. The preamplifier pulses enter the discriminator which measures their amplitude. Whenever a pulse within a certain preset amplitude range arises, the discriminator emits a pulse of standard size and shape. Since the preset amplitude range corresponds to the range of γ ray energies expected for singly backscattered source γ rays, the discriminator effectively rejects most counts due to other radiation sources, though of course it cannot reject background radiations whose energies lie within or very near to the range of γ backscatter energies.

From the discriminator, the standard pulses pass to an integrator where the count rate is converted into a 0-5 volt DC level suitable for telemetry. This is the end point of the conceptual design of the density sensor, except for the following backtrack to describe the AGC subsystem.

As described earlier, all electrical pulses from the preamplifier go to the AGC circuitry as well as to the processing electronics. The purpose of the AGC is, as its name applies, to keep constant the gain of the forepart of the detection system (i.e., NaI(Tl) crystal, photomultiplier tube, and preamplifier). Since the gain of both the scintillator and the PM tube varies significantly over the operating temperature range specified for the Martian descent, there is a need to correct for this "drift".

Otherwise, the pulses reaching the discriminator will have amplitudes which depend on the operating temperature, and so the number of pulses lying within the preset amplitude range of the discriminator will also vary independently of the backscatter count rate. A serious error in the count rate from the discriminator could result.

To compensate, a small source of Cs-137 is placed beside the scintillator, as shown in Figure 5.4-1. It emits γ rays of 662 Kev energy only. When these are detected, the output pulse height spectrum from the preamplifier is as shown lower in the same figure. Since the count rate within the 662 Kev peak of the energy spectrum remains constant (statistically) despite variations with ambient density, it can be used as a reference to maintain the system gain. As long as the count rate within the electrical pulse height range corresponding to the 662 Kev peak is kept constant, the system gain is constant also.

To achieve this, the pulses entering the AGC subsystem are routed to a discriminator which emits a standard pulse whenever a pulse corresponding to the 662 Kev energy range arrives. These standard pulses then enter a comparator unit. Provided that the system gain is constant, the count rate of these standard pulses remains constant (within statistical fluctuations). However, a system gain change alters the count rate. Depending on how the count rate changes, the comparator adjusts the high voltage supplied to the photomultiplier tube so as to return the system gain to the desired level.

This AGC applies to only the forepart of the detection system because the remainder of the processing electronics is much less sensitive to changes in the operating conditions. The AGC is also useful in compensating for voltage fluctuations in the power supplied by the MP/L batteries, although other voltage regulating devices in the system power supplies virtually eliminate such voltage fluctuations.

5.5 Detailed System Design. A more detailed description of the conceptual electronic and mechanical design of the various portions of the detection system follows.

5.5.1 Scintillator, Photomultiplier Tube, and High Voltage Power Supply. The NaI(Tl) scintillator and part of the photomultiplier tube are shown in Figure 5.5.1-1. The shielding around the crystal is tantalum and it collimates the detector to prevent the entry of γ rays from the source which have been scattered in either the shock wave or parts of the heat shield not in front of the detector. Although this shielding is relatively thin, it attenuates 100 Kev γ rays by a factor of ~100, and therefore is quite adequate for collimation. The aluminum container of the NaI(Tl) is standard and need not be discussed. The bottom of this container is transparent (often glass) so that the light scintillations within the crystal can reach the photomultiplier tube. Regarding this transfer of light photons, it is necessary to use some optical coupling which is capable of withstanding the 145°C sterilization temperature without deterioration. One method is to omit the grease commonly used for coupling and just fit the

SCHEMATIC OF SCINTILLATOR AND PHOTOMULTIPLIER TUBE*

FIG. 5.5.1-1

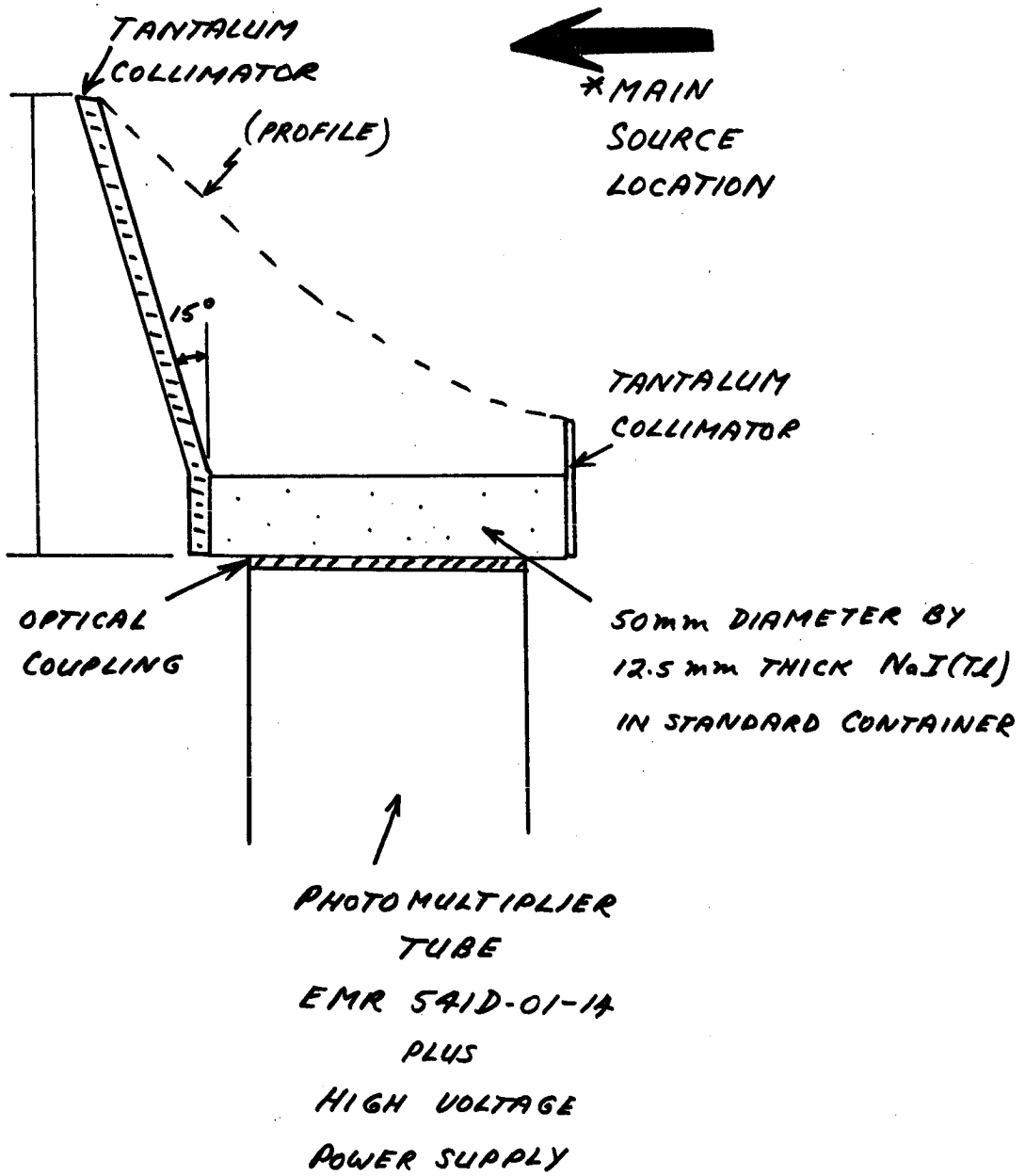

crystal and tube faces flush against each other after being most careful to get the respective faces as smooth and flat as possible.

The NaI(Tl) crystal is of standard composition and is 5 cm in diameter by 1.25 cm thick. The photomultiplier tube selected is the EMR Model 541D-01-14, which is a 14-stage end-on-window tube with a one-inch diameter, semi-transparent bi-alkali photocathode. This rugged tube is sensitive to light in the visible spectrum with peak sensitivity in the blue region. It is useful for low-light-level detection and scintillation counting. It has a typical quantum efficiency of 6% at 4100Å, and a typical room temperature anode dark current of 2×10^{-11} amperes at a multiplier gain of 10^6. Using a unique design of venetian-blind dynodes and hard-glass Kovar ring construction in an encapsulated package, the tube is capable of withstanding 100g shocks of 11 millisecond duration and operating temperature of +150°C. In the configuration selected, the high voltage power supply is packaged around the dynode rings and encapsulated into a single rugged unit whose overall dimensions are 3.8 cm diameter by 13.7 cm long. Co-Netic shielding surrounds the tube to eliminate effects of magnetic and electrostatic fields on the tube sensitivity and gain.

The photomultiplier tube power supply is packaged integrally with the photomultiplier tube. It provides voltage and current to the individual tube dynodes and is a proprietary design of Pulse Engineering of Palo Alto, California, built to Giannini specification. The power input is 18 milliamperes at 28 volts DC.

A voltage control input is also provided at a nominal +1.7 volts DC with a full range variation of ±0.5 volts DC. This provides a detector sensitivity control of three times nominal to one-third of nominal.

5.5.2 Processing Electronics and Power Supply. These include the preamplifier, the discriminator, and the integrator. All elements are assembled and packaged to withstand the specified environments. The preamplifier schematic is illustrated in Figure 5.5.2-1. It consists of a high gain DC amplifier μA702 with appropriate input impedance and feedback resistance. The emitter follower is necessary to minimize the instability due to inter-stage loading effects.

The window discriminator, illustrated in Figure 5.5.2-2 is used to select pulses in a specific region of pulse height and reject all others. It consists of two integrated level detectors (μA710). Appropriate delay and pulse reformation circuitry (SE-160) and a Nand Gate (DTL 932) provide the anticoincidence necessary to obtain the window.

Figure 5.5.2-3 illustrates the integrator schematic. It consists of a high gain DC amplifier μA702 with appropriate input and feedback impedance. Temperature compensation circuitry is necessary to correct for the zero drift of 5 μV/°C of the μA702 operational amplifier. The DC voltage output of the integrator feeds directly to the telemetry.

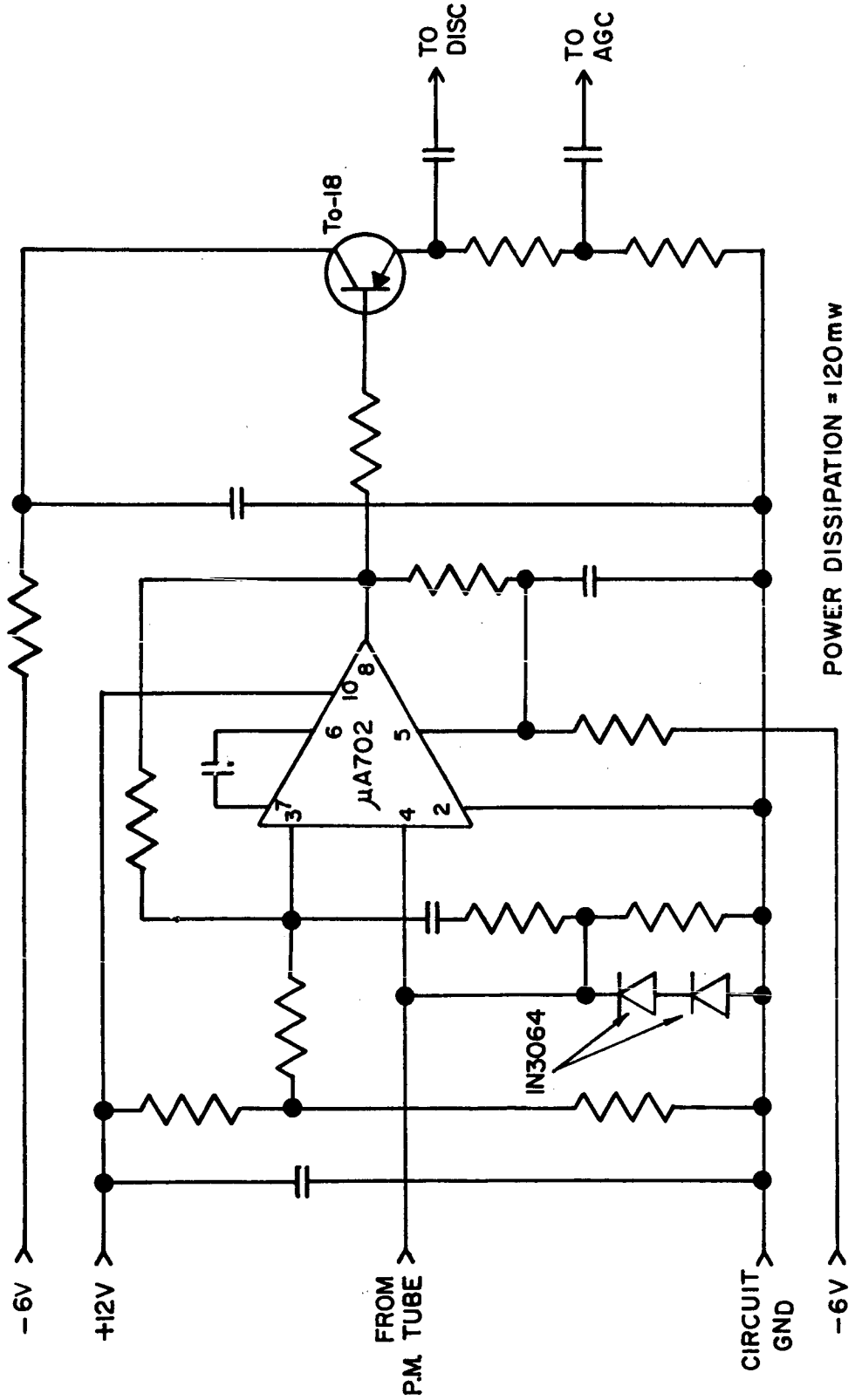

FIGURE 5.5.2-1 - SCHEMATIC OF PREAMPLIFIER

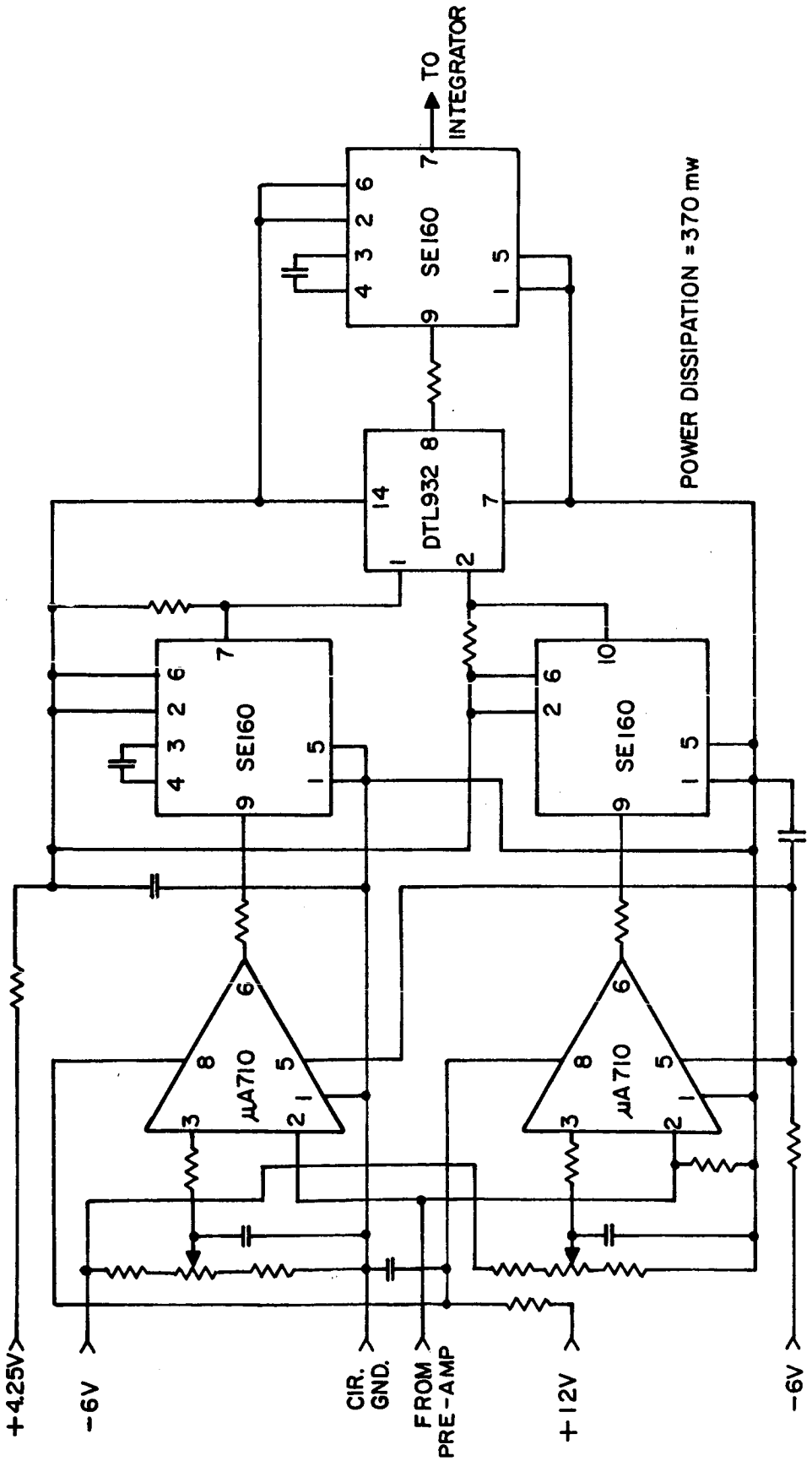

FIGURE 5.5.2-2 - SCHEMATIC OF DISCRIMINATOR

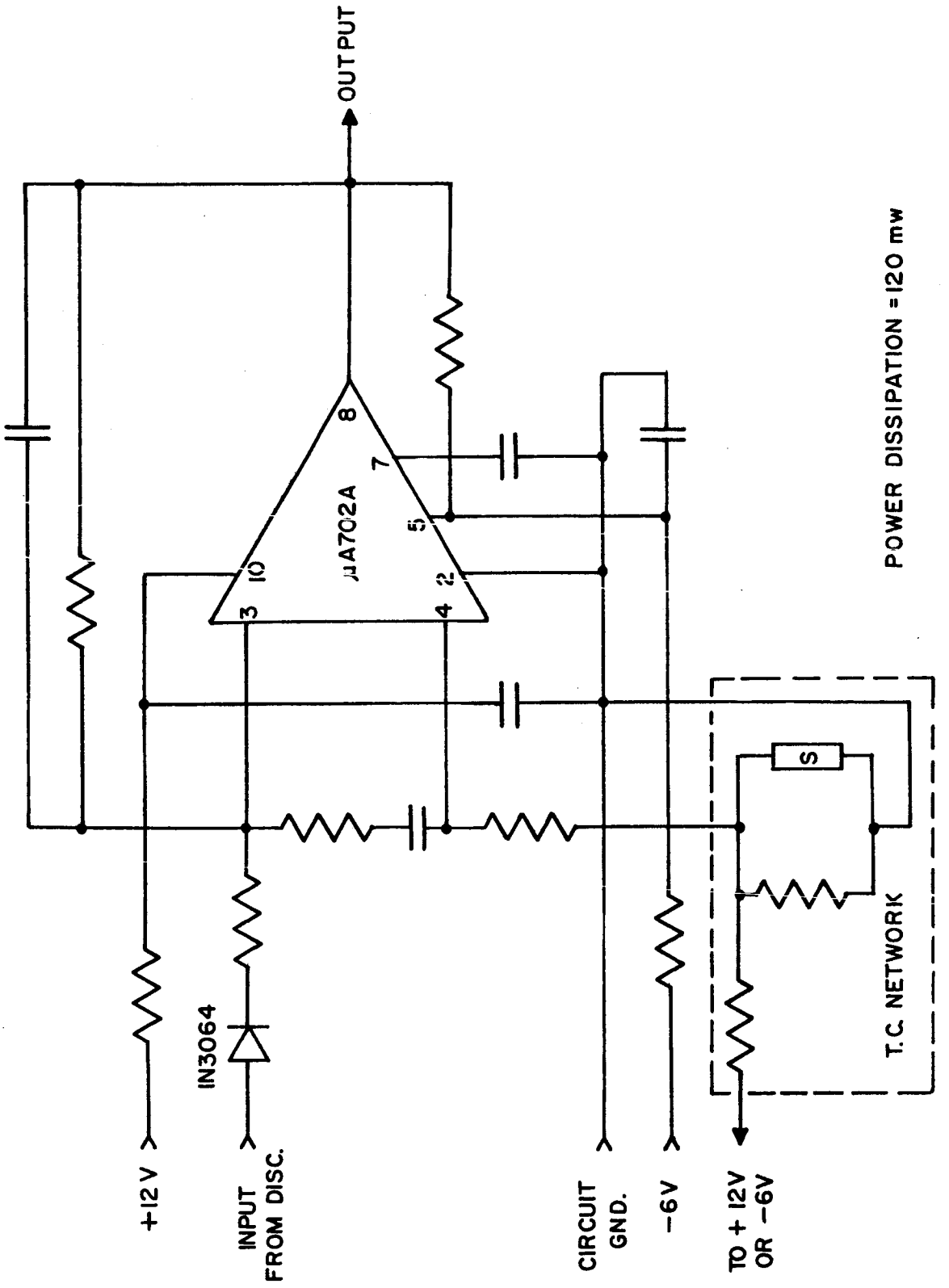

FIGURE 5.5.2-3 - SCHEMATIC OF INTEGRATOR

The regulated power supply is of the conventional design shown in Figure 5.5.2-4. The input is 24-32 volts DC and the outputs are shown for the various system elements. High voltage is also supplied from here to the proportional counter of each ablation gage, but details of this part of the power supply are presented in Chapter 6.

5.5.3 Automatic Gain Control (AGC). The source chosen for the AGC is Cs-137, which emits only 662 Kev γ rays and has a half-life of 30 years. With the source placed next to the side of the 5 cm diameter NaI(Tl) crystal, about one-tenth of all its emitted γ rays are totally absorbed in the detector, while about two-tenths will leave part of their energy therein. A source strength of 0.06 microcuries has been selected to give a total absorption count rate of approximately 200 cps. With a time constant of 10-15 seconds, the AGC will maintain the detector gain to better than ±2%. This long time constant (i.e., reaction time) is permissible because of the following anticipated operating conditions.

First, it will be switched on several minutes prior to entering the significant portion of the Martian atmosphere and so a 10-15 second time constant will be fast enough to stabilize the system. Next, as the MP/L decelerates in the atmosphere, the heat shield will ablate but the temperature rise within the density sensor will be moderate as well as slow. Hence the 10-15 second time constant.

No special safety precautions need be taken with such a minute source strength. No AEC license is required.

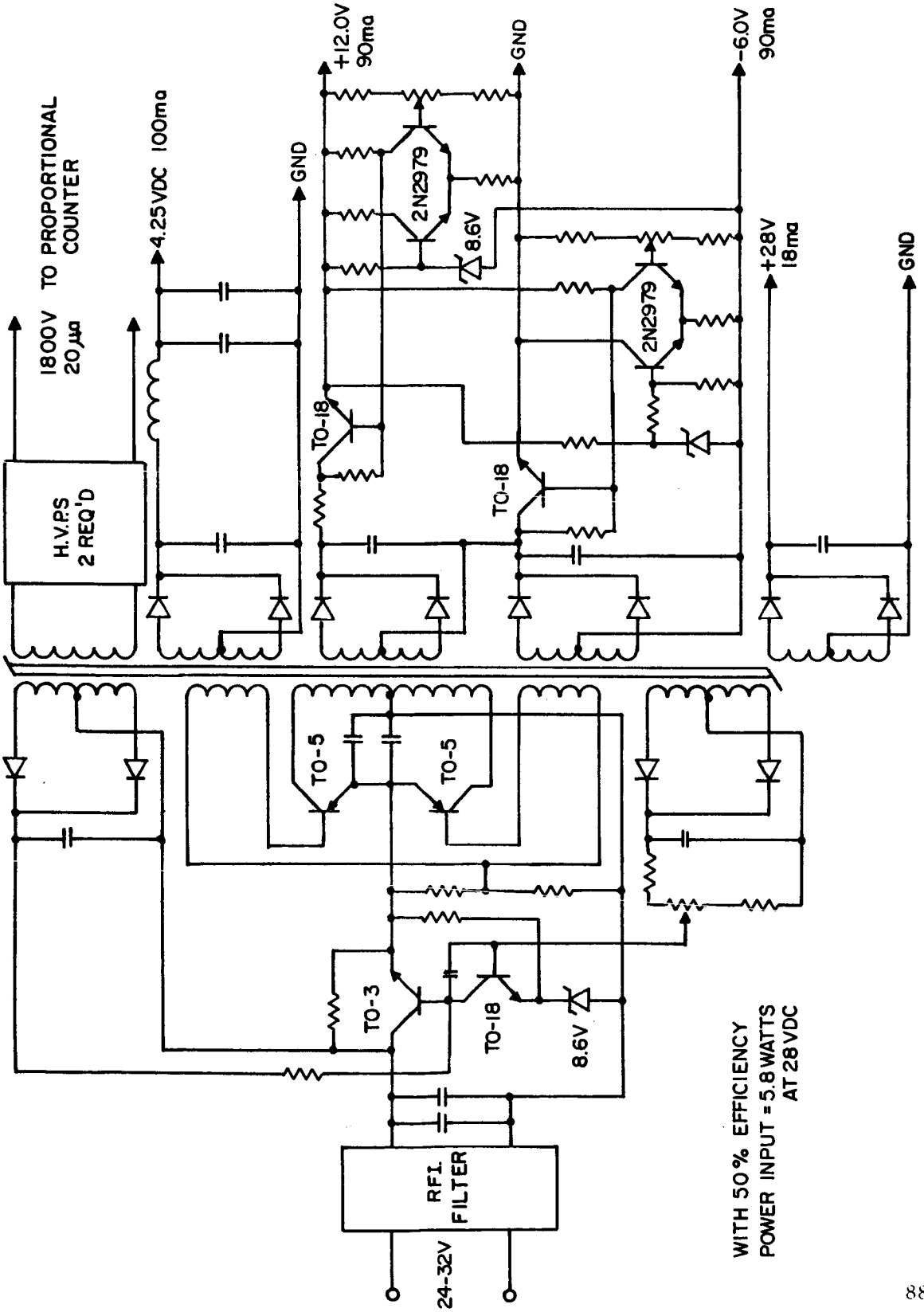

FIGURE 5.5.2-4 - SCHEMATIC OF REGULATED POWER SUPPLY

It is estimated that the error introduced into the measured density due to the presence of the AGC γ ray counts will be ±2% at 25 km in a model 3 atmosphere, and much less near to the surface. It may be possible to reduce this error by using 7.6 year Ba-133, which emits mainly ~ 300 Kev γ rays. This choice is not urgent and can easily be made by laboratory tests during the construction of the density sensor.

Figure 5.5.3-1 shows the schematic of the automatic gain control. A single level comparator detects the variation in the system gain as variations in count rate from the reference source. This comparator applies a correction signal to the photomultiplier tube high voltage power supply which causes the gain of the system to return back to the original value. Gain variations are detected by the high speed comparator μA710. A monostable multivibrator (SE 160) shapes the pulse and the integrator μA702 provides a feedback voltage through the DC amplifier to control the high voltage power supply.

5.6 Power and Mass Requirements. The power requirements are:

Photomultiplier Tube & Power Supply	0.505 watts
Automatic Gain Control	0.370 watts
Preamplifier	0.120 watts
Discriminator	0.370 watts
Integrator	0.120 watts
	1.485 watts

With a 50% efficient power supply, the power drawn from the MP/L batteries will be 2.97 watts. The ablation gages are not included.

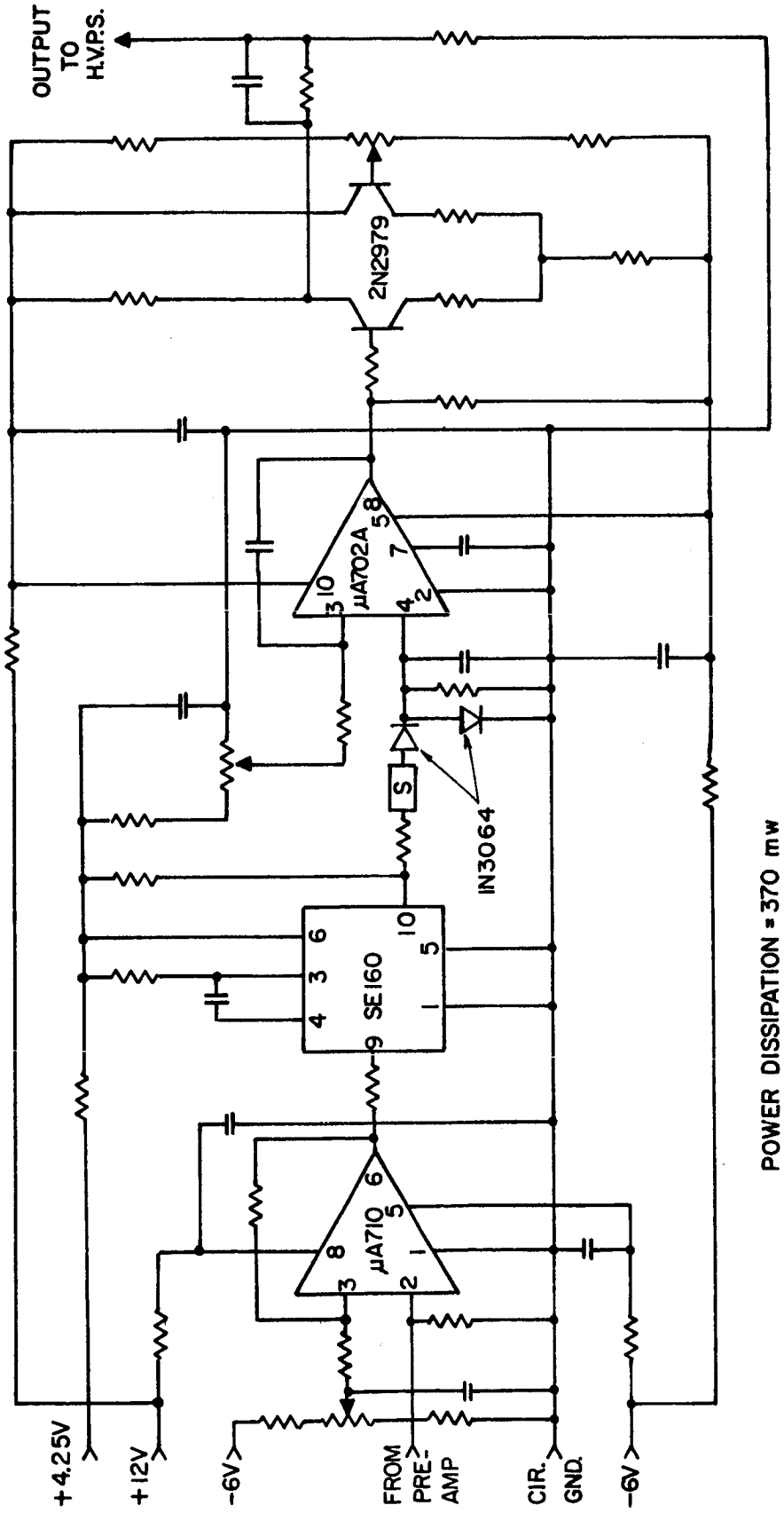

FIGURE 5.5.3-1 - SCHEMATIC OF AUTOMATIC GAIN CONTROL

The mass requirements are:

NaI(Tl) Scintillator	90 gm
Photomultiplier Tube & HV Power Supply	245 gm
PMT Shield (Collimator)	86 gm
Electronics Package	888 gm
Mounting Plate	36 gm
All Cables and Misc. Hardware	312 gm
	1657 gm

The mass of the ablation gages and their electronics is not included.

6.0 ABLATION GAGE SUBSYSTEM

6.1 Introduction and Summary. As the MP/L descends through the Martian atmosphere, the heat shield ablation is particularly severe between 25 and 5 km above the surface while the density sensor is measuring the ambient atmospheric density. Since the γ rays from the sensor must pass through the shield, backscatter, and then return through the shield to reach the detector, it is necessary to know the heat shield thickness at all times in order to calculate its effect upon the backscatter count rate, particularly since the available heat shield data indicate a count rate attenuation of about 40% prior to ablation. Therefore, the heat shield must be known to ±5% of its initial thickness so that count rate uncertainty is only ±2% (i.e., 5% of the 40% attenuation). The heat shield ablation is to be measured by the γ ray backscatter technique, which is the technique used for the density measurement. A schematic diagram of the selected ablation gage subsystem is shown in Figure 6.1-1. γ rays from the source are scattered by the heat shield and are then detected by the proportional counter. The output count rate from the detector is dependent upon the mass per unit area remaining in the heat shield. As this decreases, so does the count rate.

From the proportional counter, the output electrical pulses are counted to the processing electronics which eliminate virtually all of the extraneous background and then convert the remaining count rate into an analog 0-5 volt DC output which is fed to the telemetry system.

ABLATION GAGE OPERATION

FIG. 6.1-1

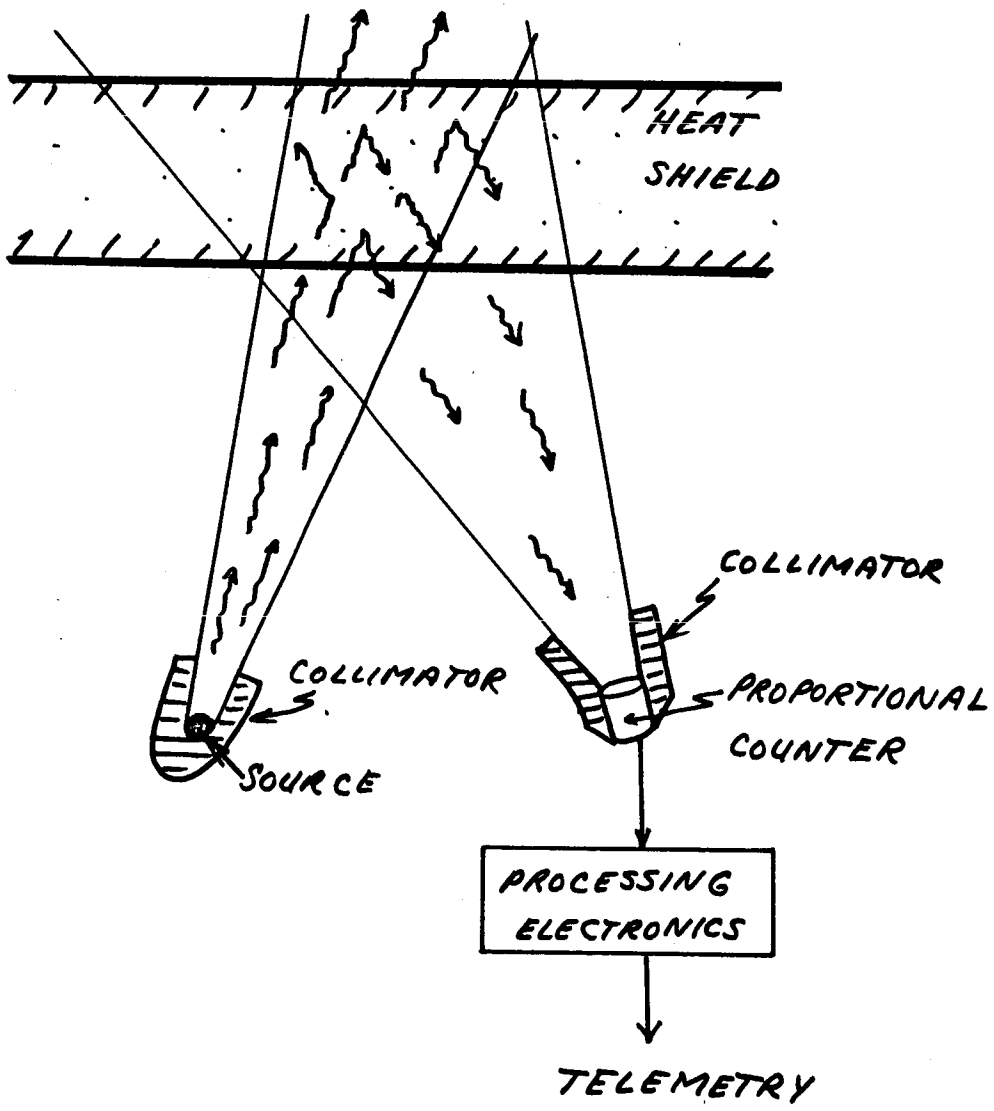

Since the heat shield ablation may vary somewhat from place to place, ablation gages are required for the heat shield over the source and over the detector. The source ablation gage utilizes the very large main γ ray source of Gd-153 to get a heat shield backscatter count rate, while the detector ablation gage has the 60 Kev γ rays from 100 millicuries of Am-241. The error introduced into the atmospheric density measurements due to the presence of this additional source is negligible.

A summary of the pertinent data for each ablation gage is given in Table 6.1-I. The next subsection presents the system hardware and the reasons for its selection.

6.2 System Selection

6.2.1 Radiation Source. Since the γ ray backscatter technique measures the remaining heat shield by noting the rate at which γ rays are scattered in it, a source is necessary for each ablation gage. Consider the gage near the Gd-153 backscatter source. Any auxiliary source used here will be swamped out by the very high backscatter rate due to the main source, so the ~100 Kev radiations from the very large Gd-153 source itself serve for the ablation gage.

Near the main detector, which is about 105 cm from the Gd-153 source, an auxiliary source is needed. The energy of this source should be such that it contributes as little error as possible to the atmospheric backscatter count rate. Therefore, a γ ray energy below the anticipated 60-100 Kev energy discrimination gate of the main detector is best. As a result, the 60 Kev γ rays

TABLE 6.1-I

SUMMARY OF ABLATION GAGE DATA

Gage Near Main Source

Mass*:	267 gm (0.59 lb)
Power:	1.42 watts from spacecraft supply
Source:	Main (Gd-153) source
Detector:	Proportional Counter

Gage Near Main Detector

Mass:	512 gm (1.13 lb)
Power:	1.42 watts from spacecraft supply
Source:	~100 mc of Am-241
Detector:	Proportional Counter

* Includes 36 grams for plate attaching gage to shield of main source.

of Am-241 are selected because their energy after backscattering in the heat shield will be ~50 Kev. They are easy to shield and are accompanied by no significant number of γ rays of other energies. Also, Am-241 is easily obtained and licensed in the source strength needed.

Therefore, the ablation gage sources consist of the main Gd-153 source for the gage near there and an Am-241 source near the main detector.

6.2.2 Detection System. Although NaI(Tl) is an excellent detector as regards efficiency and energy resolution, its use requires optical coupling, a photomultiplier tube, and possibly an automatic gain control circuit. These are available (as in the main detection system), but they are definitely complex. Therefore, a simpler detector is desirable. Among the remaining three possibilities (plastic scintillator, solid state, and proportional counter), the plastic scintillator has all the objections of NaI(Tl) and is less efficient. The solid state detector is very noisy at γ ray energy of 50 Kev and is susceptible to radiation damage. Therefore, a proportional counter is selected. Its efficiency for 50 Kev γ rays is only ~15%, but even so the resulting Am-241 source strength is acceptable. Regarding the environment criteria, proportional counters are available which operate at temperatures up to 150°C, have good gain stability despite voltage fluctuations, and can easily be ruggedized so as to survive all the expected mechanical stresses.

Both ablation gages are to utilize proportional counter LND #403, whose specifications appear in Table 6.2.2-I. It is manufactured by LND, Inc. of Oceanside, Long Island.

6.3 System Description

6.3.1 Geometry and Source Strength. The detector used with the Gd-153 source is located wherever convenient beside that source and so oriented that its field of detection includes the appropriate portion of the heat shield. Because of the very great strength of the Gd-153 source (~90 γ curies during the Martian descent), no optimization of this source-detector geometry for maximum efficiency is required. In fact, it may be possible to use a much smaller (a less efficient) proportional counter than presently selected.

For the detector ablation gage, the geometry shown in Figure 6.3.1-1 is used. The source strength is 100 millicuries of Am-241 and it produces a heat shield backscatter count rate of $\sim 10^4$ cps. The theoretical derivation of this system response is in Appendix G.

6.3.2 Processing Electronics. The main process by which the backscatter γ rays are detected in the proportional counter is photoelectric absorption. The probability of this process decreases very rapidly with energy from ~15% at 50 Kev to ~3% at 100 Kev and $\lesssim$1% at 150 Kev. Therefore, the proportional counters are relatively immune to background radiation. Nevertheless, it has been decided to incorporate energy discriminating electronics into the system, so as to preferentially select those detector output pulses corresponding to the γ rays backscattered from the heat shield.

TABLE 6.2.2-I

ABLATION GAGE PROPORTIONAL COUNTER LND #403

Diameter: 3.0 cm

Length: 3.3 cm plus ~1.8 cm of connector

Window: 2.5 cm diameter

Mass: ~113 gm

Sterilization: Counter operational between -65°C and +150°C

Radiation Damage: 5000 to 10,000 rad without significant effects

Efficiency: 50 Kev γ rays - ~15%

100 Kev γ rays - ~ several percent

Path length in xenon + methane gas is 2.5 cm

Warm-Up Time: None needed

Structural Strength: Some tubes tested to 75g static

Further ruggedization required

Operated in hard vacuum

Gain Stability: <3%/100 volts change in the 1600-2500 volt operating region

Cost: ~$275 prior to ruggedization

FIG. 6.3.1-1

ABLATION GAGE NEAR MAIN DETECTOR

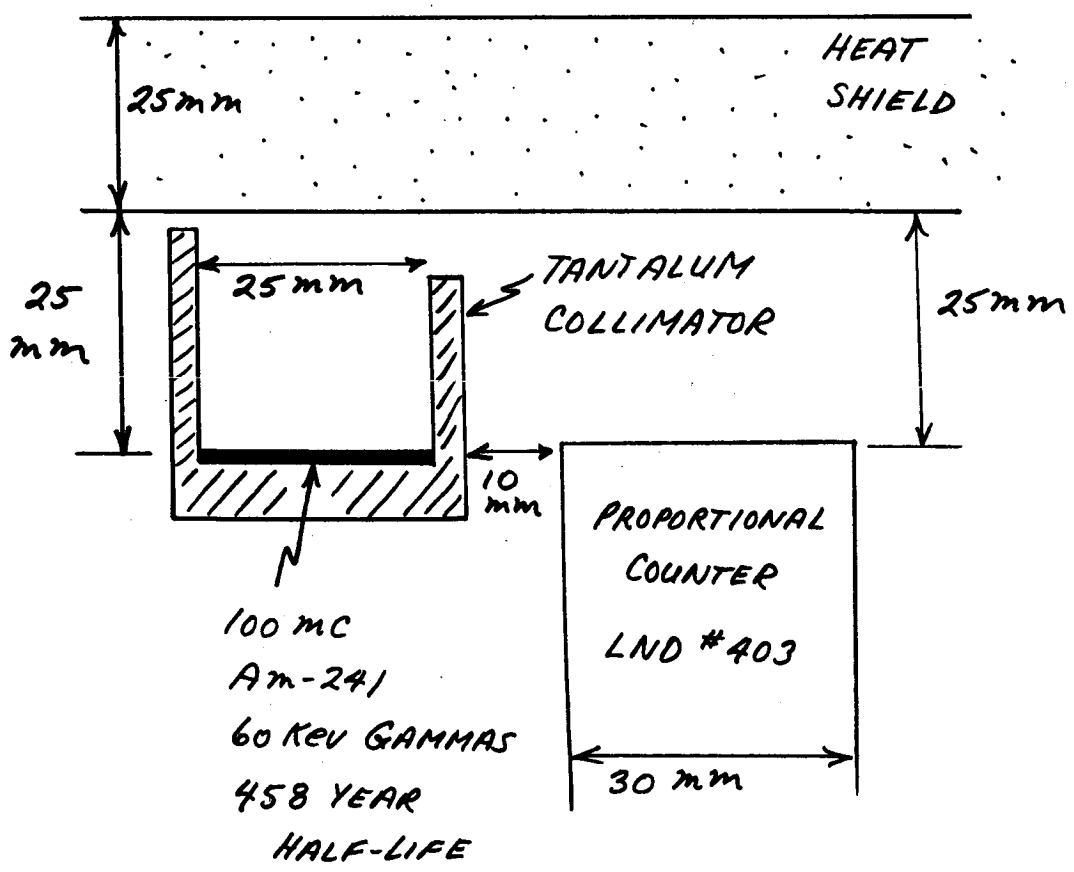

The same processing electronics (preamplifier, discriminator and integrator) are used as for the main (NaI(Tl)) detection system, and so they are not described here, though a block diagram of the ablation gage is presented in Figure 6.3.2-1.

No automatic gain control is required. When an ablation gage is activated well above the significant atmosphere, the heat shield is intact and whatever count rate is received corresponds to an unablated shield. During the descent, significant gain changes are not expected, particularly since the backscatter count rate from the ablation gage is high compared to the background--thousands of counts per second at least. When this is compared to the 230 cps expected from the main detector, and when the relative insensitivity of the proportional counter to background radiation is remembered, it can be seen that the ablation gages can omit AGC circuitry even though the main detection system cannot do so.

The power for the electronics and the proportional counter comes from the regulated power supply used for the main detector electronics. A schematic of the high voltage section is shown in Figure 6.3.2-2. The power required for each ablation gage is:

Proportional Counter & Power Supply	0.100
Preamplifier	0.120
Discriminator	0.370
Integrator	0.120
	0.710

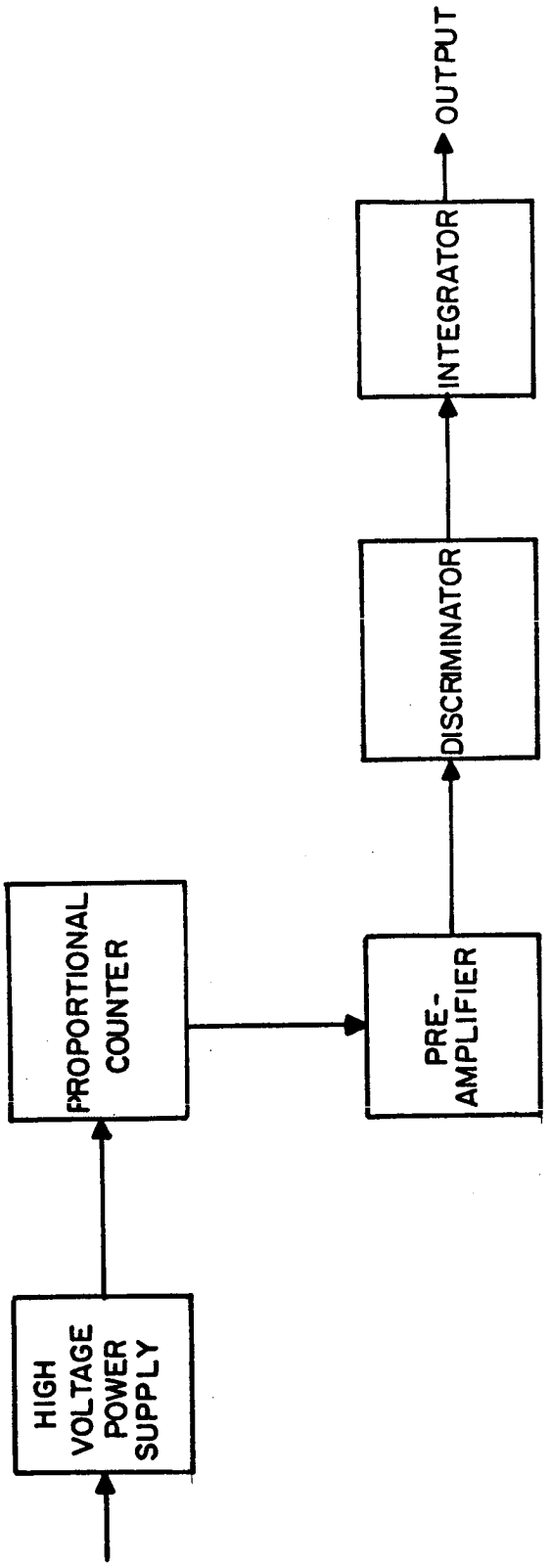

FIGURE 6.3.2-1 - BLOCK DIAGRAM OF ABLATION GAGE

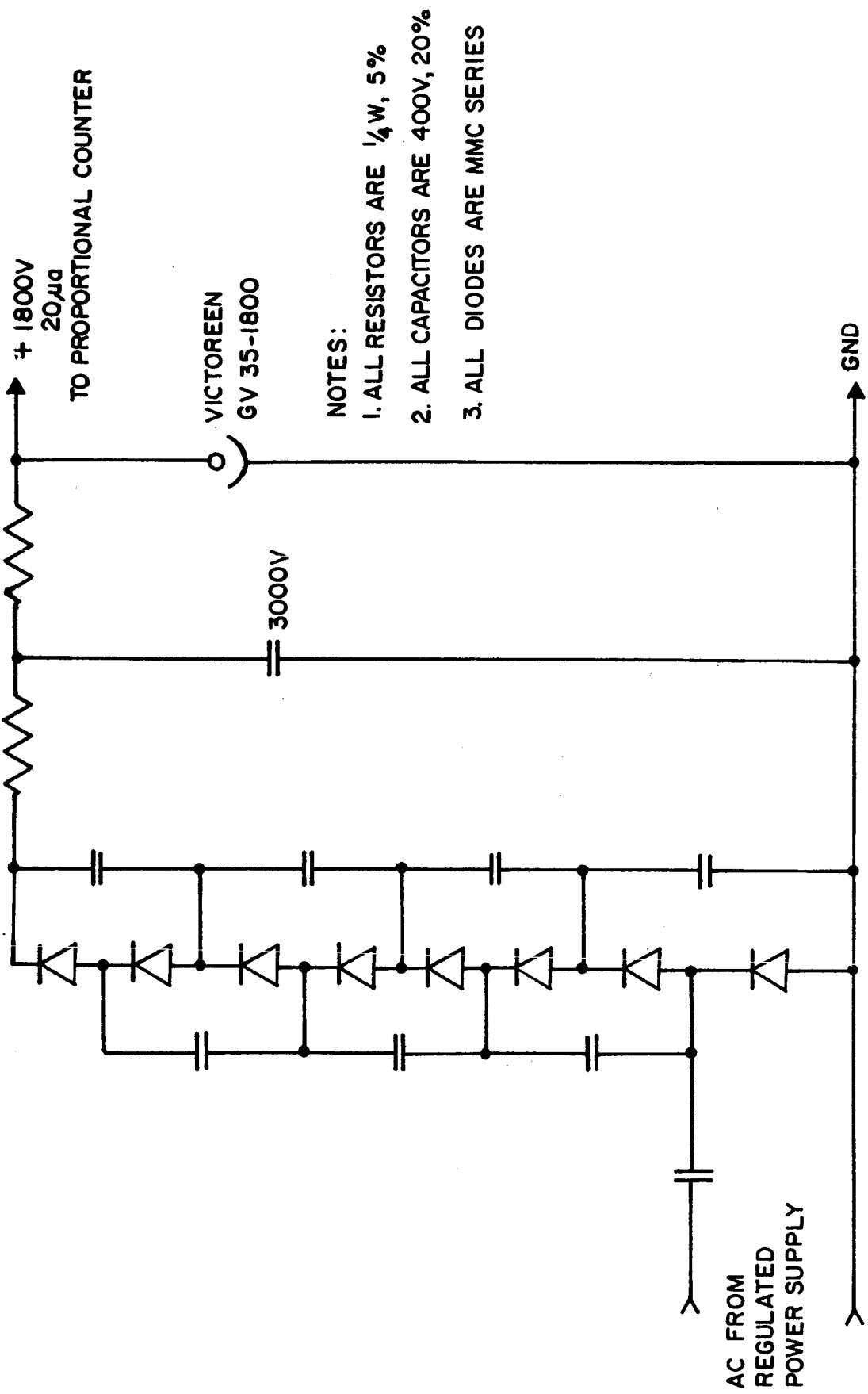

FIGURE 6.3.2-2 - HIGH VOLTAGE POWER SUPPLY FOR ABLATION GAGE

Since there are two ablation gages and the power supply is ~50% efficient, these two ablation gage subsystems require a total of 2.8 watts from the 28V DC MP/L power supply.

The total mass of the 2 ablation gages is:

2 Proportional Counters	226 grams
Shielding	336 grams
Electronics	181 grams
Mounting Plate	36 grams
	779 grams

6.3.3 Accuracy. Since the source strength has been selected so as to give the intact heat shield thickness to ±3% (one-sigma statistical fluctuation), and since the electronics are stable to ±3% over the specified temperature range, and since the gage is insensitive to all factors except the heat shield ablation, it is conservative to assign a system accuracy of ±5% of the original heat shield. That is, the mass per unit area of the heat shield over both the main source and the main detector will be known to ±.05m, or better, where m is the original mass/unit area of the shield prior to ablation.

As mentioned earlier, final calibration of the gages occurs just before the MP/L enters the significant portion of the Martian atmosphere.

7.0 SUMMARY

7.1 Introduction. The final report has presented the part-by-part conceptual design of a device to measure the density of the Martian atmosphere. This device, which will be located within a Mars Probe/Lander, uses the backscatter of γ rays to carry out the measurement; i.e., a source within the MP/L emits γ rays into the Martian atmosphere and a detector records the rate at which they are scattered back to the vehicle. As the density rises, so does the backscatter count rate.

The first step in the system design was the establishment of guidelines of constraints. Some of these (notably the mass, power, and volume goals) were obtained from the Contract Work Statement, but most were developed during consultations with NASA-LRC and AVCO/RAD personnel, and also by considering the mission profile, the MP/L vehicle structure, and other system requirements. See Chapter 2. Then, in Chapter 3, the theoretical system response was developed. From this theoretical response, the tradeoffs between various source and detector parameters were made clear, and Chapters 4, 5, and 6 were devoted to the selection of the system hardware in accordance with the aforementioned guidelines. The resulting conceptual design is summarized in the following subsection, while later subsections indicate the overall system reliability and accuracy.

7.2 Conceptual Design Summary. The overall physical arrangement of the density sensor consists of two separate parts which are labeled Assembly 1 and Assembly 2 in Figure 7.2-1.

FIGURE 7.2-1

MARS PROBE/LANDER DENSITY SENSING SYSTEM

PROPOSED MECHANICAL DESIGN

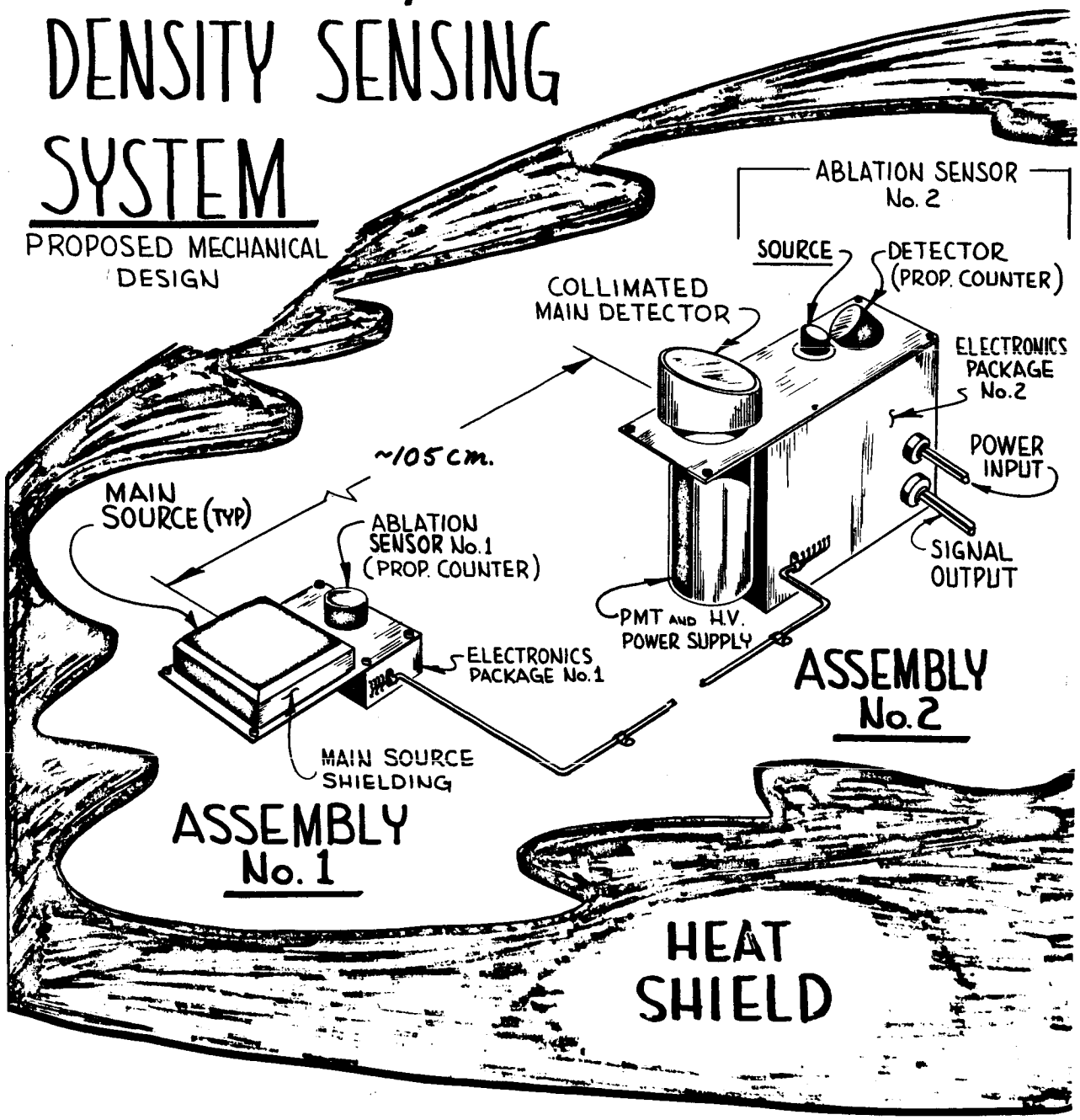

Assembly 1 consists of the main source and an ablation gage. The source consists of 480 curies of Gd-153, which emits mainly ~100 Kev γ rays, and its necessary tantalum shielding and titanium-ablation fireball protection. Sufficient material is available at ORNL to make this source, at a total cost of ~$35,000. Attached to the source shield is the proportional counter and electronics for Ablation Sensor No. 1, which measures the ablation in the heat shield over the main source. This measurement is carried out by detecting the rate at which the 100 Kev γ rays from the Gd-153 source are backscattered in the heat shield. As ablation occurs, this count rate decreases. The ablation gage accuracy is initially ±5% of the intact heat shield, but improves to ±4% when the shield is half gone. The power for the gate comes from Assembly No. 2, to which the gage also routes the 0-5V DC output signal indicative of the remaining heat shield thickness. To make this signal as meaningful as possible, the electronics accompanying the gage have an energy discriminating capability so as to reject the extraneous background radiations with energies different from those of the γ rays backscattered from the heat shield.

At a distance of approximately 105 cm, Assembly No. 2 is located. It contains the Main Detector, Ablation Sensor No. 2, the processing electronics, and the power supplies. The Main Detector consists of a 5 cm diameter by 1.25 cm thick NaI(Tl) crystal mounted on a photomultiplier tube. The crystal is collimated with tantalum. The Gd-153 γ rays, which reach this detector after being backscattered from the Martian atmosphere, produce a

light pulse in the NaI(Tl) crystal. This pulse is proportional to the energy deposited in the crystal and is converted into an electrical pulse by the photomultiplier tube. This electrical pulse in turn enters the processing electronics which reject any extraneous background pulses that do not have the same energy as the Gd-153 γ rays backscattered from the Martian atmosphere. The remainder of these electronics then puts out a 0-5 vdc signal which is routed to the telemetry and whose amplitude is governed by the count rate of those radiations within the selected energy range.

In addition to the Main Detector, Assembly No. 2 also contains Ablation Sensor No. 2, which includes a tantalum-collimated 100 millicurie Am-241 source, whose 60 Kev γrays are used to measure the heatshield thickness by the same backscatter technique as in the first ablation gage. The ablation gages differ only in that No. 2 includes a shielded radioisotope source of its own, whereas No. 1 uses the Main Source. Otherwise, both gates use a proportional counter whose output is processed to produce a 0-5 vdc signal routed to the telemetry.

The power for both ablation gages and all the density sensor electronics comes from the regulated power supply, except that the photomultiplier has its own built-in supply. These supplies are based on existing designs whose efficiencies of conversion from the spacecraft 28 vdc to the desired operational voltages are 50-60%. To be conservative, only a 50% efficiency is assumed.

TABLE 7.2-I

MASS AND POWER SUMMARY OF CONCEPTUAL DESIGN

Part	Mass (grams)	Power * (watts)
Main Source Shielding:	1070	-
Ablation Gage No. 1 and Mounting Plate:	272	1.42
Main Detector and Both Power Supplies:	1304	2.97
Ablation Gage No. 2 and Mounting Plate:	549	1.42
Cable and Miscellaneous Hardware:	312	-
TOTAL -	3507 grams (7.74 pounds)	5.81 watts

* Power drawn from 28 vdc battery supply of MP/L, including assumption of 50% efficient power supplies in density sensor itself.

The mass and power summary for the entire system is presented in Table 7.2-I. The system volume is 1600 cm^3 (97 cubic inches). The following section of this chapter describes the calibration tests, etc., required prior to carrying out the measurement of the density of the Martian atmosphere.

7.3 System Calibration and Operation Sequence. Once the density sensor has been built, it must be calibrated so that the count rates obtained while descending through the Martian atmosphere can be interpreted. The necessary calibration procedures are:

(1) Using a vacuum chamber, obtain the count rate versus density relationship with and without an intact heat shield.

(2) Repeat (1) using different heat shield thicknesses and with the ablation gages in place; this yields the relationship between the atmosphere back-scatter count rate and the ablation gate count rates as a function of the heat shield thickness. If this is impractical, use only atmospheric pressure and extrapolate. A multilayer heat shield should be used in either case to facilitate changes in the heat shield thickness.

(3) Measure all direct transmissions between the three sources and the three detectors (i.e., main source, ablation gage source, AGC source, main detector, and two ablation gage detectors. Use heavy shielding to block off all other effects.

(4) Use a multi-layered heat shield, a simulated shock wave, a vacuum chamber, and the complete density sensor to measure the multiple scatter effects within the heat shield and shock wave as a function of atmospheric pressure. Use heavy shielding to block off all other effects.

(5) Measure the lifetime of Gd-153 to ±0.1 day. The present accuracy is ~ ±1 day. This work can be done any time prior to the interpretation of the Mars data as it requires only a small Gd-153 source and a stable laboratory test arrangement.

The foregoing tests are all to be carried out on earth. However, when the descent from orbit is about to commence, the density sensor and its ablation gages should be activated so that they can do the following:

(1) The main detector uses its automatic gain control to stabilize the system gain at the desired value.

(2) The ablation gages obtain count rates corresponding to the background radiation and the intact heat shield.

(3) The main detector (once the gain has stabilized) obtains the count rate due to the background plus the backscatter from the negligible atmosphere.

(4) As the MP/L descends, variations in the ablation gage and main detector count rates indicate changes in the background radiation prior to ablation and entry into the significant atmosphere.

Once the significant atmosphere has been reached, the density sensor then carries out its designed purpose. However, the prior measurements indicated above aid in the interpretation of the data.

7.4 Radiation Safety. The density sensor contains three sources. The smallest of these, <0.1 microcuries of Cs-137, does not even require an AEC license, and poses no health hazard. The middle-sized source is 100 millicuries of Am-241. Sources of this size are presently used in commercial products of Giannini Controls and require only simple precautions, namely, do not break or handle the source capsule. The shield designed for this source eliminates all radiation hazard if several millimeters of tantalum are temporarily placed over the collimator opening during the assembly of the density sensor. Once the sensor is in the MP/L (and this temporary shield has been removed), the dose rate at a distance of 1 meter will be much less than 2.5 millirem per hour and no control area will be needed.

Finally, there is the very large main source. Its assembly will be by remote control (likely at ORNL). With its own shield and with a temporary 1 cm thick tantalum shield over the collimator opening, the dose rate at 10 cm will be ~2.5 millirem/hour, so no control area is needed. However, when the density sensor is being assembled, a geiger counter should be available to check the source if it is inadvertently dropped on the floor or otherwise grossly mishandled. Finally, once the density sensor is on the MP/L and the temporary shield has been removed and the

MP/L heat shield is in place, a 1.5 cm thick lead shield should be temporarily hung over that portion of the heat shield which is over the main source. Once this has been done, no control area will be required and the dose rate will be less than the 2.5 millirem/hour allowed by the AEC

It is therefore concluded that the radioisotope sources in the density sensor can be safely handled using simple temporary shields. This is possible because of the low γray energies emitted by the two larger sources. Radiation safety is not a serious problem.

7.5 System Reliability. A reliability analysis has been performed on the conceptual design, and the details (particularly failure rates) are found in Appendix H. For this analysis, all the component parts of each individual assembly are considered in series for a worst case condition; the worst case operating temperature is +70°C.

The analysis indicated a mean time between failures during operation of 105,000 hours. The eight-month standby time is in a non-operating condition and is well within the typical three to five years shelf life requirements of similar systems.

Therefore, if a 100-hour test and calibration period plus $\lesssim$30 minutes of operation during the Mars descent are assumed, the probability of complete mission success is 99.90%.

The probability of a partial success is 99.97% and occurs if both ablation gages malfunction. In that case, estimates must be made of the best shield ablation as a function of altitude,

and the system accuracy will become ~±20% prior to the removal of the heat shield. During the parachute phase of the descent (and after the removal of the heat shield), ablation gate malfunctions are not of any significance.

In addition to the regular MTBF reliability analysis, the possibility of radiation damage has also been considered for the three main components of the density sensor, i.e., the sources, the detectors, and the supporting electronics. Of these, the sources are quite immune to the space radiation and need not be considered further. Also, the proportional counters are specified as capable of withstanding at least 5000 rad without significant damage. This dose is well in excess of any reasonable space dose calculated from present data after allowing for the shielding provided by the bus and the MP/L structure. In addition, the NaI(Tl) detector is not degraded significantly by the calculated doses. This leaves the photomultiplier tube and the supporting electronics. The greatest danger to these is the proton flux, not the secondaries produced when this flux interacts with the MP/L vehicle, etc.

From our present knowledge of the radiation susceptibility of the photomultiplier tube and the electronics, no difficulty is expected. If these were exposed to the raw proton flux of space, the damage would apparently be significant, but inside the MP/L, which is in turn inside a sterile can, the proton fluxes are vastly reduced. Also, the packaging of the device, etc. provides additional shielding. For example, the relatively radiation-immune

NaT(Tl) crystal shields the photocathode of the photomultiplier tube, etc.

Finally, there is the Mariner 4 experience to draw upon. It accomplished the taking and transmission of pictures after ~eight months in space, a more difficult feat than measuring a count rate. Thus it appears the density sensor will suffer no significant radiation damage prior to the Martian descent.

Therefore, there is a 99.97% probability of complete success during the parachute phase of the descent, and a 99.90% probability of better than approximately ±12% accuracy between 25 km and the start of the parachute phase at ~5 km.

7.6 System Accuracy. As shown in Chapter 3.0, the system error is given by

$$\frac{\Delta\rho_m}{\rho_m} = \pm\sqrt{\left(\frac{\Delta k}{k}\right)^2 + \left(\frac{\Delta I_s}{I_s}\right)^2 + \left(\frac{\Delta I_b}{I_s}\right)^2 + \left(\frac{\Delta I_{bc}}{I_s}\right)^2} \qquad (7.6\text{-}1)$$

where: $\Delta\rho_m$ is the error in the measured density ρ_m.

Δk is the error in the calibration constant k which relates the measured density ρ_m to the rate I_s at which the γrays are scattered back from the Martian atmosphere, i.e., $\rho_m = kI_s$

ΔI_s is the error in I_s

ΔI_b is the statistical error in the background radiation count rate I_b

ΔI_{bc} is the uncertainty on the calculation of the background radiation count rate I_b.

All errors are on a one sigma basis. Note that the calibration error Δk includes the errors due to the pre-launch calibration, heat shield ablation, electronic gain variations including those due to changes in the MP/L power supply voltage, deviation of the Martian atmospheric composition from the specified models, electronic coincidence, and resolving time effects resulting from the rapid motion of the MP/L through the atmosphere.

Now that the complete conceptual design has been presented, the overall system accuracy can be calculated. This is done for altitudes of 5 and 25 km above the Martian surface and assuming a model 3 Martian atmosphere, the thinnest of the three mod specified in the Contract Work Statement. The 25 km altitude was chosen because significant aerodynamic braking of the vehicle is expected at that altitude; at 5 km, on the other hand, the slow parachute descent should have commenced, accompanied by the removal of the heat shield and consequently a sharp change in the error analysis.

Of the four error components in equation (7.6-1), the calibration error $(\Delta k)/k$ has already been evaluated in Chapter 3.0. It is ± 0.053 and ± 0.045 at 25 and 5 km, respectively. Also, the selection of the source strength has set I_s at 230 cps and 1580 cps for the respective altitudes. From these figures $(\Delta I_s)/I_s$ is ± 0.066 and ± 0.038 at 25 and 5 km. There then remain the two radiation background errors ΔI_b and ΔI_{bc}, both of which are dependent on the MP/L vehicle structure as well as on the conceptual design of the density sensor.

The detailed calculation of ΔI_b and ΔI_{bc} is presented in Appendix I, and the results are $(\Delta I_b)/I_s = \pm 0.047$ and ± 0.006, while $(\Delta I_{bc})/I_s = \pm 0.065$ and ± 0.008, at the 25 and 5 km altitudes.

A summary of the entire system accuracy is presented in Table 7.6-I. The overall one sigma accuracy is ±11.7% at 25 km and ±6.0% at 5 km, assuming a model three atmosphere and a one second sampling time.

It is very important to note that all the errors quoted above are for independent one-second sampling periods. However, when the density data are plotted, it will be possible to fit them with a smooth analytical curve whose accuracy will be markedly better than that for each separate data point. It is estimated that the accuracy may actually be improved by a factor of two by means of this curve-fitting process. However, to be conservative, the one-second interval individual sample accuracies of +11.7% and ±6.0% are quoted as the system accuracy unless otherwise specified.

TABLE 7.6-I

SYSTEM ACCURACY*

	Altitude	
	25 km	5 km
Calibration Error:		
Pre-launch Calibration	±3.0%	±3.0%
Electronic Gain Variation	±3.0%	±3.0%
Heat Shield Ablation	±2.0%	-
Resolving Time	±2.0%	-
Electronic Coincidence	±1.0%	±1.0%
Atmospheric Composition	±1.0%	±1.0%
Source Strength Statistical Fluctuations:	±6.6%	±3.8%
Radiation Background Statistical Fluctuations:	±4.7%	±0.6%
Radiation Background Prediction Uncertainty	±6.5%	±0.8%
TOTAL SYSTEM ERROR	±11.7%	±6.0%

* One sigma value assuming a model 3-atmosphere and a one-second sample time.

REFERENCES

1. Cann, Davies, Greenspan, & Owen, NASA CR-298, IIT Research Institute, "A Review of Recent Determinations of the Composition and Surface Pressure of the Atmosphere of Mars".

2. Levin, Evans, & Stevens, NASA TN D-2525, November 1964, "NASA Engineering Models of the Mars Atmosphere for Entry Vehicle Design".

3. Storm, Gilbert, & Israel, LA-2237, Physics and Mathematics, (TID-4500, 13th Ed., Rev.), April 1957, "Gamma-Ray Absorption Coefficients for Elements 1 Through 100 Derived from the Theoretical Values of the National Bureau of Standards".

4. Starfelt, Cederlund, & Lidén, International Journal of Applied Radiation and Isotopes 2, 265-273, 1957, "The Yield of Characteristic X-Rays Excited by β-Rays".

5. Reiffel, Nucleonics 13, (3), 22-24, 1955, "Beta-Ray-Excited Low Energy X-Ray Sources".

6. Ezop, IITRI 1209-9, TID-4500 (19th Ed.), "Study of the Capability of Isotopic Source of Secondary Radiation".

7. PB 121784R, U. S. Department of Health, Education and Welfare, Public Health Service, Sept. 1960, "Radiological Health Handbook".

8. Catalog of Radio and Stable Isotopes, 4th Revision, April 1963, Oak Ridge National Laboratory, Oak Ridge, Tennessee.

9. Goldman, General Electric Company, Schenectady, N. Y. 12305, June 1964 (7th edition), "Chart of the Nuclides".

10. Cohen & Wernick, Physical Review 134B, 502, May 1964.

11. Handbook of Chemistry & Physics, 45th edition, 1964-1965, The Chemical Rubber Company.

12. ORNL-11C-5, UC-23 - Isotopes - Industrial Technology, "Proceedings of Symposium on Low-Energy X and Gamma Sources and Applications Held at IITRI", October 1964, page 183.

13. Evans, "The Atomic Nucleus", McGraw-Hill, 1955.

appendix A

APPENDIX A

NATURAL RADIATION ENVIRONMENT OF THE MARS ATMOSPHERIC DENSITY SENSOR

TABLE OF CONTENTS

1.0 INTRODUCTION

This appendix is an updated and curtailed version of Engineering Report, ER-80231, which was previously submitted in preliminary form to NASA-LRC. It presents the natural nuclear radiation environment that will be encountered as the Mars Probe/Lander and its atmospheric density sensor are carried from earth to Mars. No attempt is made to calculate the radiation fluxes that will actually penetrate to the detector through the shielding afforded by the MP/L structure. The effect of the Martian atmosphere on the radiation environment is discussed in the error analysis section of the report.

From the point of view of the conceptual design, the radiation environment is important for two reasons. First, radiation damage of the density sensor may occur to such a degree that its reliability is significantly affected. Second, the background radiation during the descent to the Martian surface may cause errors in the indicated atmospheric density.

In the following sections, the radiation sources and their effects during various parts of the mission are described. The strengths of the significant sources are given in subsequent sections.

2.0 RADIATION EFFECTS DURING MISSION

2.1 Earth Pre-Launch. Any tests of the density sensor prior to launching must take into account the background due to radioisotopes in the earth's crust, solar flares, cosmic rays, and any secondary radiations produced by these latter two sources. A detailed general study of these radiations at earth sea level is omitted because the background at any test site will depend very strongly on the physical construction of the site itself and because the radiation damage on earth will be negligible even over centuries of exposure.

2.2 Earth Launch and Orbit. The radiation environment during the launch is not specified because of the very short length of this period (<1 hour) and because there is no need to operate the sensor then.

If a 100 mile orbit is used, the earth-based radioisotopes will be completely shielded out by the atmosphere, but the atmospheric shielding out of the cosmic rays and solar flares will be absent. Since the earth's magnetic field will still provide considerable shielding and since the time in orbit will be far less than the transit time to Mars, the radiation damage due to solar flares and cosmic rays during this phase will be relatively unimportant. It is also expected that any such temporary orbit will be well below the Van Allen belts and that these too will cause negligible damage.

To test the MADS while in earth orbit, considerable data must be assembled to predict the count rate to check if the apparatus is performing satisfactorily. These data and calculations are currently omitted because there is no indication that such a test will occur, and also because better data will be available at any future date when the need for such calculations arises.

Therefore, specification of the radiation environment for the earth-launch and orbit phase is omitted.

2.3 Leaving Earth Orbit. This phase extends from an altitude of 100 miles to the point at which the spacecraft has left the Van Allen belts and will not undergo a further change of trajectory except for the relatively minor mid-course maneuver. The time to leave earth orbit and attain the transit trajectory will likely be less than a day.

During this stage, the background radiation will rise because the spacecraft will pass through some portion of the Van Allen belts and also because the outward motion will take the craft into regions of space where the earth's magnetic field weakens and provides less protection against solar flares and cosmic rays.

For this phase of the mission, the Van Allen radiation belts are specified because they possess very high particle fluxes at certain points in space. Specification of the cosmic ray and solar fluxes is omitted because the Van Allen fluxes will dominate.

However, if the cosmic ray and solar particle fluxes are of interest, they can be approximated by their interplanetary values which are specified for the earth-Mars transit.

2.4 Earth-Mars Transit. This portion of the mission takes the spacecraft through space to the Mars orbit, which will likely be hundreds of miles above the planetary surface.

Since there are no plans to activate the density sensor during the transit, the only interest in the radiation environment is as regards radiation damage to the experimental apparatus. For this, both the cosmic ray and the solar radiation background must be specified. The latter will cause damage during the intense but relatively brief solar flares, while the low flux cosmic rays will steadily beat upon the apparatus during the approximately eight month transit period. No significant belts of trapped radiation near the end of this transit period were indicated by the Mariner 4 data.

2.5 Mars Descent. As the MP/L descends to the Martian surface, the density sensor is activated to determine the background count rate at altitudes well above any significant portion of the atmosphere. Contributions to the background count rate above the atmosphere may arise from:

(a) Direct interaction of cosmic ray and solar flare particles with the sensor.

(b) The cosmic rays and flare particles may interact with the MP/L structure to produce secondary radiations (γ's, neutrons, charged particles) which reach the detector. These radiations in turn can produce further radiations by interaction with the MP/L structure, etc.

(c) There will be γ rays emitted from radio-isotopes within the Martian surface layer

(d) Cosmic rays and solar particles will produce secondary radiations in the atmosphere, and some of these radiations may reach the detection system.

(e) The cosmic rays and high energy solar flare particles can interact with the Martian surface to produce γ's, protons, and neutrons which may find their way to high altitudes.

As the MP/L descends into the significant portion of the atmosphere, the background radiation becomes secondary to the count rate due to the air scattering of γ rays from the sensor's calibrated radiation source. However, the background count rate will still constitute an error in the density reading and so must be calculated using all available data, including the background measurements at the very high altitudes. As the vehicle descends deeper into the atmosphere, the radiations emitted from the surface become increasingly important. Meanwhile, the solar flare particles

decrease in both energy and number, but the very high energy cosmic ray particles are relatively unaffected. Secondary radiations produced in the atmosphere will increase with decreasing altitude (a buildup effect).

From the foregoing paragraphs, it can be seen that this last stage of the Mars mission requires specification of:

(a) The solar particle spectrum near Mars.

(b) The cosmic ray spectrum near Mars.

(c) The radioisotope radiations emerging from Martian surface.

All the other apparent sources of radiation mentioned for this stage of the mission are due to the interaction of radiations from these primary sources with the Martian surface, the Martian atmosphere, and the structure of the MP/L itself.

Radiation damage during this final phase of the mission will be negligible due to the very short time required to reach the Martian surface.

2.6 Summary. It is concluded that the following portions of the natural background radiation environment should be specified.

(a) Van Allen belts (trapped radiation belts about the earth)

(b) Cosmic Rays - near earth, but outside Van Allen belts
- between earth and Mars
- near Mars

(c) Solar Radiation (general background and flares)

- near earth, but outside Van Allen belts
- between earth and Mars
- near Mars

(d) Radioisotopes in Martian Crust

Since there is insufficient data available in some of the foregoing cases, it is necessary to extrapolate or approximate from more readily available results.

The following sections of this report specify the necessary portions of the natural background radiation environment.

3.0 VAN ALLEN BELTS OF TRAPPED RADIATION

The early model[1] of the spatial distribution of Van Allen radiation consisted of 2 concentric toroidal regions extending equatorially about the earth. The inner zone was between the geomagnetic latitudes of 25°N and 25°S and extended from approximately 600 km to approximately 10,000 km in altitude. The outer belt was represented as extending from approximately 15,000 km to approximately 70,000 km in an equatorial plane. In a meridian plane, the outer zone dipped down to lower altitudes with increasing latitude so that the outer zone extended over an altitude of from approximately 300 km to 1,500 km in the geomagnetic latitude interval from 55° to 70°.

More recent experiments indicate that the radiation belts are not separate, but that there is one large trapping region with particles of different characteristics in different sections. However, reference is still made to inner and outer belts. It must be remembered that the electron content of the inner radiation belt was increased by the Johnston Island high altitude nuclear blast. This effect is slowly disappearing, but still accounts for a noticeable portion of the electrons in the inner belt.[2] The proton content of the belts is not believed to have been altered by the nuclear blast.

3.1 Particle Fluxes in the Van Allen Belts. Flux maps[3] for the inner zone electrons and protons are available[3,4] as well as a pictorial diagram of the entire inner and outer belt electron distribution.[3] For details on the proton and electron content of the inner and outer zones,[5] see Table 3.1-I. No flux maps of the outer region comparable to those of references (3) and (4) are available.

TABLE 3.1-I

SUMMARY OF TRAPPED RADIATION ENVIRONMENT

TRAPPED RADIATIONS	ENERGY RANGE (Mev)	ENERGY SPECTRUM	PEAK INTENSITY ($cm^{-2}sec^{-1}$)
Inner Belt Protons	$E_p > 30$	$E^{-1.8}dE, 75 < E_p < 700$Mev (inner edge of belt)	3×10^4
		$E^{-4.5}dE, 0.1 < E_p < 5$Mev (outer edge of belt)	
	$E_p > 40$	$\exp(-E/306L^{-5.2})dE$	2×10^4
	$40 < E_p < 110$		2×10^4
	$E_p > 59$	$\exp(-E/460L^{-4.8})dE$	2×10^4
Electrons	$E_e > 0.6$		2×10^6
	$E_e > 0.04$	$\exp(-E/160)dE$	10^8
	$E_e > 0.04$		10^8 sterad^{-1}
	$E_e > 0.60$		10^6 sterad^{-1}
	$E_e > 0.5$	Includes Artificial Electrons	6×10^8
	$E_e > 5$		2×10^7
Outer Belt Protons	$0.1 < E_p < 5$	$\exp(-E/100)dE$	10^8
	$E_p > 1$		10^7
	$E_p > 75$		0.1
	$0.1 < E_p < 4.5$		6×10^7 sterad^{-1}
	$40 < E_p < 110$		4×10^3

TABLE 3.1-I (Cont'd)

TRAPPED RADIATIONS	ENERGY RANGE (Mev)	ENERGY SPECTRUM	PEAK INTENSITY ($cm^{-2}sec^{-1}$)
Electrons	$E_e > 0.04$	$E^{-1}dE, 40 < E_e < 150$ Kev	10^7
	$1.5 < E_e < 5$	$E^{-5}dE, 0.3 < E_e < 5$ Mev	10^4
	$E_e \geqslant 0.04$		1.5×10^8
	$E_e \geqslant 0.23$	$E^{-0.14}dE, 40 < E_e < 100$Kev	1.5×10^6
	$E_e \geqslant 1.6$		2×10^5
	$E_e \geqslant 0.04$	$E^{-(1\pm0.5)}dE$ during magnetic quiet	3×10^8
	$E_e \geqslant 0.23$		1×10^7
	$E_e \geqslant 1.6$		1×10^6
		$40\text{Kev} < E_e < 1.6$ Mev	

4.0 SOLAR RADIATION

The sun continuously emits an ionized plasma called the solar wind, but the particle energies are so low that it can be neglected.[6] The X-rays which the sun also emits have a negligible intensity at $\geq$ 20 Kev.[7] During solar flares,[7] the intensity of 1.5 to 20 Kev X-radiation rises to approximately 2.3×10^{-5} ergs/cm^2/sec. at earth orbit, which is equivalent to a 20 Kev γ-ray flux of 750/cm^2/sec. However, the flux[7] decreases very rapidly above 20 Kev. Therefore, a quiet sun poses no radiation hazard at all from either protons or X-rays, while the X-ray flux, during a flare, is negligible compared to the rest of the flare

4.1 Solar Flares. The total radiation flux due to solar flares varies by a factor of 6-10 in cycles of approximately eleven years, so missions undertaken near a solar minimum suffers markedly less radiation damage than at solar maximum. However, this possibility will be ignored at present and the conceptual density sensor design assumes the worst case.

The solar flare particle flux can be considered either from the long term or short term point of view. In the long term, the fluxes at earth orbit near solar maximum are:[8]

$\sim 6 \times 10^9$ protons/cm^2/year with energy $>$ 30 Mev

$\sim 1 \times 10^9$ protons/cm^2/year with energy $>$ 100 Mev

near solar minimum:

$\sim 1 \times 10^9$ protons/cm^2/year with energy $>$ 30 Mev

$\sim 1 \times 10^8$ protons/cm^2/year with energy $>$ 100 Mev

The time dependence of solar flares varies considerably from flare to flare, but can be roughly described by saying that the flare reaches its peak intensity about 10 hours after its onset, stays steady for several hours, and then decreases over 20 to 60 hours to the ambient particle radiation level. Different parts of the proton spectrum have different time behaviors, with the more energetic particles arriving and ending earlier. Sample time-dependent spectra are given in reference (9), and an expression for the exponential rise of the particle flux at the flare onset appears in reference (8). This latter expression is:

$$N = N_m \exp(-k\, t_m/t) \qquad (4.1\text{-}1)$$

where:
- N = number of particles/cm^2/sec. at time t
- N_m = number of particles/cm^2/sec. at flare maximum
- t_m = time between flare onset and occurrence of N_m
- t = time between flare onset and occurrence of N
- k = factor dependent on energy spectrum of flare

In addition to the time dependence of a flare, the spectral distribution of the protons is also important. The following model is suggested:[8]

$$N(>E) = 18.9N(>30\ \text{Mev}) \exp(-12.5P(E)) \qquad (4.1\text{-}2)$$

where:
- $N(>E)$ = number of protons/cm^2 with energy $> E$
- $P(E) = \dfrac{\sqrt{(E + m_o c^2)^2 - (m_o c^2)^2}}{e}$ ($\times 10^{-9}$) billion volts

E = proton kinetic energy in joules
(1 Mev = 1.602×10^{-13} joules)

$m_o c^2$ = 1.502×10^{-10} joules = 938 Mev

e = 1.602×10^{-19} coulombs

In Table 4.1-I, equation (4.1-2) is used to calculate the shape of a spectrum which has $N(> 30 \text{ Mev}) \sim 10^7$ protons/cm^2. The probabilities[8] of flares with various $N(> 30 \text{ Mev})$ values are given in Table 4.1-II. The various model flares are plotted in Figure 4.1-1.

The foregoing flare spectra are not the same shape as is the time-integrated yearly spectrum. This spectrum (tailored to fit the yearly solar proton fluxes given earlier), is applicable when the radiation effects of eight months in space are being considered. The analytical forms of this spectrum are:

(a) Near Solar Maximum

$$N(>E) = (4.86 \times 10^{10}) \exp(-.00874\sqrt{E^2 + 1876E}) \text{ protons/cm}^2\text{/year with E in Mev}$$

(b) Near Solar Minimum

$$N(>E) = (1.45 \times 10^{10}) \exp(-.0112\sqrt{E^2 + 1876E}) \text{ protons/cm}^2\text{/year}$$

The differential spectra (particles/cm^2/sec./Mev) are gotten by differentiating the appropriate integral spectrum equations with respect to E (in Mev).

TABLE 4.1-I

MODEL SOLAR FLARE

PROTON ENERGY E(Mev)	P(E) (Billions of Volts)	exp(-12.5P(E))	N(>E)*
1	0.0433	0.582	11.0×10^{7}
3	0.0750	0.392	7.4×10^{7}
10	0.137	0.185	3.49×10^{7}
30	0.239	0.0505	0.96×10^{7}
70	0.369	9.95×10^{-3}	0.188×10^{7}
100	0.444	3.89×10^{-3}	7.35×10^{5}
200	0.644	3.19×10^{-4}	6.02×10^{4}
500	1.090	1.22×10^{-6}	2.3×10^{2}
1000	1.697	6.2×10^{-10}	0.12

* $N(>E) = 18.9N(>30) \exp(-12.5P(E))$

TABLE 4.1-II

FLARE PROBABILITIES

N(E > 30 Mev) (Protons)	Probability of Occurrence/24 Hours
10^7	0.0113
5×10^7	0.0073
10^8	0.0058
5×10^8	0.0038
10^9	0.0023
5×10^9	0.0003

FIGURE 4.1-1

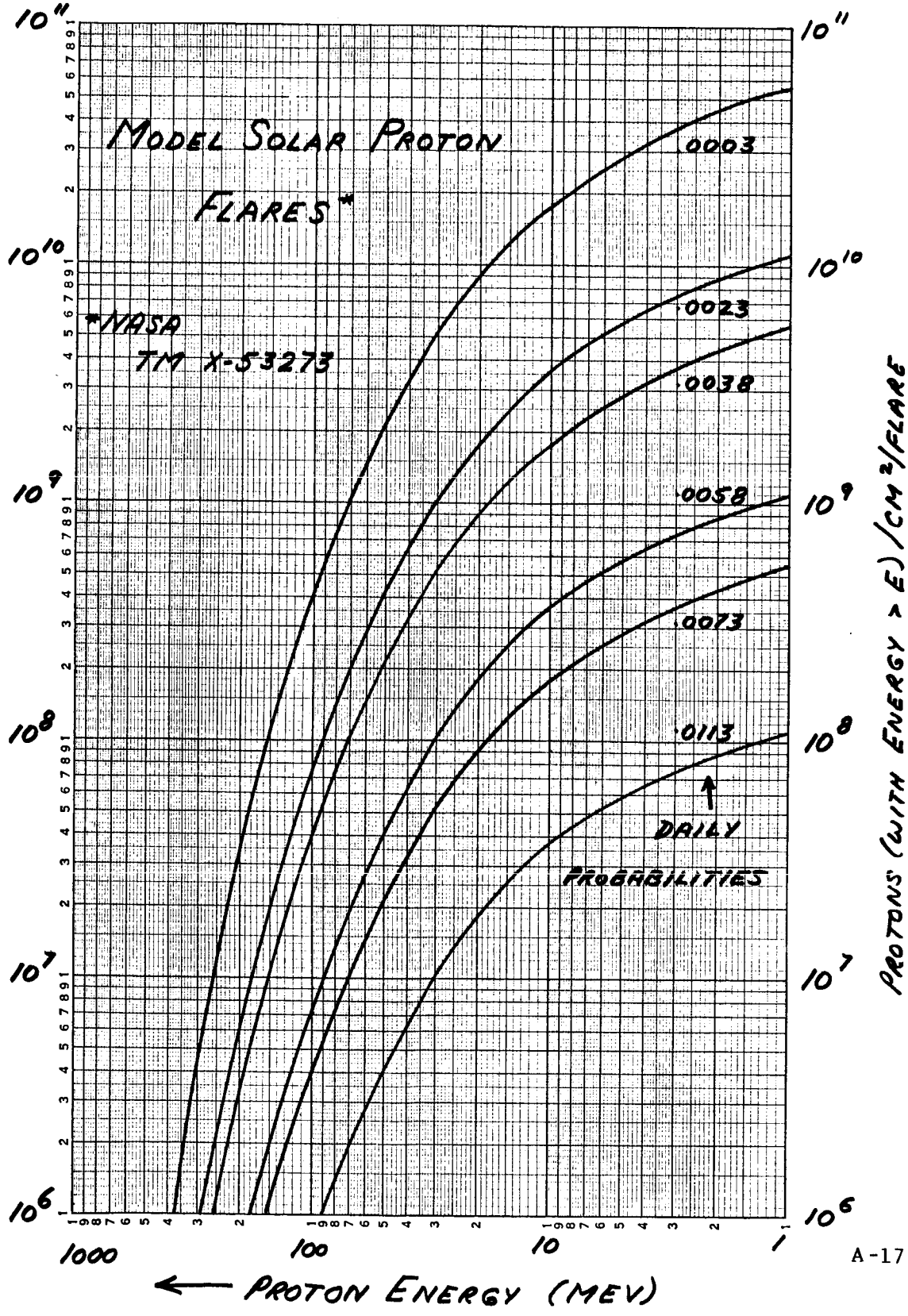
MODEL SOLAR PROTON FLARES*
*NASA TM X-53273
.0003
.0023
.0038
.0058
.0073
.0113
DAILY PROBABILITIES
PROTONS (WITH ENERGY > E)/CM²/FLARE
PROTON ENERGY (MEV)
10¹¹
10¹⁰
10⁹
10⁸
10⁷
10⁶
1000
100
10
1

4.2 Flare Fluxes Near Earth and Mars. Near earth, a noticeable flare flux reduction occurs as far out as 10 planet diameters, due to the presence of the magnetic field. However, the time required for the vehicle to reach this is negligible compared to that spent in transit to Mars, so the interplanetary solar flare environment is used even near the earth.

At the other end of the transit, Mars is believed to have an insignificant magnetic field, and so the interplanetary flare environment will apply to within several Mars diameters of the surface. At lower altitudes, allowance is necessary for the nearness of the planet if background count rates are being calculated.

5.0 COSMIC RADIATION

The composition of the galactic cosmic radiation is:[8]

~ 85% protons (H^+)

~ 14% alpha particles (He^{++})

~ 1% nuclei of elements Li→Fe in approximate cosmic abundance

The cosmic ray flux is modulated by the solar activity,[10] being a maximum about 1 year after a solar minimum and a minimum about 1 year after a solar maximum. This effect is greatest at the lower particle energies (0.5 to 30 Bev) and is due to the emission of plasma clouds from the sun. The integrated cosmic ray fluxes are:[8]

Near Solar Maximum:

~ 2.0 ±0.3 protons/cm^2/sec. (isotropic)

or ~ 7×10^7 protons/cm^2/year

Near Solar Minimum:

~ 4 protons/cm^2/sec. (isotropic)

or ~ 1.3×10^8 protons/cm^2/year

The energy range of the particles is 40 Mev to 10^{13} Mev, with the differential energy spectrum represented by:[10]

$$N(E)\ \Delta E = \frac{\Delta E}{(1+E)^n} \text{ particles/cm}^2\text{/sec.}$$

where: $N(E)\,\Delta E$ is number of particles between E & E+ΔE (E in Bev)

n is 2.1 for $2 < E < 15$ Bev

= 2.5 for $E > 15$ Bev

Figure 5.0-1 illustrates the cosmic ray spectrum.[11] Below 1 Bev the flux decreases as rapidly as above 1 Bev.

5.1 Cosmic Ray Fluxes Near Earth and Mars. The very high energies of the cosmic ray particles mean that the shielding effects of the earth's magnetic field and the Martian atmosphere can be neglected. However, since the cosmic flux is isotropic, being near a planet will reduce the flux by an amount proportional to the solid angle subtended by the planet. This effect will be negligible as regards radiation damage, but will be important for calculations of the background count rate during the Martian descent.

The cosmic flux is believed constant between earth and Mars since cosmic rays originate far outside the solar system and so should not exhibit any spatial dependence for the earth-Mars transit.

FIGURE 5.0-1

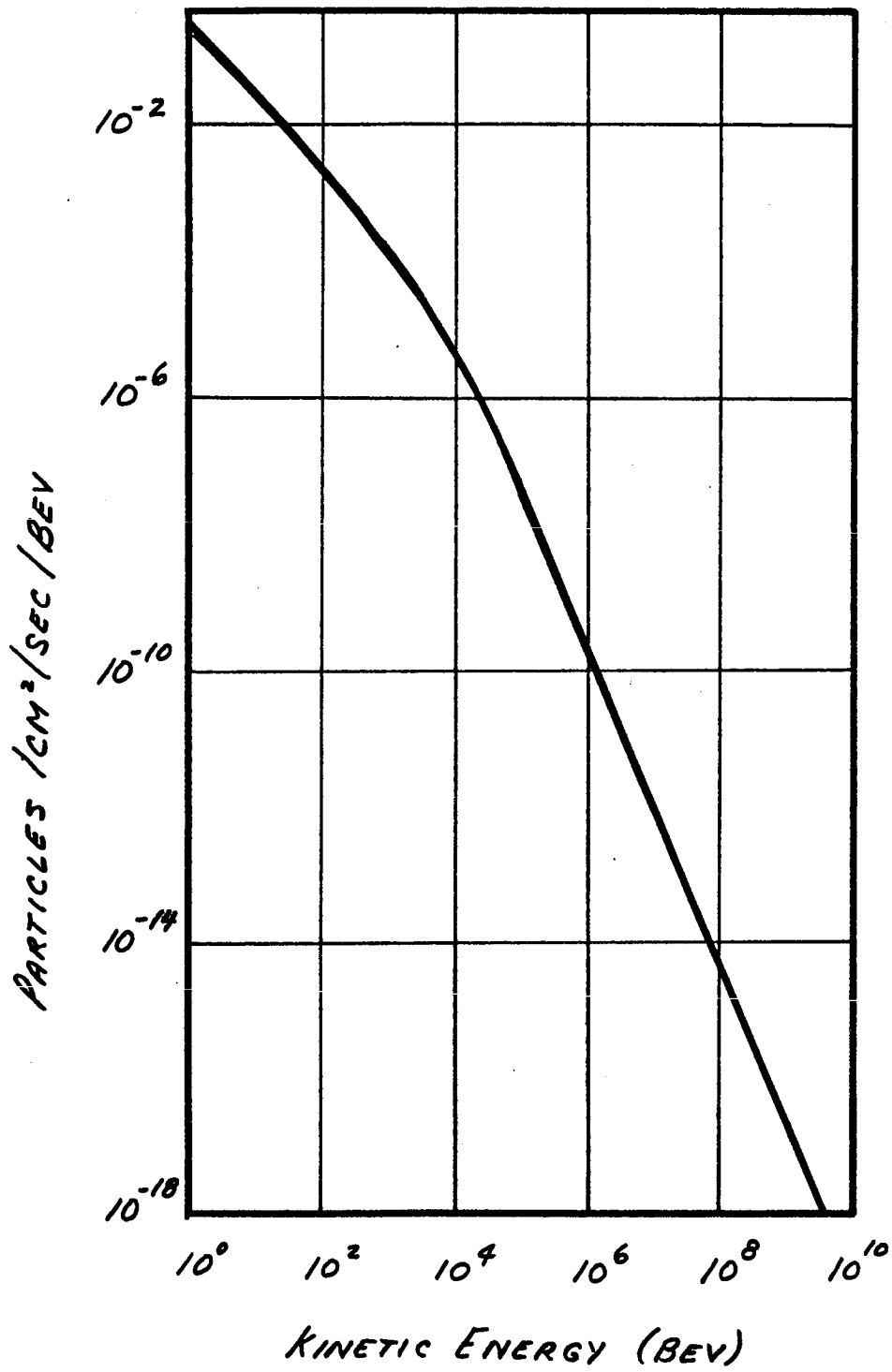

SPECTRUM OF GALACTIC COSMIC RAYS

6.0 RADIOISOTOPES IN THE MARTIAN SURFACE LAYER

In the absence of information concerning the quantitative distribution of radioisotopes near the Martian surface, it is assumed that the relative abundance of the isotopes is equal to that found on earth, with the omission of fission fragments. Since Mars is actually less dense than earth[13] (3.95g/cc versus 5.52g/cc), the relative abundance of the heavy radioactive elements on Mars may be noticeably less than that found on earth, and so this specification of the Martian surface's natural radiation is a worst case.

6.1 Types of Radiation. The radiations emitted by the surface consist of α, β, and γ rays. Assuming a maximum α particle energy of 10.5 Mev (most earth radioisotopes emit 4 to 6 Mev α's with a few as high as 10.5 Mev), the maximum α particle range[14] will be 11.5 cm of dry sea level air (on earth) which is equivalent to .014 gm/cm^2 of air. Since the model 3 Martian atmosphere has a density of 2.2×10^{-5} g/cc at Mars surface, the range of the maximum energy α particles will be $(.014)/(2.2 \times 10^{-5}) = 700$ cm or 7 meters. Therefore, there will be no natural α particle flux at altitudes $>$ 30 feet on Mars, and so α particle emissions will be ignored. Different elemental compositions of the earth and Martian atmospheres is not important here.

Regarding β particles, even those with as much as 3 Mev of energy (quite rare) will penetrate only 1.69 gm/cm^2 of air,[15] which is equivalent to a distance of $(1.69/2.2 \times 10^{-5}) = 77{,}000$ cm or approximately 2,600 feet on Mars. Also, these rare 3 Mev β's cannot reach the atmosphere if they originate $>$ 0.5 cm below the Martian surface, whereas a 2 Mev γ ray has an $\sim$ 50% chance of penetrating $\sim$ 4 cm of surface rock or $\sim$ 30,000 feet of model 3 atmosphere. The β background, therefore, will be ignored and only the γ rays will be considered, as follows.

6.2 Martian Radioisotope Abundance. The major sources[16] contributing to the γ ray spectrum at the surface are K-40 and some of the radioactive daughter products of U-238 and Th-232. The dominant sources and their radiations are:

Tl-208	2.614 Mev
Bi-214	1.76 Mev
K-40	1.46 Mev

In addition there are other much less intense γ rays from other elements in the radioactive decay series, but they are not individually apparent from the observed γ ray spectra.[17]

The production rate of the 1.46 Mev γ rays of K-40 for each gram of surface material is given by the formula:

$$N(1.46) = n(K\text{-}40) \left(\frac{.693\ C(K\text{-}40)}{\tau(K\text{-}40)}\right) \qquad (6.2\text{-}1)$$

where: $N(1.46)$ = number of 1.46 Mev γ rays/gm/sec.

$n(K\text{-}40)$ = number of K-40 nuclei/gm of material

τ(K-40) = half-life of K-40, i.e., 1.3×10^9 years
$= 4.1 \times 10^{15}$ seconds

C(K-40) = proportion of K-40 disintegrations that result in a 1.46 Mev γ

and $n(K\text{-}40) = \dfrac{(\text{proportion of K-40 per gram}) \times 6.03 \times 10^{23}}{\text{Atomic weight of K-40}}$ (6.2-2)

Because the radioisotope decay chains have had sufficient time to reach equilibrium, the half lives used for the Bi-214 and Tl-208 cases are those of the longest-lived isotopes occurring previously in their respective radioactive series, i.e., U-238 and Th-232 respectively. In addition, the numbers of U-238 and Th-232 nuclei per gram are used where n(K-40) appears in the example. The resulting production rates per gram of material for the three dominant γ rays are shown in Table 6.2-I, as well as other intermediate data and results.

However, these production rates are not the rates at which γ's emerge from the surface. These latter rates are calculated next.

6.3 γ Ray Fluxes Emerging from the Martian Surface. This flux calculation is undertaken because radiation surveys over the earth's surface differ considerably in their results and it is felt that greater accuracy can be obtained at present by calculation.

In addition to the γ ray energies tabulated in Table 6.2-I, there will be a flux of γ rays of various energies due to the decay of other portions of the U-238 and Th-232 radioisotope series. Many of these are low energy radiations which will not

TABLE 6.2-I

PRODUCTION OF 2.61, 1.76 AND 1.46 MEV γ RAYS

ISOTOPE	E_γ	HALF-LIFE (sec) (19)	CONCENTRATION (parts/10^6) (20,21)	γ-RAY ABUN-DANCE (19)	n(Isotope) /gm	$N(E_\gamma)$ /gm/sec.
K-40	1.46	4.1×10^{16} (K-40)	3.1	0.11	4.61×10^{16}	0.086
Bi-214	1.76	1.42×10^{17} (U-238)	4	?*	1.0×10^{16}	0.049
Tl-208	2.61	4.4×10^{17} (Th-232)	12	1.00	3.1×10^{16}	0.071

* Assumed $\sim$ 1.0 due to observed prominence of 1.76 Mev γ peak - a worst case

emerge from the surface and so can be neglected. Those that do emerge will be assumed to have a flux equal to 25% of the total emergent flux due to the production of 2.61, 1.76 and 1.46 Mev γ rays. The 25% assumption is based upon observed earth γ ray spectra.[17] The maximum energy of this "minor" emergent flux will be set at approximately 1.0 Mev, based upon inspection of observed spectra and the decay chains producing the γ rays. In addition, the flux due to the scattering of the three dominant γ energies in the Martian soil will also have an average energy of approximately 1.0 Mev since the most likely energies of singly scattered γ rays are approximately:

Original E_γ (Mev)	Scattered E_γ' (Mev)	Relative Production Intensities of Primaries
2.61	1.4	0.8
1.76	1.0	0.6
1.46	0.8	1.0

Thus, the spectrum of γ rays emerging from the Martian surface will consist of the three primary energies noted above, plus their scattered γ rays (centered about $\sim$ 1.0 Mev but extending up to nearly 2.6 Mev), plus the minor flux centered at 0.5 Mev and equal in strength to 25% of the sum of the foregoing.

6.3.1 Flux Calculations. To calculate the emergent fluxes, it is assumed that all γ rays emitted parallel to or away from the Martian surface are completely absorbed and never reach the atmosphere. Though some of these may actually reach the surface, they are compensated for by those which are emitted towards the surface but are scattered back towards the interior.

As in Figure 6.3.1-1, consider a source S buried a distance R below the Martian surface. From the figure, the following conclusions can be obtained for a γ ray emitted from source S at angle θ to the horizontal.

(a) The distance D through which the γ must travel if it is to reach the surface without scattering is:

$$D = \frac{R}{\sin\theta}$$

(b) The proportion P of all emitted γ rays that are emitted within angle $d\theta$ about angle θ is (for infinitesimals):

$$P = \frac{2\pi aL}{4\pi R^2} = \frac{(Rd\theta)(2\pi R\cos\theta)}{4\pi R^2} = \frac{\cos\theta\ d\theta}{2}$$

(c) Using the exponential attenuation law, the probability of a γ ray passing through distance $D = R/\sin\theta$ of matter without interaction is:

$$p = \exp(-\mu\rho D) = \exp(-\mu\rho R/\sin\theta) = \exp(-\mu m/\sin\theta)$$

FIGURE 6.3.1-1

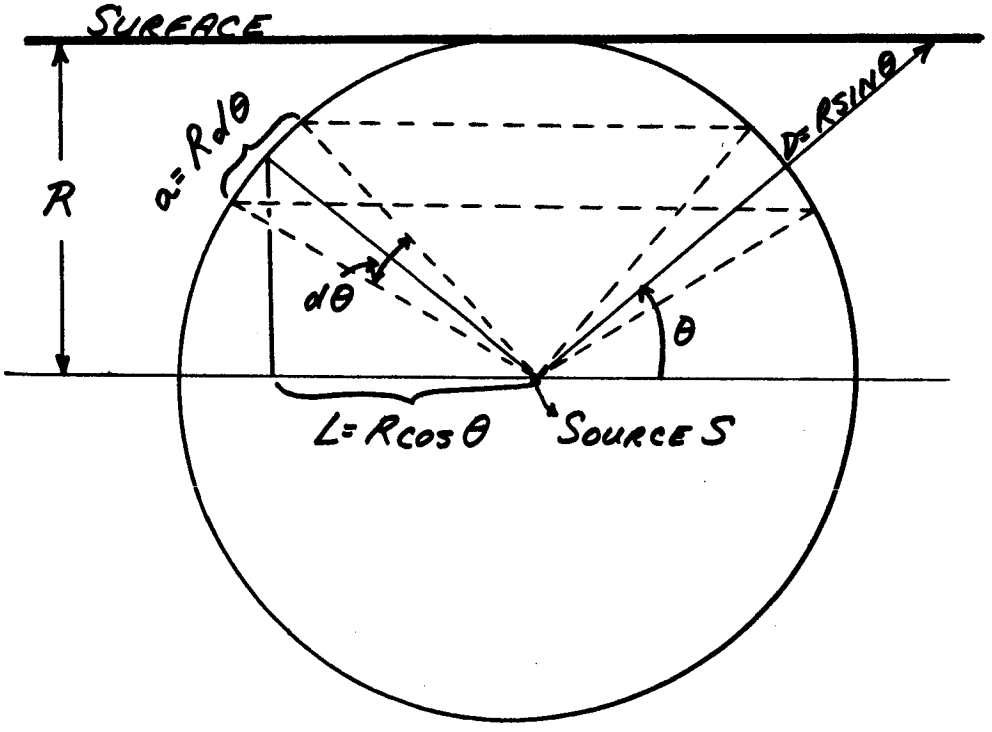

where: μ = total attenuation coefficient (cm^2/gm)

ρ = material density (gm/cc)

$m = \rho R$ = mass of material/cm^2 between source S and surface in direction perpendicular to surface

D is in cm.

Consider a column of material of 1 cm^2 cross-sectional area which is oriented perpendicular to the Martian surface. Consider an elemental mass dm within the column. If $n(E_\gamma)$ γ rays of energy E_γ are produced by each gram of material, then $n(E_\gamma)dm$ γ rays of energy E_γ are produced in dm. If angles θ and $d\theta$ are fixed, the number of γ's of energy E_γ emitted within dm at angle θ and reaching the Martian surface without interaction is:

$$dN(E_\gamma\theta) = n(E_\gamma)dm \left(\frac{\cos\theta\, d\theta}{2}\right) \exp(-\mu m/\sin\theta)$$

where m is mass of material per cm^2 between dm and surface.

If $dN(E_\gamma\theta)$ is integrated over all values of $m = 0 \rightarrow \infty$ and then over $\theta = 0 \rightarrow \pi/2$, the result is:

$$N(E_\gamma) = \int_{\theta=0}^{\pi/2} \int_{m=0}^{\infty} \frac{\cos\theta\, n(E_\gamma)}{2} \exp(-\mu m/\sin\theta)dm\, d\theta$$

$$= \int_{\theta=0}^{\pi/2} \frac{n(E_\gamma)\cos\theta\, d\theta}{2} \cdot \frac{\sin\theta}{\mu} \times \int_{m=0}^{\infty} \exp(-\mu m/\sin\theta)d(\mu m/\sin\theta)$$

$$= \int_{\theta=0}^{\pi/2} \frac{n(E_\gamma)\ \cos\theta\ \sin\theta\ d\theta}{2\mu} = \frac{n(E_\gamma)}{4\mu}$$

= number of γ rays of energy E_γ which are emitted by a 1 cm^2 column of material extending perpendicular to and below the Martian surface, and which reach the Martian surface without interaction.

The value of μ in the foregoing equation depends on the γ ray energy and also upon the atomic number of the material. Regarding this latter dependence, the composition by weight of the earth's surface[20] (assumed to be the same for Mars) is such that its nuclear properties (γ ray interactions) can be represented by those of aluminum, and so the appropriate $\mu(E_\gamma)$ interaction coefficients are:

$$\mu(2.61\ \text{Mev}) = 0.038\ cm^2/gm$$
$$\mu(1.76\ \text{Mev}) = 0.046\ cm^2/gm$$
$$\mu(1.46\ \text{Mev}) = 0.051\ cm^2/gm$$

There still remain, however, the γ ray fluxes due to the scattering of the three primary γ ray energies in the soil.

If the unscattered primary flux from an isotope emitting γ ray of energy E_γ is given by:

$$I(E_\gamma) = I_o(E_\gamma)\ \exp(-\mu m)$$

then the energy flux due to these unscattered γ rays will be:

$$L(E_\gamma) = E_\gamma I(E_\gamma) = E_\gamma I_o(E_\gamma) \exp(-\mu m)$$

However, due to the presence of scattered γ rays (originally of energy E_γ), the total energy flux from the isotope is:

$$L_t(E_\gamma) = bL(E_\gamma)$$

where the buildup factor b is greater than unity due to the presence of the degraded γ rays. From the foregoing equations, it is obvious that the energy flux due to scattered γ rays is:

$$L'(E_\gamma) = L_t(E_\gamma) - L(E_\gamma) = (b-1)\, L(E_\gamma)$$

Also, if the scattered γ rays have an average energy E_γ' then their flux will be:

$$I(E_\gamma') = \frac{L'(E_\gamma)}{E_\gamma'} = \frac{E_\gamma}{E_\gamma'}\,(b-1)\, I_o(E_\gamma) \exp(-\mu m)$$

$$= \frac{E_\gamma}{E_\gamma'}\,(b-1)\, I(E_\gamma)$$

To calculate the emergent degraded γ ray flux due to a soil radioisotope emitting γ rays of energy E_γ, substitute $\frac{E_\gamma}{E_\gamma'}(b-1)\exp(-\mu m)$ for $\exp(-\mu m)$ in the first line of the equation for $N(E_\gamma)$, i.e., now

$$N'(E_\gamma) = \int_{\theta=0}^{\pi/2} \int_{m=0}^{\infty} \frac{\cos\theta\, n(E_\gamma)}{2} \frac{E_\gamma}{E_\gamma'}\,(b-1) \exp(-\mu m)\, dm\, d\theta$$

From graphs[22] of b versus μm and E_γ, it is found that b exp(-μm) decreases by approximately a factor of 2 for each increase of one unit is μm above $\mu m = 1$, and thus (again from the graphs) the value of b exp(-μm) is:

$$E_\gamma = 1.0 \text{ Mev:} \quad b \exp(-\mu m) = 1.9(2^{-\mu m}) = 1.9(e^{-.69\mu m})$$

$$E_\gamma = 2.0 \text{ Mev:} \quad b \exp(-\mu m) = 1.4(2^{-\mu m}) = 1.4(e^{-.69\mu m})$$

$$E_\gamma = 3.0 \text{ Mev:} \quad b \exp(-\mu m) = 1.2(2^{-\mu m}) = 1.2(e^{-.69\mu m})$$

where μ is $\mu(E_\gamma)$ as before--the total interaction coefficient. These exponential equations predict too high a flux at low (μm) values, so their use constitutes a worst case.

The appropriate equations for the 1.46, 1.76, and 2.61 Mev γ rays are gotten from the preceding cases by interpolation and are:

$$1.46 \text{ Mev:} \quad b \exp(-\mu m) = 1.65 \exp(-.69\mu m)$$

$$1.76 \text{ Mev:} \quad b \exp(-\mu m) = 1.5 \exp(-.69\mu m)$$

$$2.61 \text{ Mev:} \quad b \exp(-\mu m) = 1.3 \exp(-.69\mu m)$$

By substitution of these equations, the values of $N'(E_\gamma)$ are found. For example:

$$N(1.46 \text{ Mev}) = \frac{n(1.46)}{4\mu(1.46)}$$

$$N'(1.46 \text{ Mev}) = \left[\frac{1.65n\ (1.46)}{4(.69)\mu(1.46)} - \frac{n(1.46)}{4\mu(1.46)}\right]\left(\frac{E_\gamma}{E_\gamma}\right)$$

$$= 1.39\left(\frac{E_\gamma}{E_\gamma}\right)\left(\frac{n(1.46)}{4\mu(1.46)}\right)$$

Table 6.3.1-I shows the primary and degraded fluxes emerging from the Martian surface due to the presence of the isotopes K-40, Bi-214 and Tl-208. The last column, which is arbitrarily 25% of the sum of the foregoing fluxes, represents the contributions of the other numerous but less important members of the radioactive decay chains. Their average energy is about 0.5 Mev. Note that the average scattered γ ray energy E_γ' is assumed to be 50% of the original energy E_γ. This assumption is based on the observation of γ ray spectra emerging through thick absorbers. The fluxes of Table 6.3.1-I lie within the range of the observed fluxes of references (16) and (24), after the latter are corrected for the detector efficiency and the altitude of observation.

There are two final points to consider. Although the unscattered fluxes will still have the primary energies as given in Table 6.3.1-I, the degraded fluxes will have continuous energy distributions with the primary energy as the maximum possible in each case. No attempt is made to predict these continuous distributions. Instead, they will be added together and assumed to be approximately mono-energetic at $\sim$ 1.0 Mev.

The second and final point is a note that certain types of rocks have greater than average concentration of radioisotopes. It is therefore recommended that the tabulated fluxes be doubled when calculating the radiation background during the descent through the Martian atmosphere.

TABLE 6.3.1-I

ESTIMATED γ RAY FLUXES EMERGING FROM MARTIAN SURFACE DUE TO NATURALLY-OCCURRING RADIOISOTOPES

Isotope	E_γ (Mev)	Primary Flux γ's/cm^2/sec.	Scattered Flux γ's/cm^2/sec.	Minor Flux γ's/cm^2/sec.
K-40	1.46	.42	1.17	.40
Bi-214	1.76	.27	.62	.22
Tl-208	2.61	.47	.82	.32
TOTALS		1.16	2.61	0.94

REFERENCES

(1) "A Study of Space Radiation Shielding Problems for Manned Vehicles", FZK-144, 8 June 1962, General Dynamics, Forth Worth, page 23.

(2) "Computer Analysis of Radiation Shielding", AMRL-TDR-64-11, Biophysics Laboratory, WPAFB, February 1964, page 13.

(3) "The Natural Environment for the Manned Orbiting Laboratory System Program (MOL)", AFCRL-64-845, 25 October 1964, last 3 pages and also pages 8 & 9.

(4) "The Space-Radiation Environment and Its Interactions With Matter", REIC Report No. 37, Battelle Memorial Institute, Jan. 15, 1965, pages 17-20.

(5) Ibid, pages 22 and 23.

(6) See Reference (2), page 28.

(7) "Space Radiation Guide", AMRL-TDR-62-86, Biomedical Laboratory, WPAFB, August 1962, page 14.

(8) "Space Environment Criteria Guidelines for Use in Space Vehicle Development", NASA TM X-53273, R. E. Smith, Aero-Astrodynamics Laboratory, MSFC, Huntsville, May 27, 1965.

(9) "Manned Spacecraft: Engineering Design & Operation", Purser, Faget & Smith, Fairchild Publications, Inc., page 100.

(10) See Reference (2), page 27.

(11) See Reference (2), page 29.

(12) Aviation Week, page 16, 7-26-65.

(13) Handbook of Chemistry & Physics, 37th Edition, page 3076.

(14) "The Atomic Nucleus", R. D. Evans, McGraw-Hill, 1955, page 650.

(15) "Energy Loss and Range of Electrons and Positrons", NBS Circular 577, page 21.

(16) "The Natural Radiation Environment", Adams and Lowder, University of Chicago Press, 1964, page 747 and onward.

(17) Ibid, page 750.

(18) See Reference (13), page 3073.

(19) Handbook of Chemistry and Physics, 45th edition, pages B-11 to B-79.

(20) Ibid, page F-81.

(21) "The Chart of the Nuclides", David T. Goldman, General Electric Co., 8/64.

(22) Radiological Health Handbook, PB 121784R, U. S. Department of Health, Education & Welfare, Sept. 1960, pages 147-150.

(23) "Gamma-Ray Absorption Coefficients for Elements 1 through 100 Derived from the Theoretical Values of the National Bureau of Standards", LA-2237, Los Alamos Scientific Laboratory.

(24) See Reference (16), pages 705 to 736.

appendix B

APPENDIX B

THE INTERACTION OF ELECTROMAGNETIC RADIATIONS WITH MATTER

THE INTERACTION OF ELECTROMAGNETIC RADIATIONS WITH MATTER

The possible interactions between γ rays and matter are the 9 combinations of the 3 kinds of interactions and the 3 effects of interaction listed below.* Note that mesonic interactions have been omitted since they require energies upwards of 100 Mev, which is vastly in excess of the photon energies to be used.

Kind of Interaction	Effect of Interaction
(1) Interaction with atomic electrons	(a) Complete absorption
(2) Interaction with nucleons	(b) Elastic scattering (coherent)
(3) Interaction with electric field surrounding nuclei or electrons	(c) Inelastic scattering (incoherent)

The contributions of the 9 possible combinations are as follows:

(1a) Photoelectric Absorption - The γ ray energy is completely transferred to an electron which is thus forced out of its orbit about the atom. The net result is a high speed free electron which has a negligible chance of contributing to the detector count rate.

(1b) Rayleigh Scattering - The tightly bound atomic electrons act in unison to scatter the γ without change in energy. The permissible Rayleigh scattering angles are small; e.g., 60 to 70% of the Rayleigh scatters are confined to deflections of less than 15° for 0.1 Mev γ rays interacting with aluminum. For 0_2 and N_2, etc., the angles are even less. Since it is planned to detect γ's that have been scattered through well over 90°, Rayleigh scattering will be a negligible contributor.

* Reference: "The Atomic Nucleus", page 672, R.D. Evans, pub. by McGraw-Hill, New York, 1955.

(1c) Compton Effect - This has no angle limitations, although certain angles are indeed more probable, and is the major contributor. In Compton scattering, a γ ray scatters from a single electron in an orbit about a nucleus. The electron is freed from its orbit, thus absorbing some of the original photon's energy. The energy of the scattered photon depends on its original energy, the energy required to free the electron, and the angle of scattering.

(2a) Nuclear Photodisintegration - The γ ray enters the nucleus and gives all its energy to a single nucleon, thus ejecting said nucleon. For the γ ray energies contemplated, this process is impossible.

(2b) Nuclear Thomson Scattering - Here, γ rays scatter without energy loss with the nucleus as a whole - a negligible effect.

(2c) Nuclear Resonance Scattering - In this area, the photon is absorbed by the nucleus and is then re-emitted without energy loss. All angles to the original photon's direction are equally probable. However, this form of interaction is very rare and can be neglected.

(3a) Pair Production - The photon enters the electric field and is converted into an electron and a positron. A minimum γ ray energy of 1.02 Mev is necessary, but the probability of this effect does not approach that of the Compton effect until photon energies well in excess of 1.02 Mev.

(3b) Delbruck Scattering - This scattering without energy loss from the electric field is so unlikely that it has not been definitely detected yet.

(3c) Not detected and therefore negligible.

appendix C

APPENDIX C

SELECTION OF THE SOURCE-DETECTOR GEOMETRY AND CALCULATION OF SOURCE STRENGTH

1.0 INTRODUCTION

The first step in this appendix is a more rigorous development of the scattering theory beyond the simple outline given in Chapter 3 of Part I. This theory is then used to select the source-detector geometry and to calculate the necessary source strength of 100 Kev γ rays. This strength is 20 γ curies when source and detector are 105 cm apart and have collimator half angles of $\sim 45°$, and when a backscatter count rate of 230 cps is required at 25 km in the model 3 Martian atmosphere. A detector of 5 cm diameter by 1.25 cm thick NaI(Tl) is assumed.

2.0 SCATTERING THEORY

Consider Figure 2.0-1. The source and the detector are located in a plane and are separated by distance r. The flat detector face with area A_d lies in this plane. A point source is assumed. Angles ψ and θ are measured from the source-detector line. ϕ is measured from the detector plane and in a direction perpendicular to the source-detector line, as shown. Scattering center C is defined by the angles ψ, θ and ϕ, and so subtends the fraction

$$\frac{(Sd\psi)(S\sin\psi d\phi)}{4\pi S^2} = \frac{\sin\psi \; d\psi \; d\phi}{4\pi} \qquad (2.0\text{-}1)$$

of the total solid angle around the source, where S is the distance of C from the source.

Accordingly, the rate at which primary energy γ rays from the monoenergetic source are scattered in C is:

FIGURE 2.0-1

SOURCE-DETECTOR GEOMETRY

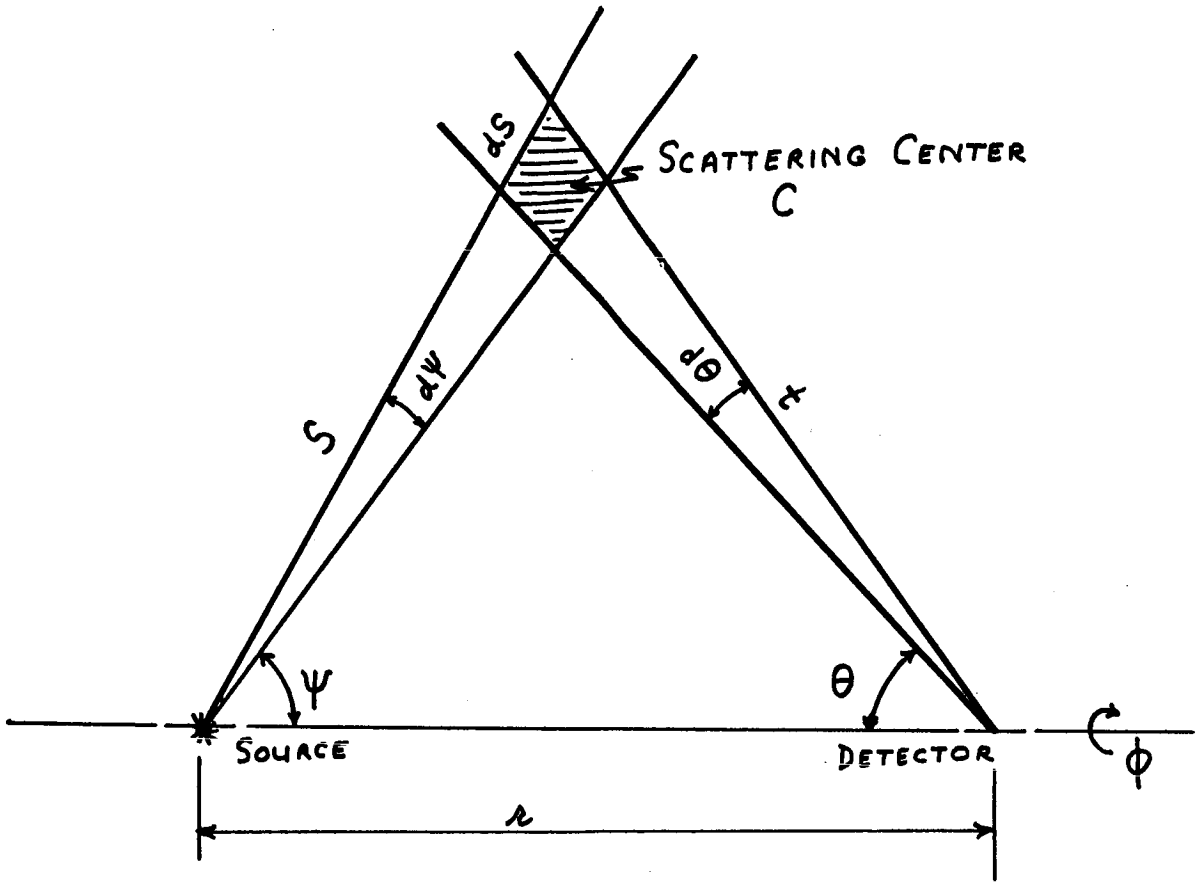

$$I_c = I_o \, \beta\left(\frac{\sin\psi \, d\psi \, d\phi}{4\pi}\right) \mu\rho dS \quad \gamma\text{'s/sec.} \tag{2.0-2}$$

where: I_o is the source strength, γ's/second

β is the attenuation factor due to the heat shield and shock wave

μ is the atmospheric scattering coefficient, in cm^2/gm

ρ is the atmospheric density, gm/cc

dS is the thickness of the scattering center C, in cm

Of the I_c primary energy photons scattered at C, the number detected is:

$$I_s' = \frac{I_c \, A_d \, \epsilon_d \, \sin\theta \, \sin\phi}{4\pi t^2} \tag{2.0-3}$$

where: A_d is the detector area

ϵ_d is the detector efficiency

t is the distance of the detector from the scattering center C

Therefore:

$$I_s' = \frac{I_o \, \beta\mu\rho \, A_d \, \epsilon_d \, \sin\psi \, \sin\theta \, \sin\phi \, d\psi \, d\phi \, dS}{16\pi^2 t^2} \tag{2.0-4}$$

From Figure 2.0-1, it can be shown that:

$$t = \frac{r \sin\psi}{\sin(\pi-\theta-\psi)} = \frac{r \sin\psi}{\sin(\theta+\psi)} \tag{2.0-5}$$

$$S = \frac{r \sin\theta}{\sin(\pi-\theta-\psi)} = \frac{r \sin\theta}{\sin(\theta+\psi)} \qquad (2.0\text{-}6)$$

and: $$dS = \frac{\sin(\pi/2)td\theta}{\sin(\theta+\psi)} = \frac{td\theta}{\sin(\theta+\psi)} \qquad (2.0\text{-}7)$$

so: $$I_s' = \frac{I_o \beta\mu\rho A_d \epsilon_d \sin\theta \sin\phi \, d\theta \, d\psi \, d\phi}{16\pi^2 r} \qquad (2.0\text{-}8)$$

Thus, the total count rate due to all the scattering centers is:

$$I_s = \int I_s' \, dV \quad \text{(i.e., integrate over all scattering centers)}$$

$$= \frac{I_o \beta\mu\rho A_d \epsilon_d}{16\pi^2 r} \iiint \sin\theta \sin\phi \, d\theta \, d\psi \, d\phi \qquad (2.0\text{-}9)$$

The limits of integration are:

(a) ϕ: $\phi = \phi_o \longrightarrow (\pi-\phi_o)$, i.e., use a geometry which is symmetric with respect to the source-detector plane. No loss of generality since source-detector plane is arbitrary.

(b) θ: $\theta = \theta_o \longrightarrow (\pi-\psi)$, i.e., there can be no scattering centers for $\theta > (\pi-\psi)$ since then there is no intersection between the "beams" from source and detector.

(c) ψ: $\psi = \psi_o \longrightarrow (\pi-\theta_o)$, i.e., same effect as for θ upper limit.

When the integration has been carried out, the result is:

$$I_s = \frac{I_o \beta\mu\rho A_d \epsilon_d \cos\phi_o}{8\pi^2 r} \left[\sin\theta_o - \sin\psi_o + \cos\theta_o(\pi-\theta_o-\psi_o)\right] \qquad (2.0\text{-}10)$$

3.0 SELECTION OF SYSTEM GEOMETRY

In the foregoing equation, ϕ_o, θ_o, ψ_o and r depend on the system geometry, and remain to be chosen. Their values depend on the shock wave thickness. From the present knowledge of the MP/L and the likely location of the density sensor on one side of the vehicle nose, a shock wave thickness of 30 cm is reasonable. Since the heat shield will be no more than 2.5 cm thick and the source and detector can each be placed ~ 3.8 cm behind the shield, the geometry defining parameters must be chosen so that all scattering centers are at least 36 cm from the source-detector line. However, this allows $\phi_o = 90°$ only, since the greater radius of curvature of the shock wave (as seen along the MP/L axis) means that the scattering centers for $\phi_o < 90°$ will sometimes be in the shock wave. Accordingly, require that no scattering center be closer to the source-detector line than distance D = 46 cm. A reasonable vehicle configuration and density sensor location will then let ϕ_o be 45°. The remaining parameters, θ_o, ψ_o and r are then chosen.

First, let $\psi_o = \theta_o$, i.e., both source and detector have symmetrical collimation, a normal procedure for optimizing systems. The term $\left[\sin\theta_o - \sin\psi_o + \cos\theta_o(\pi - \theta_o - \psi_o)\right]$ in the expression for I_s becomes simply $(\pi - 2\theta_o)\cos\theta_o$ and since $\cos\theta_o = r \sin\theta_o / 2D$, it is the expression

$$(\pi - 2\theta_o)\,\frac{r \sin\theta_o}{2D} \qquad (3.0\text{-}1)$$

that must be maximized. Standard methods show that this maximum occurs at $\theta_o = 41°$, so $r = 2D/\tan 41° = 2.30D = 105$ cm (3.45 feet).

Therefore, the system geometry is defined by:

$r = 105$ cm

$\phi_o = 45°$

$\theta_o = 41°$

$\psi_o = 41°$

and the detector count rate is:

$$I_s = 1.10 \times 10^{-4} I_o \beta\mu\rho A_d \epsilon_d \text{ counts/second} \qquad (3.0\text{-}2)$$

This expression is approximate because it assumes an isotropic source and isotropic scattering in each scattering center, neither of which are quite true. Scattering in the atmosphere prior to and after reaching the scattering region is ignored as well, but this is a very good approximation for the atmospheric densities being considered. In view of the limited data available regarding the MP/L vehicle structure, greater detail is not warranted in the geometry optimization process.

Note that I_s is the count rate due to primary energy γ rays from the source which reach the detector after only one scatter (in the atmosphere).

4.0 SOURCE STRENGTH

To obtain the source strength I_o as a function of the back-scatter count rate I_s, the parameters β, μ, ρ, A_d and ϵ_d must be known. A 100 Kev γ source is assumed. In view of the system geometry, it is assumed that the average γ ray penetrates the heat shield at an angle of 30° to the perpendicular. For a 2.5 cm heat shield of 0.5 gm/cc Refrasil-like material, 59% of the γ rays will penetrate the heat shield over both the source and the detector without interaction. Therefore:

$$\beta = 0.59 \qquad (4.0\text{-}1)$$

Losses in the shock wave are negligible ($\ll$ 1%). Next there is the scattering coefficient μ, which is:

$$\mu = 0.125 \text{ cm}^2/\text{gm} \qquad (4.0\text{-}2)$$

for all the specified model Martian atmospheres.

For system accuracy calculations, an altitude of 25 km in the specified model 3 atmosphere is used. The ambient density there is[2]:

$$\rho = 2.31 \times 10^{-6} \text{ gm/cc} \qquad (4.0\text{-}3)$$

Finally, there are the detector parameters A_d and ϵ_d. A likely detector is NaI(Tl) of 5 cm diameter by 1.25 cm thick. This has:

$$A_d = 20 \text{ cm}^2 \qquad (4.0\text{-}4)$$

$$\epsilon_d = 1.0 \text{ for 100 Kev } \gamma \text{ rays} \qquad (4.0\text{-}5)$$

Using the foregoing parameters, the source strength I_o is:

$$I_o = 2.67 \times 10^9 I_s \qquad (4.0\text{-}6)$$

where I_s is the desired backscatter count rate.

There remains only the angular dependence of the scattering to be considered. For the specified system geometry, an average scattering angle of 150° is assumed. For 100 Kev γ's scattering at this average angle, formulas in reference (13) are used to calculate a correction factor of 1.18. Therefore:

$$I_o = 3.15 \times 10^9 I_s \qquad (4.0\text{-}7)$$

and so the necessary source strength for I_s = 230 cps is:

$$I_o = \frac{3.15 \times 10^9 \times 230}{3.7 \times 10^{10}} \qquad (4.0\text{-}8)$$

$$= 19.6\ \gamma \text{ curies}$$

However, this is only the source strength needed during the descent through the Martian atmosphere. A greater strength source must be obtained if there is to be source decay during the eight-month transit to Mars.

appendix D

APPENDIX D

RESOLVING TIME ERROR

RESOLVING TIME ERROR

The MP/L will travel a significant vertical distance in a one-second sampling period. Assuming a linear variation of density over the one-second interval, the altitude corresponding to the average density is one-half second earlier than the altitude at the readout time. This half-second time shift in altitude correlation is easily compensated for during data reduction. The deviation from a linear density change over this one-second period will, however, introduce an error. The magnitude of this error may be determined as follows. It can be assumed conservatively that the density variation with altitude for a sampling period is the exponential function:

$$\rho = \rho_o e^{-\beta h}$$

where: h_1 = altitude at start of the averaging interval

h_3 = altitude at end of the averaging interval

h_2 = altitude at the altitude center of the averaging interval

The measured density reading is the average over the interval, i.e.,

$$\rho_m = \frac{\int_{h_1}^{h_3} \rho_o e^{-\beta h} \, dh}{h_3 - h_1}$$

$$= \frac{\rho_o (e^{-\beta h_1} - e^{-\beta h_3})}{\beta (h_3 - h_1)}$$

The fractional deviation of this measured density from the actual density ρ_2 at the interval center is:

$$\frac{\rho_\epsilon}{\rho_2} = \frac{\rho_m - \rho_2}{\rho_2} = \frac{e^{-\beta(h_1-h_2)} - e^{-\beta(h_3-h_2)}}{\beta(h_3-h_1)} - 1$$

If Δh is the vertical travel over the interval, then:

$$\frac{\rho_\epsilon}{\rho} = \frac{e^{-\beta\Delta h/2} - e^{+\beta\Delta h/2}}{-\beta\Delta h} - 1$$

Expanding the exponentials gives:

$$\frac{\rho_\epsilon}{\rho} = \frac{(\beta\Delta h)^2}{24} + \frac{(\beta\Delta h)^4}{1920} + \ldots\ldots$$

For $\beta\Delta h < 1$, the second and successive terms can be neglected. Thus:

$$\frac{\rho_\epsilon}{\rho} = \frac{(\beta\Delta h)^2}{24}$$

The maximum β is obtained from the model 3 atmosphere profile at 25 kilometers altitude. This is 0.14 km^{-1}. The maximum vertical velocity expected is 5 km/second and much less if the MP/L is not coming down vertically at that altitude. The maximum velocity fractional error expected is thus:

$$\frac{\rho_\epsilon}{\rho} = \frac{(.14 \times 5)^2}{24} = 2.04 \times 10^{-2}$$

or: $\pm 2.0\%$

appendix E

APPENDIX E

GENERATION OF SOURCE ENERGY GUIDELINES

TABLE OF CONTENTS

1.0 INTRODUCTION

This appendix generates the maximum γ ray energy limits used in selecting the γ ray source energy for the density sensing apparatus. The problem of the presence of additional γ rays of higher energy than those used to measure the density is considered, and limitations are placed upon the strength of these unwanted radiations.

The appendix commences by defining the density-sensing system and determining the thickness of the required shielding. Specific shielding mass calculations are then carried out for γ-radioisotope, X-ray tube, and hybrid sources. From these calculations, the guidelines emerge and are summarized in section 7.0.

Note that the calculations are simple and generally produce lax guidelines, so some sources which meet them may later be found to be unacceptable. However, the preliminary source search is kept reasonably non-restrictive since there are relatively few suitable sources.

2.0 SOURCE STRENGTH AND SIZE

As in Part I of the report, a source strength of 20 γ curies during descent serves as a guide to calculations. If a γ-radioisotope with a concentration of 200 curies/gram and a density of 5 gm/cm^3 is used, the source can be a sphere of .02 cm^3 volume, with a radius of $\sim$ 2 mm. In practice, however, the source strength (and size) must be increased to allow for self-absorption and radioactive decay.

Therefore, the γ-radioisotope source is assumed to be 20 γ curies (7.4×10^{11} γ's/sec) radiating from a sphere of 4 mm radius. The sizes of hybrid sources and X-ray tubes are discussed later.

3.0 DETECTOR COUNT RATE

The detector is a NaI(Tl) disc 5 cm in diameter by 1.25 cm thick. It is oriented edge on to the source and presents a target area of $5 \times 1.25 = 6.25$ cm^2 for the direct source to detector transmission. Since it is located 105 cm (3.45 feet) from the source, the total intensity of γ rays upon it due to an unshielded 20 γ curie source is:

$$\frac{7.4 \times 10^{11} \times 6.25}{4\pi(105)^2} = 3.4 \times 10^7 \ \gamma\text{'s/second}$$

Virtually all of these will interact with the detector, though the probability of total absorption declines as the energy rises. However, direct transmission γ rays will reach the detector with more energy than those γ rays which have backscattered in the atmosphere, as shown by the energies corresponding to a 150° angle of scatter.

E_γ = 100 Kev: E'_γ (150° scatter) = 73 Kev

E_γ = 200 Kev: E'_γ (150° scatter) = 116 Kev

E_γ = 300 Kev: E'_γ (150° scatter) = 143 Kev

Since energy discriminating electronic circuits are included in the conceptual design, many of the counts due to direct transmission will be rejected.

For a 100 Kev source and the proposed source-detector geometry, the wide range of acceptable scattering angles in the atmosphere will lead to a backscatter energy range of 71 to 84 Kev. This will in turn be broadened by the detector energy resolution to perhaps 60 to 100 Kev. Therefore, about 50% of the 100 Kev direct transmission counts will be rejected. A similar survey for the 200 and 300 Kev sources indicates that the electronics will achieve a rejection rate of about 90% for each. At higher energies, this rejection rate rises. Accordingly, the maximum estimated count rates due to the unshielded source are:

E_γ = 100 Kev: 2×10^7/second

E_γ = 200 Kev: 4×10^6/second

E_γ = 300 Kev: 4×10^6/second

Throughout this subsection, only 5 cm diameter by 1.25 cm thick NaI(Tl) is considered because this is the detector size finally chosen and because a highly efficient detector is needed to keep the source strength as low as 20 γ curies and the source cost below $50,000. A larger detector size means a rapid increase in its mass and the mass of the necessary photomultiplier tube.

4.0 NECESSARY SHIELD ATTENUATION FACTORS AND THICKNESS

Bearing in mind the backscatter count rate of 230 cps at 25 km in a model 3 atmosphere, it is decided that the direct transmission should not exceed 100 cps within the energy range acceptable to the electronics. Even so, this background will have a one-sigma statistical fluctuation of ±10 cps which constitutes a ±4.4% error in 230 cps. In practice, the average direct transmission will still likely be ±6% or more if a rate of 100 cps is allowed, since the average direct transmission rate cannot be exactly calibrated out. In the actual system design, this rate is reduced somewhat, but even if the 100 cps is accepted, the shielding will be called upon to attenuate the γ ray fluxes by factors of 4×10^4 (at 200 and 300 Kev) to 2×10^5 at 100 Kev. The required thickness of tantalum shielding is indicated below. The shielding density ρ is 16.6 gm/cm^3 and its thickness d is derived by standard methods.

E_γ (Kev)	Attenuation Factor	d (cm)
100	2×10^5	0.20
200	4×10^4	1.1
300	4×10^4	2.5

These results are used in the next section to calculate the masses of the required shielding.

5.0 SHIELDING MASSES

As discussed in section 2.0 of this appendix, the γ radioisotope is considered as a sphere of r_2 = 4 mm radius, and the shielding about it is spherical. For an X-ray tube, where the source is a spot of several millimeters radius on a metal target enclosed in a glass tube, a different shielding shape is needed. From practical experience, the X-ray tube itself is expected to have a 1.3 cm radius and a length of perhaps 8 cm. However, due to the shape of the radiation pattern emitted by the tube, a cylindrical shield of r_2 = 1.3 cm inside radius by L = 2.5 cm length is assumed. Finally, there is the hybrid source. If it involves an on/off mechanism, it will require a shield at least as great as that for the X-ray tube since the β emitting radioisotope will have to be spread out so its β's can reach the target with an appreciable portion of their original energy. If, however, there is no on/off device, the β emitter and its target can be powdered and pressed together into a ball perhaps no larger than that of the γ radioisotope. Both cases are listed in the table of necessary shielding masses below.

E_γ (Kev)	Shield Thickness d(cm)	Shield Mass (gm) γ Isotope	X-Ray Tube	Hybrid On/Off	Hybrid Constant
100	0.20	10.6	73	73	10.6
200	1.1	235	530	530	235
300	2.5	1690	1660	1660	1690

The formulas used for the above calculations are:

(a) γ Radioisotope

$$\text{Mass} = \frac{4}{3}\pi\rho((d + r_2)^3 - r_2^3)$$

$$= 69.5((d + .4)^3 - .064)$$

(b) X-Ray Tube

$$\text{Mass} = \pi L\rho((1.3 + d)^2 - 1.3^2)$$

$$= 130d(d + 2.6)\text{gm}$$

(c) Hybrid Source

(i) With on/off capability, same mass as for X-ray tube.

(ii) Without on/off capability, same mass as for γ radioisotope.

From the foregoing calculated shield masses, it can be seen that the 2 pound (about 900 gm) mass allotment for shielding will eliminate all sources above roughly 250 Kev.

6.0 SOURCE IMPURITIES

In addition to emitting γ rays of an energy suitable for atmospheric density measurement, a source may emit other energies of γ rays. If these energies are lower, they cause little or no trouble, particularly as regards shielding. However, higher energies can lead to a considerable increase in the required shielding mass. Consider a 20 γ curie γ radioisotope which also emits 1.0 Mev γ rays with a relative abundance of 5%. Suppose also that 3% of the 1 Mev flux reaching the detector is counted in the selected energy range. The count rate from an unshielded source is then:

$$(5.3 \times 10^7) \times (.05) \times (.03) = 8 \times 10^4/\text{second}$$

Allowing only 100 of these means a factor of 800 shielding attenuation is required. The required shield thickness for this is about 7 cm of tantalum. This is very excessive and so stringent guidelines are adopted regarding the impurity γ ray energies allowed in a source.

7.0 SUMMARY

The following guidelines have been adopted for γ-ray source selection.

(a) The main emission (used for density measurements) must be $\geq$ 50 Kev.

(b) The main emission (used for density measurements) must be $\leq$ 250 Kev.

(c) The relative abundance of γ rays above 0.3 Mev must be $<$ 10%.

(d) The relative abundance of γ rays above 0.4 Mev must be $<$ 3%.

(e) The relative abundance of γ rays above 0.7 Mev must be $<$ 1.0%.

(f) The relative abundance of γ rays above 1.0 Mev must be $<$ 0.5%.

appendix F

APPENDIX F

SHIELDING OF THE MAIN γ RADIOISOTOPE SOURCE

1.0 INTRODUCTION AND SUMMARY

This appendix shows that 6.4 mm (0.25 in.) of tantalum shielding will reduce the direct transmission between the source and detector to approximately 11 cps for the main source selected in Part I of this report. The source strength of Gd-153 will be 90 γ curies (i.e., 3.3×10^{12} γ ray emissions from the source) and it will be located 105 cm from the 5 cm diameter by 1.25 cm thick NaI(Tl) detector. Energy discriminating electronics are assumed for the 11 cps background estimate. The statistical fluctuation of the 11 cps will constitute a ±1.4% error in the 230 cps atmospheric backscatter count rate expected at 25 km in the model 3 Martian atmosphere.

2.0 MATERIAL

Tantalum or heavy metal #170 will be used. These have densities of 16.6 and 17.0 gm/cc respectively and approximately equal shielding capabilities per unit mass. A preliminary examination indicates that the heavy metal (90% tungsten, plus copper, iron, nickel and cobalt) is not quite as effective as the tantalum.

3.0 γ RAY SPECTRUM FROM THE SOURCE

The Gd-153 source is expected to be pure in the sense that radiations from any other isotopes present therein will be negligible by comparison with the Gd-153 radiations. The latest information (R. L. Cohen and J. H. Wernick - Phys. Rev. 134B, p. 502, May/64) gives the following spectrum--γ ray transition strengths are relative.

E_γ(Kev)	Rel. Strength
54	< 0.1
68	< 0.04
70	8.1
75	0.26
83	0.70
89	0.23
97	100
103	73
152	< 0.6
173	< 0.6

For calculation purposes, the 97 and 103 Kev γ rays are assumed to be 100 Kev γ's.

4.0 SOURCE STRENGTH

The source strength will be 90 γ curies during the Mars descent. Such a source emits $90(3.7)10^{10} = 2.73 \times 10^{12}$ 100 Kev γ's per second into 4π solid angle. The emission rate of the 152 and 173 γ's is:

$$\frac{2 \times 0.6}{170} \times 2.73 \times 10^{12} = 1.9 \times 10^{10}/\text{sec. for each energy}$$

The factor of 2 appears because about 1/2 of the 100 Kev γ's are lost to internal conversion, but the 152 and 173 Kev γ's are nearly unaffected. The actual emission rate may be less (much less).

5.0 GEOMETRICAL ATTENUATION AND DETECTOR EFFICIENCY

The detector is 5 cm in diameter and 1.25 cm thick. It is positioned edge on to the source and so presents an effective area of 6.25 cm^2. Since it is located 105 cm from the source, the geometric efficiency of the detector is:

$$\frac{6.25}{4\pi(105)^2} = \frac{1}{22,000}$$

It should be noted that if the source is closer to the detector, say separated by only 35 cm, the source strength will decrease by a factor of 3, but the geometrical efficiency will rise by a factor of 9. Nevertheless, the resulting factor of 3 increase in the attenuation to be supplied by the shield will not increase the shield weight by as much as the mass decreases due to the need for only 1/3 as much source--assuming the same specific activity is used for the source material. Therefore, the source-detector arrangement is a worst case from the point of view of shielding mass required.

Using the geometrical attenuation factor of 22,000, the resulting (unshielded) γ ray fluxes reaching the detector are:

100 Kev: 1.24×10^8/sec.

152 Kev: 8.6×10^5/sec.

173 Kev: 8.6×10^5/sec.

Since the detector of NaI(Tl) is edge on to these γ rays, it is virtually 100% efficient.

6.0 TANTALUM ATTENUATION

The attenuation factors for different combinations of γ ray energy and tantalum shield thickness have been calculated and listed in Table 6.0-I.

These attenuation factors are for photoelectric absorption alone and thus are somewhat conservative.

TABLE 6.0-I

Thickness (mm) → / E_γ (Kev) ↓	0.1	0.2	0.5	1.0	2.0	5.0	10.0
60	1.43	2.06	6.05	3.7+1	1.35+3	6.7+7	4.5+15
80	3.25	*1.06+1	3.6+2	1.3+5	1.75+10	3.9+25	--
100	1.90	3.59	2.45+1	6.0+2	3.6+5	7.8+13	--
152	1.23	1.50	2.78	7.70	5.9+1	2.7+4	7.3+8
173	1.15	1.33	2.04	4.17	1.74+1	1.25+3	1.56+6

* 1.06 + 1 means 1.06×10^1, etc.

7.0 DESIRED ATTENUATION AND THE NECESSARY SHIELDING

Any 100 Kev γ rays reaching the detector will be totally absorbed and will probably get into the wide energy gate necessitated both by the poor energy resolution of the detector ($\sim$ 20% fwhm at 100 Kev), and by the wide range of energies possible for singly scattered photons of 100 Kev original energy. Assume all 100 Kev γ's reaching the detector are counted.

Fortunately, the average direct transmission rate will be constant throughout the Mars descent, and may be almost calibrated out by experiments performed before the launch from earth. The main "error" will be the statistical fluctuation in the direct transmission. It is assumed that 16 cps will be allowed--thus constituting a $\leq \pm 2\%$ error in the 230 cps (backscattered) at 25 km in a model 3 atmosphere. Therefore, the shield attenuation required for the 100 Kev γ's will be $(1.25 \times 10^8)/16 = 7.7 \times 10^6$, minimum. This is provided by less than 3 mm of tantalum.

In addition, there will be counts due to the 152 Kev γ's. Due to their higher energy, it is assumed that only 1/4 of these will enter the electronic energy window. Again allowing 16 cps, the necessary shield attenuation factor becomes:

$$8.6 \times 10^5 \times \frac{1}{16} \times \frac{1}{4} = 1.34 \times 10^4$$

which is provided by $<$ 5 mm of tantalum.

Note that 5 mm of tantalum will reduce the 100 Kev intensity to $\ll$ 1 count/second.

Finally, there are the 173 Kev γ rays. About 1/10 of those reaching the detector will be counted in the window. Thus, the necessary shield attenuation factor becomes:

$$8.6 \times 10^5 \times \frac{1}{16} \times \frac{1}{10} = 5.4 \times 10^3$$

This is provided by 6.1 mm of tantalum (which reduces the 152 Kev count rate to ~ 1/sec.).

Therefore, to be conservative, a 6.35 mm (0.25 inch) tantalum shield will be assumed. The γ fluxes reaching the detector and being totally absorbed and then counted will be as follows--(the electronic energy window is assumed to pass all 100 Kev γ counts, 1/4 of all 152 Kev γ counts, and 1/10 of all 173 γ counts--a rather pessimistic assumption).

E_γ (Kev)	Total Flux at Detector (per second)	Count Rate (per second)
100	0.00	0.00
152	~ 4	~ 1
173	~ 100	~ 10

appendix G

APPENDIX G

ABLATION GAGE SYSTEM RESPONSE

1.0 INTRODUCTION

This appendix calculates strength of the Am-241 source to be used in the ablation gage which monitors the heat shield located near the main detector. Since the strength of this source is not a critical design problem, only a simple theoretical calculation is carried out. Then, the resulting source strength is arbitrarily increased to provide a margin of safety.

The chosen source is 100 mc of Am-241 and it produces a back-scatter count rate of at least 10,000 cps when the heat shield is intact. The statistical fluctuation in this count rate is the same as the count rate due to the outer 3% of the heat shield when the heat shield is intact. As ablation occurs, the system accuracy (as a percentage of the intact heat shield) improves to ±1.5% when half the shield is gone.

The system geometry and shielding are also presented.

2.0 SYSTEM RESPONSE DERIVATION

Consider the schematic gage of Figure 2.0-1. The γ rays from the collimated source emerge in a cone and strike the heat shield. The collimation of the detector includes the portion of the source cone which lies within the heat shield.

The rate I_1 at which 60 Kev γ rays emerge from the source collimator is related to the total source strength I_o by:

$$I_1 = \epsilon_c I_o$$

FIGURE 2.0-1

ABLATION GAGE SCHEMATIC

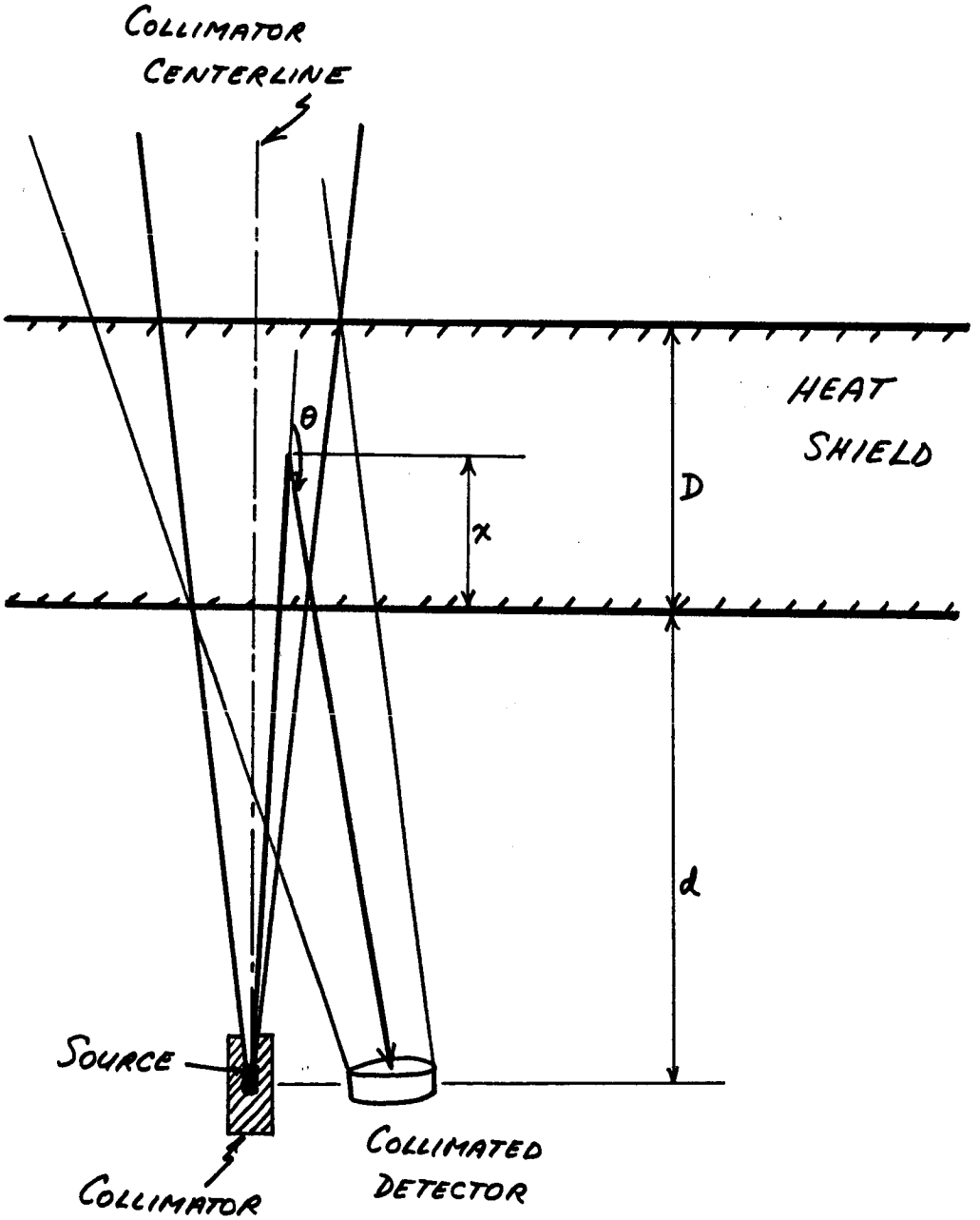

where ϵ_c is the collimation efficiency. For simplicity, it is assumed that all the γ rays travel along the indicated centerline of the cone rather than spread throughout the cone.

The rate at which unscattered 60 Kev γ rays reach a depth x within the heat shield is then:

$$I_x = I_1 \exp(-\mu_1 \rho x)$$

where μ_1 is the total interaction coefficient for 60 Kev γ rays in the heat shield, and ρ is the heat shield density.

The number of γ rays scattered into 4π solid angle from the infinitesimal thickness dx of shield at depth x is:

$$N_x = I_x \, (1-\exp(-\mu_s \rho dx))$$

$$= \mu_s \, \rho \, I_x \, dx$$

where μ_s is the scattering coefficient for 60 Kev γ rays in the shield.

The rate at which these N_x scattered γ rays are detected is:

$$N_x \, w(\theta) \exp(-\mu_2 \rho x/\cos\theta) \, \frac{A_d \, \epsilon_d}{4\pi((x+d)/\cos\theta)^2}$$

where: $w(\theta)$ is the angular dependence of the γ ray scattering

θ is the angle through which the γ rays are scattered

μ_2 is the heat shield total interaction coefficient for the scattered γ rays

A_d is the detector area

ϵ_d is the detector efficiency

d is the distance of the detector from the heat shield

Therefore, the total count rate due to the detection of primary γ's which have undergone one scatter in the heat shield of thickness D is:

$$N = \int_{x=0}^{x=D} \frac{I_o \epsilon_c \exp(-\mu_1 \rho x) \mu_s \rho w(\theta) \exp(-\mu_2 \rho x/\cos\theta) A_d \epsilon_d dx}{4\pi(x+d)^2/\cos^2\theta}$$

$$= \frac{I_o \epsilon_c \mu_s \rho A_d \epsilon_d}{4\pi} \int_o^D \frac{\exp(-\mu_1 \rho x - \mu_2 \rho x/\cos\theta)\ w(\theta)\ dx}{(x+d)^2/\cos^2\theta}$$

The evaluation of the integral is complex and is not warranted because the source size is not a critical matter. Therefore, an averaging scattering angle of $\theta = 150°$ is assumed, since this is approximately the scattering angle from the middle of the heat shield for the selected system geometry. Using $\theta = 150°$, one gets:

$$N = \frac{0.5\ I_o \epsilon_c \mu_s \rho A_d \epsilon_d}{4\pi} \int_o^D \frac{\exp(-\rho x(\mu_1 + 1.3\mu_2))dx}{(x+d)^2}$$

$$= L\ J$$

where:

$$L = \frac{0.5\ I_o \epsilon_c \mu_s \rho A_d \epsilon_d}{4\pi}$$

$$J = \int_o^D \frac{\exp(-kx)dx}{(x+d)^2}$$

where $k = \rho(\mu_1 + 1.3\mu_2)$

Using standard integration tables:

$$J = e^{kd}\left[\frac{-e^{-k(x+d)}}{(x+d)} - k\left(\ln(x+d)\frac{-k(x+d)}{1.1!} + \frac{k^2(x+d)^2}{2.2!} - \frac{k^3(x+d)^3}{3.3!} + \ldots\right)\right]_{x=0}^{x=D}$$

By substituting the appropriate parameters, the detector count rate N can be determined.

3.0 SELECTED ABLATION GAGE

The parameters of the actual ablation system shown in Figure 3.0-1 are:

$\rho = 0.5$ gm/cc

$\mu_1 = .230$ cm^2/gm

$\mu_s = .162$ cm^2/gm

$\mu_2 = .320$ cm^2/gm

$\epsilon_d = 0.15$

$\epsilon_c = 0.05$ (using a collimator half angle of $\sim 25°$)

$A_d = 4.90$ cm^2

$D = 2.5$ cm

$d = 2.5$ cm

Therefore $k = 0.5(.23 + .43) = 0.33$

$J = 0.137$

$L = 1.18 \times 10^{-4}\ I_o$

$N = LJ = 1.61 \times 10^{-5}\ I_o$

If $N = 10^4$ cps, $I_o = 6 \times 10^8$ cps or 16 γ mc, where a γ mc is 3.7×10^7 γ rays/second. Due to self absorption in the Am-241, the actual source strength is ~ 60 mc.

FIGURE 3.0-1

ABLATION GAGE SYSTEM

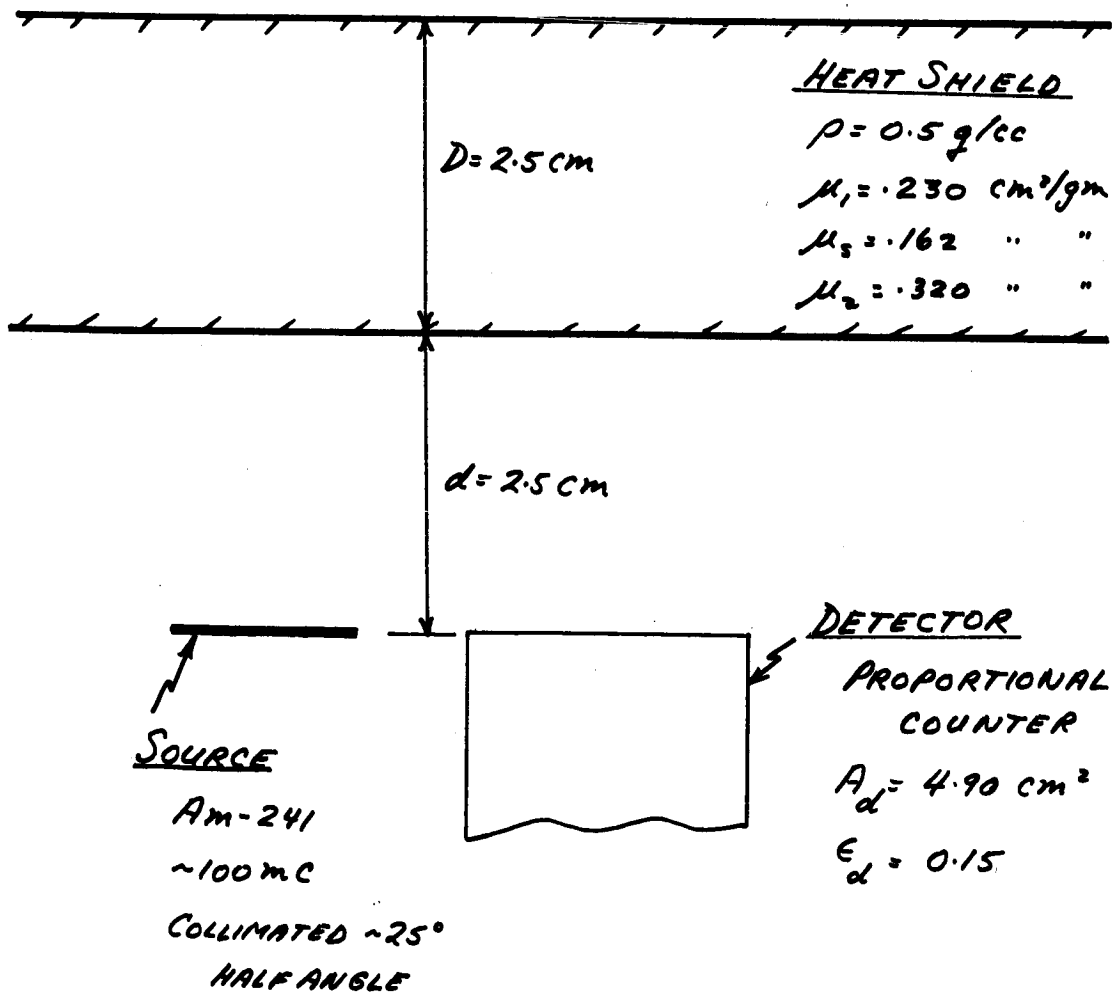

Next, consider the system accuracy by evaluating the integrand:

$$I = \frac{e^{-kx}\,dx}{(x+d)^2}$$

for the outer 1% of the heat shield, i.e., dx = 0.025 cm, x+d = 5 cm, x = 2.5 cm, and k = 0.33. The result is:

$$I = \frac{e^{-.83}(.025)}{25} = .00044$$

Therefore, the change in count rate due to the removal of the outer 1% of the shield is $\Delta N = .00044L$, and since $N = .137L$,

$$\frac{\Delta N}{N} \text{ (outer 1\%)} = \frac{.00044}{.137} = .0032$$

i.e., the last 1% of the shield alters the count rate by 0.32%. Therefore, the last 3% of the shield accounts for 1% of N, i.e., $.01 \times 10^4 = 100$ cps, which is the one-sigma statistical uncertainty in N. Therefore, the gage has an error of ±3% due to source statistical fluctuations when the heat shield is intact.

When the heat shield is half gone, the original count rate of 10,000 cps is reduced to ~8000 cps, and the thin outer skin layer equal to 1.5% of the original shield contributes ~90 cps, which is the statistical fluctuation in 8000 cps. Thus, the system error (due to source fluctuations alone) is reduced to ±1.5% when half the shield has gone.

Since the selected electronics are stable to ±3%, and since the maximum source fluctuation error of ±3% is independent of the electronic error, an overall accuracy of ±5% is reasonable. To provide a margin of safety, a 100 mc source is specified.

The only remaining point to discuss is the shielding of the source. This shielding is needed to shield the proportional counter and the main detector (NaI(Tl)) from the source. Although a collimation efficiency of 5% corresponding to a collimator half angle of 25° was used in the calculations, there is no need to be so restrictive, provided the aforementioned necessary shielding is provided. Accordingly, the shielding indicated in Figure 3.0-2 is used. It is tantalum, and each millimeter of it attenuates the 60 Kev γ rays by a factor of 75. Its total mass is 308 grams (0.68 pounds) and it permits a negligible count rate of ~2 cps in the proportional counter. The proportional counter is not shielded since the low energy sources (Gd-153 and Am-241) are already well shielded, while the Cs-137 is very, very small and contributes negligibly because the counter is insensitive to its high energy γ rays. As regards extra vehicular radiation, neutrons and most γ rays are almost completely ignored. This leaves protons, whose intensity could reach 1000 cps, but which are very strongly discriminated against by the processing electronics. If further study indicates that proportional counter shielding is desirable, some mass can be saved by a careful redesign of the Am-241 shield and used for the proportional counter without increasing the system mass. Beryllium or carbon is suggested as the shielding material.

FIGURE 3.0-2

ABLATION GAGE SOURCE & SHIELD

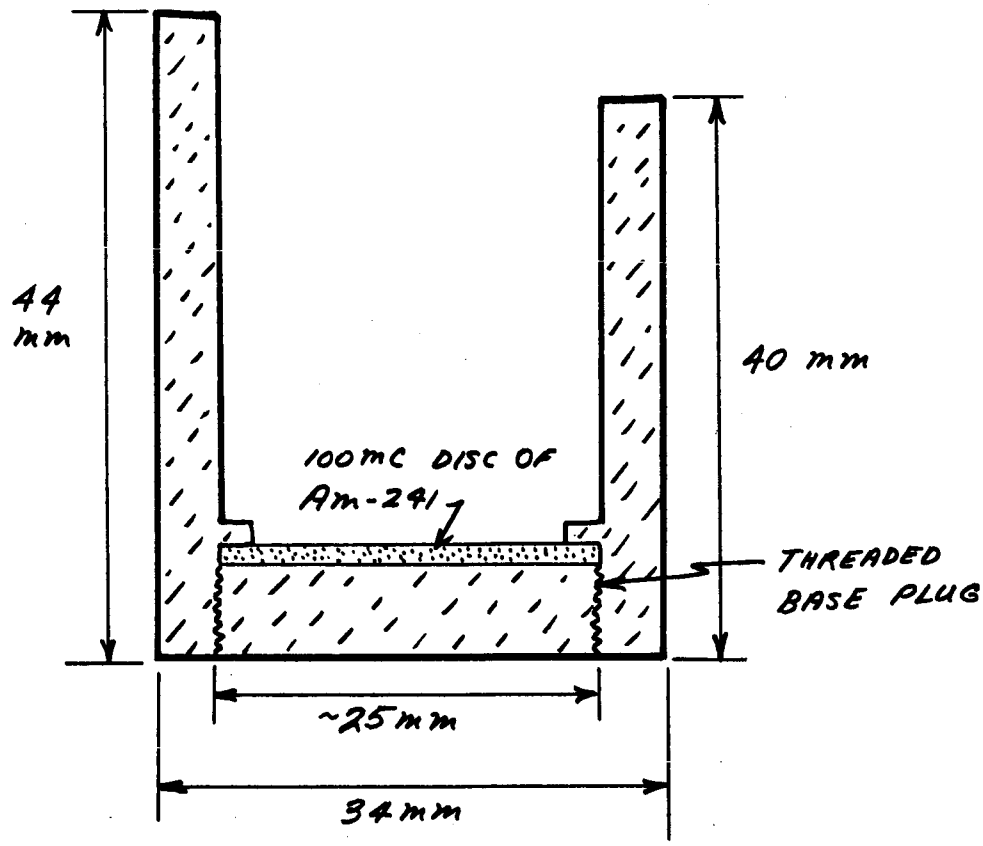

THE AM-241 SOURCE AND 6mm THICK BASE PLUG SCREW INTO REST OF COLLIMATOR

appendix H

APPENDIX H

SYSTEM RELIABILITY

A brief reliability analysis has been performed on the system. For this analysis all component parts of each individual assembly were considered in series for a worst case condition, and the worst case operating temperature was +70°C. The stress ratio is $(\frac{\text{applied voltage or power}}{\text{rated voltage power}}) = 0.3$. Table I, Numerical Analysis, shows the assemblies with their associated component failure rates. Table II shows the failure rate apportionments. The sources of failure rates are as follows:

A. Failure rate "lower limit" based on AVCO Rate Handbook (April 1962)

B. Best estimate for special parts when no failure rates are specified in handbook and not enough data has been collected for accurate apportionment.

C. Failure rate based on Fairchild test data. Tests conducted by MIT on the Micrologic (900 Series) RTL Integrated Circuits (similar to DTL Series) to be used on the Apollo Guidance Computer indicated an average failure rate of $\approx .02 \times 10^{-6}$ F/hr at a 60% confidence level.

The total failure rate for each component is equal to the failure rate base multiplied by the K_A factor. The K_A factor was obtained from the AVCO Failure Rate Handbook. Figure 1 shows the block diagram and the math model giving a mean time between failure of 105,000 hours. Assuming a 100 hour system test and calibration

period and a 30 minute operation time, the probability of mission success is 0.999. More than one-half of the failure probability is in the ablation gage system.

The eight-month standby time will be in a non-operating condition, and is well within typical three to five year shelf life requirements of similar systems.

TABLE I

NUMERICAL ANALYSIS FOR MARS PROBE/LANDER DENSITY SENSING SYSTEM

ASSEMBLY	COMPONENT	FAILURE RATE BASE (10^{-6}F/HR)	K_A FACTOR	QTY.	FAILURE RATE BASE (10^{-6}F/HR)
Source Assembly	Co-60 Source	.001	1	9	.009
Crystal Assembly	Calibration Source	.003	1	1	.003
	Scintillator Material	.010	1	1	.010
	Optical Coupling	.040	1	1	.040
				TOTAL	.053
Regulated Power Supply	RFI Filter	.080	1	1	.080
	Capacitor, S. Tantalum	.012	1	10	.120
	Capacitor, Ceramic	.011	0.5	3	.016
	Resistor, Metal Film	.004	1	23	.092
	Resistor, W.W. Variable	.020	1.8	3	.108
	Diode, Si, Zener	.040	0.2	3	.024
	Diode, Silicon	.021	0.2	12	.050
	Transistor, Silicon	.100	0.1	9	.090
	Inductor	.011	1	1	.011
	Transformer, Power	.500	1	1	.500
				TOTAL	1.091
Photomultiplier Tube and High Voltage Power Supply	Capacitor, S. Tantalum	.012	1	1	.012
	Capacitor, Ceramic	.011	0.5	46	.253
	Resistor, Composition	.005	2	33	.330
	Transformer, Pulse	.170	1	1	.170
	Transistor, Silicon	.100	0.1	4	.040
	Photomultiplier Tube	1.000	1	1	1.000
				TOTAL	1.805
Automatic Gain Control	Capacitor, S. Tantalum	.012	1	10	.120
	Capacitor, Ceramic	.011	0.5	1	.006
	Diode, Silicon	.021	0.2	2	.008
	Resistor, Metal Film	.004	1	27	.188
	Resistor, W.W., Variable	.020	1.8	3	.108
	Transistor, Silicon	.100	0.1	2	.020
	Integrated Circuit (μA710)	.017	1	1	.017
	Integrated Circuit (SE160)	.020	1	1	.020
	Resistor, Thermal	.040	1	1	.040
				TOTAL	.527

TABLE I (Cont'd)

ASSEMBLY	COMPONENT	FAILURE RATE BASE (10^{-6}F/HR)	K_A FACTOR	QTY.	FAILURE RATE BASE (10^{-6}F/HR)
Preamplifier	Capacitor, S. Tantalum	.012	1	3	.036
	Capacitor, Ceramic	.011	0.5	4	.022
	Resistor, Metal Film	.004	1	12	.048
	Diode, Silicon	.021	0.2	2	.008
	Transistor, Silicon	.100	0.1	1	.010
	Integrated Circuit (μA702)	.017	1	1	.017
				TOTAL	.141
Discriminator	Capacitor, S. Tantalum	.012	1	5	.060
	Capacitor, Ceramic	.011	0.5	2	.011
	Integrated Circuit (μA710)	.017	1	2	.034
	Integrated Circuit (SE160)	.020	1	3	.060
	Integrated Circuit (DTμL932)	.020	1	1	.020
	Resistor, Metal Film	.004	1	15	.060
	Resistor, W.W., Variable	.020	1.8	2	.072
				TOTAL	.317
Integrator	Capacitor, S. Tantalum	.012	1	4	.048
	Capacitor, Ceramic	.011	0.5	1	.011
	Resistor, Metal Film	.004	1	9	.036
	Resistor, Thermal	.040	1	1	.040
	Diode, Silicon	.021	0.2	1	.004
	Integrated Circuit (μA702A)	.017	1	1	.017
				TOTAL	.156
High Voltage Power Supply	Capacitor, Ceramic	.011	0.5	8	.046
	Resistor, Metal Film	.004	1	2	.008
	Diode, Silicon	.021	0.2	8	.034
	Capacitor, Paper-plastic	.010	1	1	.010
	Regulator Tube (Victoreen)	1.000	1	1	1.000
				TOTAL	1.098
Proportional Counter Tube		1.000	1	1	1.000

TABLE II

FAILURE RATE BASES

COMPONENT	FAILURE RATE BASE 10^{-6}F/HR	FAILURE RATE SOURCE
Capacitor		
1. Plastic	.010	A
2. Ceramic	.011	A
3. Solid Tantalum	.012	A
Diode, Silicon		
1. Power	.021	A
2. Switching	.021	A
3. Zener	.040	A
Filter, RFI	.080	B
Inductor, RF	.011	A
Integrated Circuits		
1. DC Amplifier (μA702A)	.017	C
2. Differential Amplifier (μA710)	.017	C
3. Dual Buffer (DTμL932)	.020	C
4. Monostable Multivibrator (SE160G)	.020	C
5. Quad Gate (DTμL946)	.028	C
Resistor		
1. Metal Film	.004	A
2. Composition	.005	A
3. W.W. Variable	.020	A
4. Thermal	.040	B
Transistor, Silicon	.100	A
Transformer		
1. Pulse	.170	B

TABLE II (Cont'd)

COMPONENT	FAILURE RATE BASE 10^{-6}F/HR	FAILURE RATE SOURCE
Tube		
1. Photomultiplier	1.000	B
2. Counter Tube	1.000	B
3. Victoreen	1.000	B
Miscellaneous		
1. Radioactive Source (Co-60)	.001	B
2. Calibration Source	.003	B
3. Scintillator Material	.010	B
4. Optical Coupling Assembly	.040	B

NOTE: The value of these failure rates is prior to temperature and electrical stresses.

FIGURE 1

LOGIC DIAGRAM AND MATH MODEL

LOGIC DIAGRAM

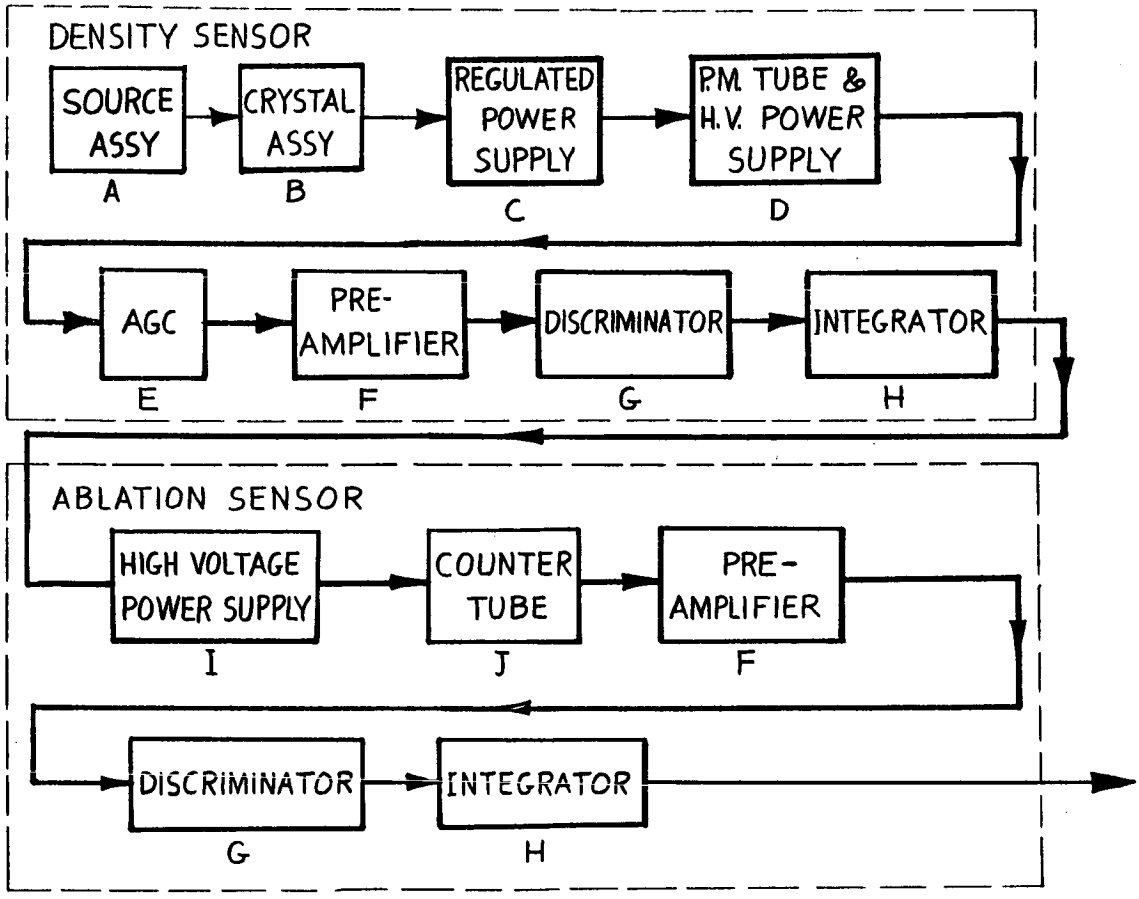

(CONTD)

LOGIC DIAGRAM AND MATH MODEL (CONTD)

MATH MODEL

$$\lambda \text{ SYSTEM} = \lambda \text{ DENSITY SENSOR} + 2\ \lambda \text{ ABLATION SENSOR}$$

$$= \left[\lambda A + \lambda B + \lambda C + \lambda D + \lambda E + \lambda F + \lambda G + \lambda H\right] + \left[2(\lambda I + \lambda J + \lambda K + \lambda L + \lambda M)\right]$$

$$= \left[.009 + .053 + 1.091 + 1.805 + .527 + .141 + .317 + .156\right] \times 10^{-6}$$

$$+ \left[2(1.098 + 1.000 + .141 + .317 + .156)\right] \times 10^{-6}$$

$$= \left[4.099 \times 10^{-6}\right] + \left[5.424 \times 10^{-6}\right]$$

$$\boxed{\lambda \text{ SYSTEM} = 9.523 \times 10^{-6} \text{ F/HR}}$$

$$\boxed{\text{MTBF} \approx \frac{1}{\lambda} \approx 105{,}000 \text{ HOURS}}$$

LEGEND:

λA THRU J = FAILURE RATE OF REFERENCE ASSEMBLIES (SEE TABLE I)

SYSTEM = ONE (1) DENSITY SENSOR AND TWO (2) ABLATION SENSORS

FIGURE I

appendix I

APPENDIX I

CALCULATION OF THE SYSTEM ERROR DUE TO BACKGROUND RADIATION

TABLE OF CONTENTS

1.0 INTRODUCTION

During the descent through the Martian atmosphere, there will be a background radiation count rate I_b which is added to the backscatter count rate I_s despite the use of energy-discriminating electronics. This is due to the fact that a portion of the background radiation reaching the detector produces a light pulse therein whose magnitude lies within the range of magnitudes expected for the Gd-153 γ rays that are backscattered from the Martian atmosphere. The background count rate arises as follows:

(a) Cosmic rays and solar flare particles produce γ rays, protons, neutrons, etc., by interacting with the density sensor, the MP/L vehicle, the Martian atmosphere, and the Martian planetary surface.

(b) There is direct transmission to the detector from the three radioisotope sources in the density sensor.

(c) Some γ rays from the source reach the detector by means of scattering within the shock wave and the MP/L structure.

(d) There are radioisotopes in the Martian surface layer.

In this appendix, the total background count rate I_b that manages to pass through all the energy discriminating electronics is calculated and this calculated rate is labeled I_{bc}. There are two errors associated with I_{bc} that contribute an error to the density measurement.

First, even if the calculated background I_{bc} is exactly equal to the average true background $\bar{I}_b$, the actual background I_b recorded during a one-second sample period will fluctuate randomly from $\bar{I}_b$ with a statistical distribution having a one-sigma value of $\sqrt{\bar{I}_b}$. Since I_{bc} is a prediction of $\bar{I}_b$, the statistical uncertainty ΔI_b in $\bar{I}_b$ is taken as:

$$\Delta I_b = \sqrt{I_{bc}}$$

Since it is not likely that the calculated background I_{bc} will exactly equal the average background $\bar{I}_b$, there is an additional error ΔI_{bc} which is the statistical uncertainty in the accuracy with which I_b is approximated by I_{bc}. This uncertainty is estimated at less than one-third of I_{bc}, since considerable on-the-spot background data will be available due to the activation of the density sensor prior to its descent into the significant Martian atmosphere. In addition, the direct transmission and multiple scattering background from the radioisotope sources within the MP/L can be accurately predicted by means of tests prior to the launch.

In the following sections of this appendix, the detailed calculation of the background count rate I_{bc} is presented.

2.0 THE DETECTION SYSTEM

The detector is a 5 cm diameter by 1.25 cm thick NaI(Tl) crystal encased in 0.75 mm of aluminum on its outer face and sides. The inner face is in contact with the photomultiplier tube which is assumed to provide shielding equivalent to at least 0.75 mm of alunimum. In addition, the crystal has a tantalum collimator of 0.6 mm thickness which is increased to 2 mm on the side toward the Gd-153 source; this covers the 1.25 cm deep sides and also projects about 5 cm forward from the crystal side nearest the Gd-153 source in order to discriminate against Gd-153 γ rays which scatter in the shock wave and heat shield.

Radiations which interact with the crystal have their resultant electrical pulses rejected unless these are the same magnitude as those due to totally absorbed γ rays of 60-100 Kev energy.

3.0 ALTITUDES FOR ERROR CALCULATIONS

The system accuracy is calculated at altitudes of 5 and 25 km above the Martian surface. At 25 km, the atmosphere causes significant heat shield ablation, and so its density is of considerable interest; at approximately 5 km, the parachute sequence is expected to be underway, with the result that the heat shield is gone and there is a significant change in the error analysis. It is possible to calculate the system accuracy at other altitudes, but a preliminary study indicates that the accuracy is only a slowly varying function of altitude, and thus there is no need for further accuracy calculations at intermediate positions.

4.0 DIRECT TRANSMISSION FROM THE SOURCES TO THE DETECTOR

4.1 Automatic Gain Control Source. The AGC uses a calibration source consisting of 0.06 microcuries of Cs-137. This emits 2000 γ rays per second of 662 Kev energy into 4π solid angle. Due to the position of this source, about 900 of these γ rays enter the crystal, and about 600 interact in some way with the crystal. From standard data tables[1] it is found that approximately 200 of these are totally absorbed and approximately 400 deposit from zero to 500 Kev in the crystal. Therefore, in a 40 Kev range, the average number of counts is:

$$\frac{40}{500} \times 400 = 32 \text{ per second}$$

This average is independent of altitude and can be exactly measured during pre-launch tests, but it does have a one-sigma statistical fluctuation of $\pm\sqrt{32} = 5.66$.

4.2 Ablation Gage Source. The ablation gage near the main detector consists of 100 millicuries of Am-241 (60 Kev γ rays). Due to self-absorption, its actual strength is no more than 1.5×10^9 γ's/second into 4π solid angle. Since the detector has a side area of $5 \times 1.25 = 6.25$ cm^2 and is located 5 cm from this source, its geometric efficiency is:

$$\frac{6.25}{4\pi(5)^2} = 0.02$$

Also, the Am-241 is shielded by 4 mm of tantalum which attenuates the radiation flux by a factor of 1.5×10^7. Next, the shielding about the NaI(Tl) further reduces the γ flux by a factor of 10.

Finally, only one-half of the 60 Kev γ rays reaching the detector are accepted by the electronics because the statistical fluctuation in the size of the resulting electrical pulses means that half are outside the 60-100 Kev range.

In conclusion, the background count rate due to direct transmission from the 100 mc Am-241 source to the NaI(Tl) detector is:

$$1.5 \times 10^9 \times 0.02 \times \frac{1}{1.5 \times 10^7} \times \frac{1}{10} \times \frac{1}{2} = 0.1/\text{second}$$

which is negligible.

4.3 Main Sensor Source. At 300 days before the Martian descent, the main source is 480 curies of Gd-153. However, the half-life of 236 days for this radioisotope reduces this to 199 curies during the actual descent. These 199 curies emit the following number of γ rays each second.

E_γ (Kev)	Emissions Per Second
70	1.5×10^{11}
~100	3.4×10^{12}
152	3.7×10^{10}
173	3.7×10^{10}

Without shielding between the source and detector, the γ ray fluxes reaching the latter would be reduced by the geometric factor (inverse square law) of:

$$\frac{6.25}{4\pi(105)^2} = 4.52 \times 10^{-5}$$

since the detector crystal subtends only that proportion of the solid angle about the source.

However, the shielding about the source is at least 6.4 mm of tantalum in all directions except out the collimator. In addition there is the equivalent of ~2mm of tantalum shielding about the detector. As a result, this radiation background count rate is only 0.5/second.

4.4 Summary for Direct Transmission. The direct transmission amounts to 33 cps, which can be calibrated during pre-launch to ±2 cps. Its statistical fluctuation is $\pm\sqrt{33} = \pm 5.8$ cps.

5.0 SCATTERING WITHIN THE VEHICLE AND SHOCK WAVE

There are two basic cases to be considered here. First, there are those γ rays which leave the source through the collimator opening, scatter in the heat shield or shock wave, and then reach the detector somehow. Then there are those γ rays which escape through the source shielding and reach the detector after a scatter in the vehicle structure or in the shock wave. Both of these cases contain a number of sub-cases.

5.1 Collimator Scatterings. The heat shield is 2.5 cm of 0.5 gm/cc material with the nuclear scattering properties of magnesium. The nuclear properties of the shock wave are represented by nitrogen, and the maximum possible shock wave density is six times that of the ambient atmosphere. Only an altitude of 25 km is considered since the shock wave and heat shield are expected to be gone once the parachute sequence is underway at ~5 km. The numbers of γ rays from the source that are scattered in the heat shield opposite the source collimator opening are:

E_γ (Kev)	Heat Shield Scatters (25 km)	Shock Wave Scatters (25 km)
70	1.3×10^9	7×10^4
100	2.2×10^{10}	1.1×10^6
152	2.1×10^8	1.1×10^4
173	2.0×10^8	1.0×10^4

The next step is to calculate how many of these get to the detector. Consider those which reach the detector without any other intervening interactions. The number of such counts due to a particular original energy of γ rays is the scattering rate given for that energy in the above table multiplied by each of:

(a) The geometric efficiency of the detector - the detector subtends ~1/22,000 of the solid angle.

(b) The attenuation factor in the heat shield. Use the energy of the scattered γ ray in the calculations.

(c) The attenuation factor in the 2 mm of tantalum shielding around the detector crystal on the side facing the main source. It is important here to use the scattered γ ray energy when calculating this attenuation.

(d) The probability that the electrical pulse caused by the γ rays will be accepted by the energy-discriminating electronics.

After considering all the above, the total resulting count rate is 20 cps.

Next, consider the case when the γ's scattered in the heat shield and shock wave undergo a second interaction prior to reaching the detector. There are two such cases; the second interaction may be so located that the doubly scattered γ must still pass through the 2 mm detector shield, or, the second scatter may occur on that portion of the heat shield or shock wave that lies in the detector's field of view. Consider the former case. The count rate so resulting is much less than the 20 cps of the previous paragraph because the doubly scattered γ rays are distributed into 4π solid angle geometry. Thus, most of those originally scattered in the general direction of the detector are scattered away from it on the second interaction. Those that were originally scattered away have the disadvantage of a large geometrical attenuation plus more attenuation in the heat shield. Also, large angle scatters are less likely. As a result, this case accounts for no more than 5 counts/second.

Calculations for secondary scatters in the field of view of the detector have also been carried out and a count rate of 12 cps resulted.

Therefore, the total background count rate at 25 km due to γ's which leave the source through the collimator and scatter in the heat shield is 37 cps, which has a statistical fluctuation of ± 6.1 cps.

5.2 Background Through Source Shield. There still remains the count rate due to γ's which leave the source through its tantalum shield. These are distributed into $\sim 4\pi$ geometry and their rates are:

E_γ (Kev)	Outgoing Rate Through Source Shield
70	10
100	0.0
152	$\sim 10^5$
173	$\sim 4 \times 10^6$

Since the numbers in the above table are much smaller than those in the preceding table concerning the number of scatters in the heat shield, it is clear that their contribution to the background will be much less. In fact, they contribute no more than several cps.

5.3 Summary. Therefore, the total background count rate due to γ rays from the source that scatter in the vehicle structure and shock wave is conservatively taken as 40 cps, which can be calibrated to ±10 cps during the pre-launch. It has a statistical fluctuation of $\pm\sqrt{40}$ cps. At 5 km, this background will be down to <5 cps, which is predictable to ±2 cps.

6.0 MARTIAN SURFACE RADIOISOTOPES

As shown in Appendix A, the γ ray fluxes emerging from the Martian surface are not expected to exceed:

E_γ (Mev)	Flux* γ's/cm^2/sec.
~0.5 (secondaries)	1.88
~1.0 (secondaries)	5.22
1.46 (primaries)	0.84
1.76 (primaries)	0.54
2.61 (primaries)	0.94

* Double the fluxes calculated to emerge from the earth's surface. This allows for variations in the radioisotope content of the Martian surface rocks.

Those energies marked as primary are the primary γ ray energies from K-40, Bi-214, and Tl-208, respectively. The secondaries centered at ~1.0 Mev are due to the scattering of the foregoing primaries in the Martian crust. The ~0.5 Mev secondaries are due to a multitude of less prominent and lower energy γ rays in the Bi-214 and Tl-208 decay chains.

6.1 Sample Background Calculations. The detailed calculation of the background count rate due to the foregoing five categories of γ radiation emerging from the Martian surface is too long to present in its entirety. Therefore, a sample calculation is performed in this subsection to show the general technique that is used. A model 3 atmosphere is used at all times.

Consider the 2.61 Mev primaries. Assume that they emerge from the surface at an average angle of 45°. Since the thickness of the model 3 atmosphere between 0 and 25 km is 26.33 gm/cm^2, the average 45° angle path to the detector must traverse 26.33/(sin 45°) = 37.3 gm/cm^2 of atmosphere. Since the specified gases comprising this atmosphere as N_2 and CO_2, each of which has 0.50 orbital electrons per atomic mass unit, their γ ray scattering and absorption properties can accurately be represented by those of air; air is mainly N_2 and O_2, each of which has the 0.50 ratio also. Accordingly, the γ ray interaction coefficients for air are used[2].

Since 0.94 γ rays of 2.61 Mev are emitted from each cm^2 of the surface, the number incident on 20 cm^2 of detector at 25 km altitude is:

$$(0.94)(20)\ \exp(-.039 \times 37.3) = 4.4 \text{ per second}$$

where 0.039 cm^2/gm is the interaction coefficient for air and 37.3 gm/cm^2 is the average path through which a 2.61 Mev γ ray must travel if it is to reach the detector without an interaction in the atmosphere.

Since the detector is an average of 6.5 gm/cm^2 of NaI(Tl), due to the 45° average angle, the probability that an incident 2.61 Mev γ ray will interact with it is $1 - \exp(0.038 \times 6.5) = 0.219$. Therefore, the 4.4 incident γ rays of 2.61 Mev produce only 4.4(.219) = 0.96 interactions/second. Using standard data tables[1], it is possible to estimate that 0.16 of these interactions result in total absorption; i.e., an electrical pulse corresponding to 2.61 Mev of γ ray energy is provided by the detector,--and promptly

rejected by the 60-100 Kev energy gate in the processing electronics. However, the remaining 0.80 pulses/second are spread over ~0-1.6 Mev, and a 40 Kev wide region contains an average of:

$$0.80 \times \frac{0.040}{1.600} = 0.020/\text{second}$$

Thus, an average background count rate of ≤ 0.02/second is expected at 25 km due to 2.61 Mev primary γ rays emerging from the Martian surface.

The methods used in this example have been simple and straightforward, and have neglected the shielding effects of the MP/L vehicle structure, etc. Therefore, it is quite likely that the background count rate so calculated is on the high side. However, to be conservative, these simple methods are used in all the background calculations of this section 6. If so desired, a very complex and more accurate set of calculations could be carried out on a computer, but at this stage in the system design it is not worthwhile.

6.2 Summary: Background Due to Surface Radioisotopes. The calculated background count rates at 25 and 5 km due to γ emitting radioisotopes in the Martian surface are 5 and 7 cps respectively, and these are estimated to have prediction uncertainties of ±3 and ±4 cps respectively.

As explained in other parts of the report, the α's and β's can be neglected.

7.0 COSMIC RAY BACKGROUND

Cosmic rays produce a background count rate when they interact with the detector, the MP/L vehicle, the Martian atmosphere, or the Martian surface. In the latter 3 cases, it is the secondaries and tertiaries produced by the interactions that reach the detection system and cause a count.

The calculation of this count rate is too complex to be presented here, as it is necessary to follow the progress of the primary, secondary and tertiary radiations through the atmosphere. Therefore, the pertinent techniques used to calculate the background are presented for each of the four interaction categories mentioned in the preceding paragraph, but first it is necessary to define the calculation guidelines.

7.1 Calculation Guidelines. Calculations are carried out only for altitudes of 5 and 25 km in the model 3 atmosphere. The primary cosmic ray flux of ~4 protons/cm^2/sec. is halved to 2.0/cm^2/sec. because the planet Mars shields out half of them. Their average energy is assumed to be 5 Bev. The processing electronics are assumed to reject all counts not equivalent to totally absorbed 60-100 Kev γ rays. In this connection, it is necessary to note that 1 Mev deposited in NaI(Tl) by a proton does not produce as large a light pulse as does 1 Mev from a γ ray. See reference 3 for details of the light-producing efficiencies of different particles. The interaction probabilities for various proton and neutron energies are from references 4 and 5, and the average number of secondary particles produced by each such interaction is found in reference 5 also.

7.2 Interactions with the Detector. The background count rate from the interaction of primary cosmic rays with the NaI(Tl) is <0.1 cps because virtually every incoming particle leaves many Mev of energy in the detector and so does not contribute. Only those particles passing through an edge can hope to leave only a very little amount of energy and so contribute to the background.

7.3 Interactions with the MP/L Structure. The structure is assumed composed of two parts. First, a 9 kilogram sphere of lead located only 20 cm from the detector was used to represent the high atomic number instrumentation and shielding that may be located nearby. Second, the remainder of the vehicle is represented by a 1260 kg sphere of carbon located 105 cm from the detector. This represents the heat shield and other light-alloy structures of the vehicle.

When the 5 Bev primaries strike the above two configurations, they produce mainly high energy protons, neutrons and γ rays, which go on to cause further interactions leading to lower energy particles and γ's. When particles or γ's escape from the MP/L vehicle, they are assumed lost, since the rarity of the atmosphere makes their return to the detector very unlikely. The total count rate from the MP/L structure interactions is 5 cps at all altitudes (due to the penetration of the primary cosmics to all altitudes), with a prediction uncertainty of ± 3.

7.4 Interaction with the Martian Atmosphere. The methods used here are the same as in paragraph 7.3 above. Some of the particles are lost to outer space and some reach the surface. Note that each neutron that does not escape into space is eventually captured in either the atmosphere or ground, and so produces γ rays. Also, the rarity of the atmosphere permits the neutrons to exist for >10 seconds in the atmosphere, thus causing a buildup in the neutron flux.

The calculated background from interactions with the atmosphere is 5 cps at all altitudes, with a prediction uncertainty of ± 3.

7.5 Interaction with the Martian Surface. The calculation techniques are the same as for 7.4 above. The results are 20 cps at 25 km and 30 cps at 5 km, with respective prediction uncertainties of ± 8 and ± 10.

8.0 SOLAR FLARE BACKGROUND

Solar flares have greatly varying sizes and energy distributions, but their large particle flares are offset by their much lower average energy (10-100 Mev compared to 5 Bev for cosmic rays). Therefore, they are much attenuated by the vehicle structure and also by the atmosphere itself. Also, the particles usually lose all their energy by ionization rather than by nuclear interactions which produce secondary radiations. And when a nuclear interaction does occur, the number of secondary radiations produced is far lower than for the higher energy cosmic rays.

Bearing these facts in mind, calculations were carried out using the same techniques as for the cosmic rays. From tabulated flare sizes and probabilities[6], a 1% per day flare was selected, i.e., a flare size which has a 1% daily probability of occurrence during the period of maximum solar activity. Then, it was assumed that the descent was occurring during the most intense portion of the flare. The resulting background was 10 cps at 25 km and 5 cps at 5 km, with respective prediction uncertainties of ±5 and ±2 cps. In practice, selection of the moment of descent from orbit by the earth controllers will likely lessen the solar flare background.

9.0 SUMMARY

The summary of the background radiation count rates is presented in Table 9.0-I.

TABLE 9.0-I

BACKGROUND RADIATION COUNT RATES (PER SECOND)

RADIATION SOURCE	STATISTICAL UNCERTAINTY 25 km	STATISTICAL UNCERTAINTY 5 km	PREDICTION UNCERTAINTY 25 km	PREDICTION UNCERTAINTY 5 km
Cosmics Interacting with Vehicle	$\pm\sqrt{5}$	$\pm\sqrt{5}$	±3	±3
Cosmics Interacting with Atmosphere	$\pm\sqrt{5}$	$\pm\sqrt{5}$	±3	±3
Cosmics Interacting with Surface	$\pm\sqrt{20}$	$\pm\sqrt{30}$	±8	±10
Solar Flare (1%/day)	$\pm\sqrt{10}$	$\pm\sqrt{5}$	±5	±5
Surface Radioisotopes	$\pm\sqrt{5}$	$\pm\sqrt{7}$	±3	±4
Direct Transmission from Sources to Detector	$\pm\sqrt{33}$	$\pm\sqrt{33}$	±2	±2
Scattering of Source γ rays in Vehicle and Shock Wave	$\pm\sqrt{40}$	$\pm\sqrt{5}$	±10	±2
Root of Sum of Squares	±10.9	±9.5	±14.8	±12.3
Fractional Error, Assuming I_p = 230 and 1580 at 25 and 5 km respectively	±0.047	±0.006	±0.065	±0.008
Symbol	ΔI_b	ΔI_b	ΔI_{bc}	ΔI_{bc}

APPENDIX I

REFERENCES

1. Nuclear Data Tables, Part 3, 1960, by J. B. Marion and available from Superintendent of Documents, page 59.

2. The Atomic Nucleus, R. D. Evans, McGraw-Hill, 1955, page 713.

3. J. B. Birks, "The Theory and Practice of Scintillation Counting", Macmillan Company, 1964.

4. Neutron Cross Sections, 1958, BNL - 325 Second Edition.

5. Douglas Report SM-46334, December 1964, "Secondary Nucleons Produced in High Energy Nuclear Reactions"

6. NASA TM X-53273, "Space Environment Criteria Guidelines for Use in Space Vehicle Development", May 27, 1965.